GLASILO SLOVENSKIH TEKSTILCEV • SLOVENE JOURNAL FOR TEXTILE AND CLOTHING TECHNOLOGY, DESIGN AND MARKETING

tekstilec

3/2023 • vol. 66 • 161–248
ISSN 0351-3386 (tiskano/printed)
ISSN 2350 - 3696 (elektronsko/online)
UDK 677 + 687 (05)

http://www.tekstilec.si

tekstilec (ISSN: 0351-3386 tiskano, 2350-3696 elektronsko) je znanstvena revija, ki podaja temeljne in aplikativne znanstvene informacije v fizikalni, kemijski in tehnološki znanosti, vezani na tekstilno in oblačilno tehnologijo, oblikovanje in trženje tekstilij in oblačil. V prilogah so v slovenskem jeziku objavljeni strokovni članki in prispevki o novostih v tekstilni tehnologiji iz Slovenije in sveta, prispevki s področja oblikovanja tekstilij in oblačil, informacije o raziskovalnih projektih ipd.

tekstilec *(ISSN: 0351-3386 printed, 2350-3696 online) the scientific journal gives fundamental and applied scientific information in the physical, chemical and engineering sciences related to the textile and clothing industry, design and marketing. In the appendices written in Slovene language, are published technical and short articles about the textile-technology novelties from Slovenia and the world, articles on textile and clothing design, information about research projects etc.*

Dosegljivo na svetovnem spletu/*Available Online at*
www.tekstilec.si

Tekstilec je indeksiran v naslednjih bazah/*Tekstilec is indexed in*
Emerging Sources Citation Index – ESCI (by Clarivate Analytics) za 2022:
Journal Impact Factor (JIF): 0.7; Journal Citation Indicator (JCI): 0.25
Leiden University's Center for Science & Technology Studies: 2021:
SNIP 0.777
SCOPUS/Elsevier za 2022: Q3, SJR 0.2, Cite Score 1.8, H Index 14
Ei Compendex
DOAJ
WTI Frankfurt/TEMA® Technology and Management/
TOGA® Textile Database
World Textiles/EBSCO Information Services
Textile Technology Complete/EBSCO Information Services
Textile Technology Index/EBSCO Information Services
Chemical Abstracts/ACS
ULRICHWEB – global serials directory
LIBRARY OF THE TECHNICAL UNIVERSITY OF LODZ
dLIB
SICRIS: 1A3 (Z, A', A1/2); Scopus (d)

tekstilec

Ustanovitelja / *Founded by*
- Zveza inženirjev in tehnikov tekstilcev Slovenije / *Association of Slovene Textile Engineers and Technicians*
- Gospodarska zbornica Slovenije – Združenje za tekstilno, oblačilno in usnjarsko predelovalno industrijo / *Chamber of Commerce and Industry of Slovenia – Textiles, Clothing and Leather Processing Association*

Revijo sofinancirajo / *Journal is Financially Supported*
- Javna agencija za raziskovalno dejavnost Republike Slovenije / *Slovenian Research Agency*
- Univerza v Ljubljani, Naravoslovnotehniška fakulteta / *University of Ljubljana, Faculty of Natural Sciences and Engineering*
- Univerza v Mariboru, Fakulteta za strojništvo / *University of Maribor, Faculty for Mechanical Engineering*

Sponzor / *Sponsor*
Predilnica Litija, d. o. o.

Izdajatelj / *Publisher*
Univerza v Ljubljani, Naravoslovnotehniška fakulteta / *University of Ljubljana, Faculty of Natural Sciences and Engineering*

Revija Tekstilec izhaja pod okriljem Založbe Univerze v Ljubljani / *The journal Tekstilec is published by the University of Ljubljana Press*

Revija Tekstilec izhaja šestkrat letno (štirje znanstveni zvezki in dve strokovni prilogi) / *Journal Tekstilec appears six times a year (four scietific issues and two proffessional supplements)*

Revija je pri Ministrstvu za kulturo vpisana v razvid medijev pod številko 583.
Letna naročnina za člane Društev inženirjev in tehnikov tekstilcev je vključena v članarino.
Letna naročnina za posameznike 38 € za študente 22 €
za mala podjetja 90 € za velika podjetja 180 €
za tujino 110 €

Cena posamezne številke 10 €

Na podlagi Zakona o davku na dodano vrednost sodi revija Tekstilec med proizvode, od katerih se obračunava DDV po stopnji 5 %.

Imetnik računa / *Account holde*r:
Univerza v Ljubljani,
Naravoslovnotehniska fakulteta,
Askerceva 12, 1000 Ljubljana, SI-Slovenija

Transakcijski račun / *Bank Account:*
SI56 01100–6030708186, Banka Slovenije,
Slovenska 35, 1000 Ljubljana, SI-Slovenija
SWIFT / *SWIFT Code*: BSLJSI2X

Naslov uredništva / *Editorial Office Address:*
Uredništvo Tekstilec, Snežniška 5, SI–1000 Ljubljana
Tel. / *Tel.*: + 386 1 200 32 00, +386 1 200 32 24
Faks / *Fax*: + 386 1 200 32 70
E–pošta / *E–mail*: tekstilec@ntf.uni–lj.si
Spletni naslov / *Internet page*: http://www.tekstilec.si;
https://journals.uni-lj.si/tekstilec

Lektor za slovenščino / *Slovenian Language Editor* Milojka Mansoor
Lektor za angleščino / *English Language Editor*
Glen Champagne, Barbara Luštek Preskar

Oblikovanje platnice / *Design of the Cover* Tanja Nuša Kočevar
Oblikovanje / *Design* ENOOKI Kraft, Mitja Knapič s.p
Oblikovanje spletnih strani / *Website Design* Jure Ahtik

Tisk / *Printed by* DEMAT d.o.o.

SCIENTIFIC ARTICLES/
Znanstveni članki

Tanja Nuša Kočevar
University of Ljubljana, Faculty of Natural Sciences and Engineering, Department of Textiles, Graphic Arts and Design, Aškerčeva 12, 1000 Ljubljana, Slovenia

3D Printing on Textiles – Overview of Research on Adhesion to Woven Fabrics

3-D tisk na tekstil - pregled raziskav o adheziji na tkane tekstilije

Scientific review/*Pregledni znanstveni članek*
Received/Prispelo 7-2023 • Accepted/Sprejeto 7-2023

Corresponding author/*Korespondenčna avtorica*:
Assist. Prof. Dr. Tanja Nuša Kočevar
E-mail: tanja.kocevar@ntf.uni-lj.si
Tel. +386 1 200 32 80
ORCID: 0000-0002-5568-5719

Abstract

3D printing on textiles has great potential to influence developments in various industries. It enables the production of new, potentially personalised products in areas such as technical textiles, protective clothing, medical products, fashion, textile and interior design. 3D printing can also contribute to waste-free production processes. In the method of 3D printing on textiles, the material is applied directly to the textile substrate to create 3D objects, patterns or designs on the surface. The fused deposition modelling (FDM) technology, where thermoplastic filaments are extruded and deposited in thin layers based on a 3D model, is widely used for this purpose. A precise control of factors such as temperature and speed is essential in FDM to regulate the flow of polymer material during the printing process. The most commonly used polymer for 3D printing on textiles using FDM is polylactic acid (PLA). Acrylonitrile butadiene styrene (ABS) is another widely used material, known for its low shrinkage rate and high printing accuracy, while thermoplastic polyurethane (TPU) is used due to its exceptional mechanical properties, e.g. tensile strength, flexibility, durability and corrosion resistance. Good adhesion between 3D printed objects and the textile surface is essential for the production of quality products. Adhesion depends on various factors, e.g. textile properties, printing parameters and the type of polymer used. The composition of the woven fabric, including the areal density, warp and weft density, yarn count, fabric thickness and weave pattern, significantly affects the adhesion strength of the 3D printed polymer. When considering double weaves, which allow different materials in the upper and lower layers, better adhesion properties are found than at single weaves. A cross-sectional analysis revealed that the polymer penetrates deeper into a double-woven fabric, resulting in improved adhesion. In general, the study highlights the advantages of double weaves for 3D printing applications on textiles.
Keywords: 3D printing, adhesion, woven fabric, double fabric

Izvleček

3-D tisk na tekstil vpliva na razvoj različnih industrij. Omogoča izdelavo novih, potencialno personaliziranih izdelkov na področjih, kot so tehnične tekstilije, zaščitna oblačila, medicinski pripomočki, moda, oblikovanje tekstilij in

interierja. 3-D tisk pripomore tudi k proizvodnim procesom brez odpadkov. Pri 3-D tisku na tekstil se material nanaša neposredno na tekstilno podlago, da se na površini tekstila ustvarijo različni 3-D objekti ali vzorci. V ta namen se pogosto uporablja tehnologija modeliranja s spajanjem slojev (FDM), pri kateri se termoplastični filamenti ekstrudirajo in nalagajo v tankih plasteh glede na oblikovani 3-D model. Natančen nadzor dejavnikov, kot sta temperatura in hitrost, je pri tehnologiji FDM bistvenega pomena za uravnavanje pretoka polimernega materiala med tiskanjem. Najpogosteje uporabljeni polimer za 3-D tiskanje na tekstil s tehnologijo FDM je polimlečna kislina (PLA). Akrilonitril butadien stiren (ABS) se prav tako pogosto uporablja, ker ima nizko stopnjo krčenja in omogoča visoko natančnost tiskanja, medtem ko se termoplastični poliuretan (TPU) uporablja zaradi izjemnih mehanskih lastnosti, kot so natezna trdnost, prožnost, trpežnost in odpornost proti koroziji. Dobra adhezija med 3-D natisnjenimi predmeti in tekstilno površino je bistvenega pomena za izdelavo kakovostnih izdelkov. Adhezija je odvisna od različnih dejavnikov, kot so lastnosti tekstila, parametri tiskanja in vrsta uporabljenega polimera. Konstrukcija tkanin, vključno s ploskovno maso, gostoto osnove in votka, finostjo preje, debelino tkanine in vezavo, pomembno vpliva na adhezijo 3-D natisnjenega polimera. Pri dvojnih tkaninah, ki omogočajo uporabo različnih materialov v zgornjem in spodnjem sloju, je bila ugotovljena večja adhezija kot pri enojnih tkaninah. Analiza prečnega prereza je pokazala, da polimer prodre globlje v dvojno tkanino, zaradi česar je adhezija boljša. Na splošno so raziskave pokazale prednost uporabe dvojnih tkanin za aplikacijo 3-D tiska na tekstil.

Ključne besede: 3-D tisk, adhezija, tkanina, dvojna tkanina

1 Introduction

Three-dimensional (3D) printing is an additive manufacturing (AM) technology that produces objects by depositing material in thin layers. The deposited layers of material are bonded together in different ways depending on the 3D printing technology and the material used [1]. The technology has great potential to influence developments in many areas of the textile and fashion industry. In addition to the production of new, possibly personalised products in the fields of technical textiles, protective clothing, medical products, fashion, textiles, interior design etc., it can influence the modernisation of processes with a view to waste-free production [2, 3]. In textile and apparel design, 3D printing is used in three different forms, i.e. direct printing on textiles, printing of rigid elements that can be assembled into flexible textile-like structures and printing of elastic materials that resemble textiles. Each of these forms can be realised with different printing technologies [4]. In 3D printing on textiles, the material is applied directly to the textile substrate and the desired 3D objects, patterns or designs are created on its surface. The fused deposition modelling (FDM) technology is usually used for this purpose. In addition, stereolithography (SLA) [5] and PolyJet technology, where aesthetic, detail and surface finishes are the most important, can be used [6]. In FDM, a 3D printer uses the process in which thermoplastic filaments are extruded and deposited in thin layers based on a previously designed 3D model [7]. During this process, the printer ensures precise control over factors such as temperature and speed to regulate the flow of the polymer material [8].

In the workflow of 3D printing on textiles, 3D models should first be created in a 3D computer application and exported as stl files for slicing in a suitable software where the parameters for the 3D printing process are defined. Fixing a textile substrate to the printer bed to achieve stability and precise alignment of the threads is an important step in the workflow, as it affects the accuracy of the print. Some researchers mentioned fixing textiles with tape on the print bed [9] or using lacquer [10]. In addition, special mounting frames [11] can be prepared

for precise positioning of a textile and clamps [12, 13] can be used for fastening to prevent the textile from slipping during the printing process.

The most common polymer for 3D printing on textiles using the FDM technology is polylactic acid (PLA). This polymer is predominantly used for all applications on a textile substrate. One of the notable advantages of PLA is its low extrusion temperature, which is typically around 210 °C. In addition, PLA is a biopolymer; thus, its biodegradability and renewability make it an environmentally friendly choice for 3D printing [14, 15].

Acrylonitrile butadiene styrene (ABS) is, along with PLA, one of the most widely used materials in FDM. It has a relatively low glass transition temperature and very good processing properties. While the shrinkage rate during the cooling process is low, the printing accuracy and dimensional stability are high [16]. ABS is also frequently used and tested in 3D printing on textiles [17–19].

Another material used for 3D printing is thermoplastic polyurethane (TPU). It has exceptional mechanical properties, e.g. tensile strength, abrasion resistance, hydrolytic stability, flexibility, durability and corrosion resistance. The polymer is composed of various soft and hard segments. These segments contribute to the unique properties and behaviour of TPU [20]. Tests have also shown that synthetic fabrics such as polyester, polyamide and laminated neoprene are compatible with TPU filaments. Direct 3D printing of TPU filaments onto neoprene can therefore offer many potential functional applications, e.g. protective clothing and other aesthetic 3D decorations [21, 22].

Polyethylene terephthalate (PET) copolymer is a modified version of polyethylene terephthalate in which additional monomers or additives are incorporated into the polymer chain. This modification can introduce specific properties and characteristics that make it suitable for 3D printing applications on textiles. It requires slightly higher temperature for 3D printing than PLA (240 °C). It has better mechanical properties than PLA and is also recyclable. Polyethylene terephthalate copolymer with glycol modification (PETG) was tested by Ercegović et al. for use in car interiors [23]. In the study, three different polymers were printed on the composite with a porous knit of polyester fibres (PET) on the front side. TPU polymers were found to have better adhesion properties than PLA and PETG, while TPU has a more polar character among the polymers and is hence suitable for printing on most textile substrates.

As the field of 3D printing continues to evolve, researchers and manufacturers are constantly exploring novel materials that expand the range of possibilities and enhance the capabilities of printed objects. These new materials bring forth diverse properties such as increased strength, improved flexibility, enhanced heat resistance, and even specialised functionalities like conductivity or bio-compatibility [24]. New thermoplastic filaments used in recent research for 3D printed polymer adhesion to textiles include polyamide combined with percentage of carbon fibres or glass fibres and high-performance polyolefin with percentage of glass fibres, which have strong mechanical properties and can withstand much higher temperatures than PLA, for example [25]. Furthermore, the adhesive forces between these new materials and textile substrates can vary significantly. Different materials may exhibit stronger or weaker bonding properties with specific types of fabrics or textile constructions. This allows for customisation and optimisation of the bonding process to achieve desired levels of adhesion and durability between the 3D printed objects and textile substrates.

2 Use of 3D printing on textiles

3D printing on textiles has become an important technology for manufacturing new products in recent years, at a time when new 3D technologies are on the rise and proving useful in many fields. One important area is medicine, particularly prosthetics, where customised products such as orthopaedic devices can

be made [2], combining soft and flexible textile material with 3D printed material that provides a firm support. In these cases, knitted materials are usually used for the textile substrate. 3D printing on textiles can also be used for protective clothing [22]. Other area is textile for garment production, considerably textile design. Spahiu et al. made some experiments where 3D printed patterns were printed on a textile substrate for modifying the drape of a fabric [26]. 3D printing is also used for fabric surface decoration [27]. An open-pore fabric can be used as a substrate where adhesion is not a problem as the printed polymer can tightly bound into the open pores of the textile. The textile decorated by 3D printing can then be used to make garments [28], as shown in Figure 1.

Figure 1: Detail of fabric decorated with 3D printing (photo: Manca Drusany)

Many other 3D printing on textiles design projects are featured on the website of the company STRARASYS, which collaborates with numerous fashion and textile designers [29]. A breakthrough technique involves additive manufacturing on stretched fabrics that, once released, undergo a remarkable metamorphosis from a flat 2D pattern to a dynamic 3D geometry [30]. The literature review shows that 3D printing on textiles enables the versatility of new aesthetic and functional properties that will further expand the scope of applications; moreover, various textiles substrates can be enriched with some additional visual and physical properties through 3D printing [31, 32]. Recently, 4D printing (4DP), an advanced technology that combines functional materials and 3D printing, has been developing. It introduces time as the fourth dimension and enables the development of smart materials with versatile properties. By combining the 3D printing technology with textiles, dynamic and adaptable structures can be created that can change shape or properties based on external stimuli or environmental conditions. This integration of 3D printing with textiles expands the capabilities of 4D printing by incorporating the inherent properties and behaviour of the textile material into the final printed object. The key feature of 4DP is the shape memory effect (SME), which allows printed objects to respond to external stimuli, e.g. heat, moisture, electricity, magnetic fields. By leveraging SME, the 4DP technology eliminates the inherent rigidity of 3D printed prototypes and opens possibilities for complex smart textiles and fashion items in various industries [33].

3 Adhesion of 3D printed polymer on textile substrate

For the versatile use of polymer-textile composites, it is important that the 3D printed polymer bonds to the textile with sufficient force. A prerequisite for the production of quality products is therefore good adhesion of the 3D printed objects to the textile surface [11]. Adhesion between the polymer and the substrate is enabled by three primary mechanisms, i.e. mechanical coupling, molecular bonding and

thermodynamic adhesion. These mechanisms play a critical role in establishing a strong and durable bond between the polymer material and substrate surface. Mechanical coupling or interlocking considers the mechanical penetration of the adhesive into the pores and voids of the solid surface, and is based on the penetration of the adhesive into the surface of the substrate. Molecular bonding is the predominant mechanism generally accepted as an explanation for adhesion between two closely spaced surfaces. In this process, intermolecular forces occur between the adhesive and the substrate, including dipole-dipole interactions, van der Waals forces and various forms of chemical interactions, e.g. ionic, covalent and metallic bonds. While the thermodynamic theory assumes that the adhesive adheres to the substrate at the interface due to interatomic and intermolecular forces, if close contact is achieved, only an equilibrium process is required at the interface [34]. In studies, it was found that when some polymers are printed on various textile substrates, physical interlocking bonds are formed without any chemical bonding between the polymer and the substrate material [17, 22]. The intensity of adhesion depends on factors from three different categories in the printing process, i.e. textile properties, printing parameters and the type of polymer printed [35]. These are also the main areas of interest for research in the field of adhesion of 3D printed objects to the textile substrate. The research is mainly conducted on woven and knitted fabrics; however, our focus in the article is on the adhesion of 3D printed polymer to woven fabrics.

3.1 Methods for testing adhesion

In the revised literature, three methods are used to quantify the adhesion of 3D printed parts to a textile substrate, i.e. a perpendicular tensile test, a shear test and a T-peel test. It was found that these tests are all suitable for evaluating the adhesion properties [37]. T-peel is the most used adhesion test which is usually performed according to the standard DIN 53530 [13, 17, 36–41]. Sometimes, the adhesion test was also conducted visually and experientially, as in the case of a study in which different textile substrates were 3D printed with different polymers in the form of snap and zip fasteners, and the composites were observed to see how they behaved when the functionalised fabric was washed [18].

3.2 Observing morphology

The morphology of 3D printed objects on textile substrates also provides information about possible physical bonding. The surface of the fabric has a significant effect on the adhesion properties; thus, observing the surface of the printed textiles plays an important role in the study of adhesion. The morphology of the fabric is closely related to the adhesion of the 3D printed polymer, as it allows the molten polymer to penetrate the pores of the fabric

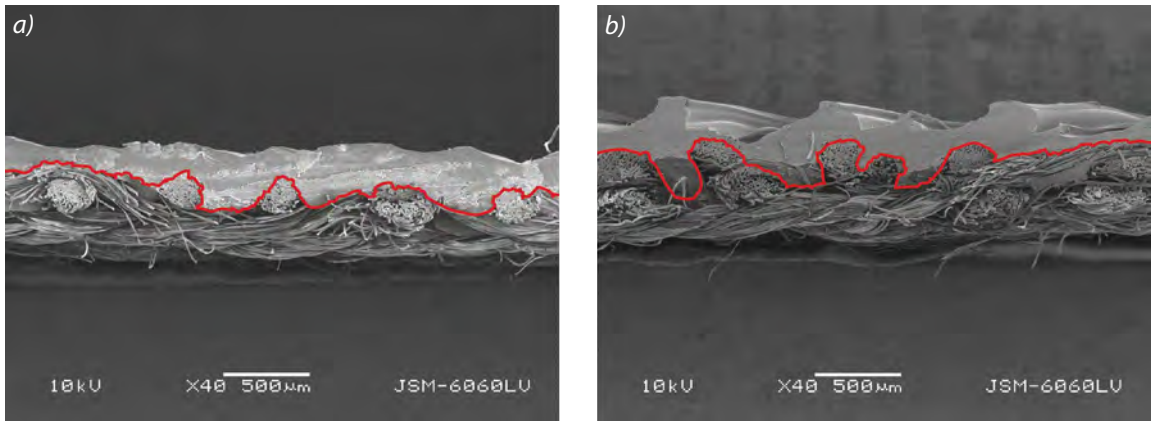

Figure 2: Cross-section of 3D printed fabrics: a) simple fabric, b) double fabric, both fabrics are cut in warp direction and printed at z-distance z = 0.25 mm, 40· magnification [11]

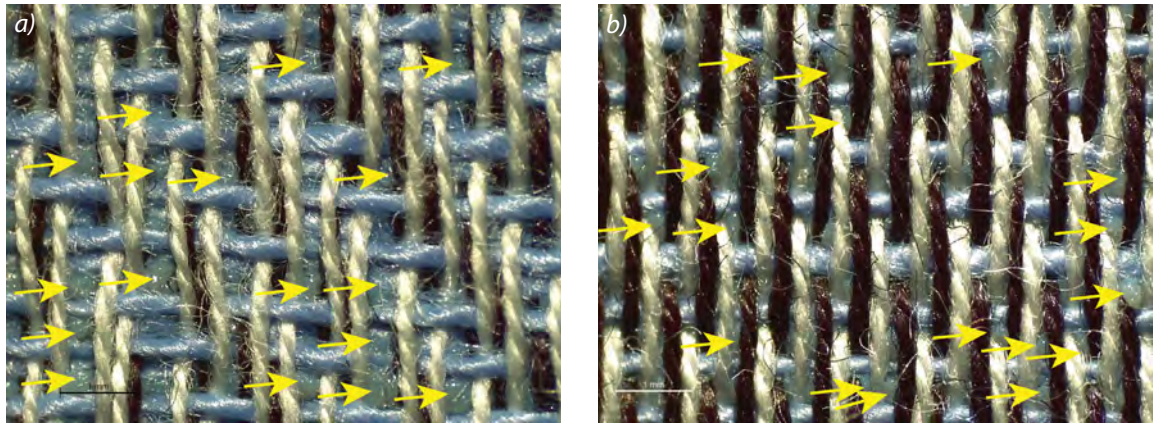

Figure 3: Images acquired with optical microscope, 20· magnification, of back of fabrics 3D printed with constant z-distance (z = 0.25 mm): a) double fabric, b) simple fabric, where deposits of penetrated molten polymer are marked [11]

structures [17, 40]. The images show how the printed polymer coats the threads in a fabric or protrudes through the textile substrate. Optical microscopes, confocal laser scanning microscopes or scanning electron microscopes are generally used to optically evaluate the composites, surfaces and their cross-sections [37–39, 41]. Figures 2 and 3 show the images taken with the scanning electron microscope and the optical microscope for the adhesion study.

3.3 Influence of 3D printing parameters on adhesion

Among the parameters of 3D printing, according to the research of most authors, the distance of the print head from the print bed or the textile substrate, i.e. the so-called z-distance, is the most important [17]. Other parameters, e.g. printing speed and temperature, print bed temperature and nozzle size, different infill orientations of the first printed layer [40] etc., also influence adhesion between the textile substrate and 3D printing polymer. Printing at a lower nozzle position is clearly advantageous for the adhesion [9]. Nevertheless, as the distance decreases, the adhesion force increases until reaching a minimum distance where the nozzle gets clogged by the filament [38]. Göksal et al. [25] suggest the necessary optimisation of the z-distance to achieve sufficient adhesion between the two materials, while the importance of this printing parameter proposes further research to optimise this value without first performing a series of tests, such as measuring the force the textile fabric exerts against the nozzle or polymer flow.

3.4 Influence of woven fabric composition on adhesion

The most influential parameters affecting the properties of woven fabrics are the warp and weft raw materials, warp and weft count, warp and weft density, and the type of weave. These parameters have a significant effect on the structure and appearance of the woven fabric [42]. All the revised research has clearly confirmed that the adhesion strength of the 3D printed polymer depends on the fabric structure. Subsequently, much research has been conducted on how specific construction parameters of the textile substrate itself affect the adhesion of the 3D printed polymer.

The following influencing factors were analysed on woven fabrics in relation to the adhesion strength of 3D printed polymer to the textile substrate: areal density [13], warp and weft density [13, 43, 44], yarn count [13], fabric thickness [9, 13, 45], weave patterns, e.g. plain weave, twill, broken twill, satin and hopsack [43, 44, 46, 47].

Yarn count

Yarn count is a numerical expression that defines yarn fineness. The count is a number indicating the mass per unit length in the direct system (e.g. Tex system) or the length per unit mass of yarn in the indirect system (e.g. metric count system – Nm). Yarn count can be tested using the ASTM D1059-01 or ISO 7211-5 standard. Few studies have been conducted examining only yarn count for its effects on adhesion. Mpofu et al. [13] concluded in their research that the adhesion force increases with increasing yarn count or yarn diameter. Silvestre et al. [10] also led a study in which the conductive material (PLA graphene) was printed on various woven textile substrates. It was found that the adhesion of the printed polymer to the textile substrate was greater at higher thread count. This could indicate that increasing the warp and weft thread count increases the yarn diameter and consequently the surface area to which the polymer adheres on the fabric.

Warp and weft density

Warp and weft density refers to the number of threads per unit length in warp and weft direction. The testing of warp and weft density (ends/cm, wefts/cm) is performed in accordance with the ISO 7211-2 standard. When considering the influence of warp and weft density on adhesion, it was generally found that higher warp and weft density results in a lower adhesion force [13, 47, 49]. In one of the research projects [44], weft densities (weft/cm) were predefined in the weaving process, which enabled a precise and systematic observation of the adhesion force. The findings were the same as at other studies, i.e. the highest adhesion force was found at the lowest weft density and the lowest adhesion was found at the highest weft density.

The observed phenomenon can be attributed to the relationship between warp and weft density and fabric cover factor. As the warp and weft density increased, the fabric cover factor decreased. This reduction in the fabric cover factor led to a decrease in fabric pores, limiting the diffusion of the polymer into the fabric. Consequently, the reduced diffusion resulted in lower adhesion force [13]. This can be explained by the fact that as the density of weft yarns increases, the polymer can hardly enclose individual yarns. As a result, the polymer has less surface area available to adhere to the fabric, which reduces the adhesion force [44].

Fabric thickness

Multiple studies have consistently demonstrated a direct association between fabric thickness and adhesion force, indicating that an increase in fabric thickness corresponds to a subsequent increase in adhesion force. These findings emphasise a positive relationship between these two variables, suggesting that thicker fabrics generally exhibit higher adhesion forces [13, 44, 45, 48, 50]. These good adhesion results may be due to the bonds of the printed polymer with the fibres on the top of the textile as well as inside the textile structure, which should provide enough open areas for the molten polymer to penetrate inside [17, 18, 45]. However, in a study performed by Störmer et al. [9], the results of the adhesion test regarding the fabric thickness unexpectedly showed the highest adhesion force for a thin fabric.

Fabric material, type of yarn

The studies of adhesion properties were conducted on textile substrates with different raw material compositions. Most frequently, investigations were implemented on cotton and polyester (PES), other materials were tested as well. In general, it was found that better adhesion can be achieved if the textile surface is roughened or hairy as shown for the polyester (PES), cotton (CO) and wool (WO) sample [22]. In some cases, it has been established that certain combinations of materials do not produce high adhesion force, e.g. PLA polymers on polyamide (PA) fabric, since the two polymers are not compatible [47].

In later research, Demir at al. [51] compared jute, flax and cotton fabrics regarding adhesion between 3D printed PLA and textile substrate. The aim of the research was to investigate the influence of fabric

treatments on adhesion, untreated samples also being tested and compared. Untreated flax fabrics woven in plain weave were found to adhere better than cotton twill fabrics, which have no notable pores on the fabric surface. On the other hand, lower adhesion strength was measured on more porous jute fabrics than on flax fabrics.

Weave pattern

Several studies have been conducted on the effects of weave pattern on the adhesion of 3D printed polymer to a textile substrate. Mainly plain weave, twill and satin were tested, next to broken twill weave, hopsack and satin. In most cases, adhesion was found to be higher with twill compared to plain weave [43]. In a study by Malengier et al. [36], it was also established that a plain weave fabric reaches the least adhesion compared to twill and satin. In that study, they showed that the twill fabric was the best textile substrate for the 3D printing of PLA filament, regarding the adhesion. In a study by Silvestre et al. [10], better adhesion was achieved in the satin fabric than in twill and plain weave.

Comparison of simple and double fabrics

A recent study by Čuk et al. investigated the adhesion of 3D printed polymers to textile substrates, specifically comparing double-weave structures with simple fabrics. Simple weave fabrics consist of a single set of warp and weft threads interwoven in a weave pattern, creating a single-layer fabric, while double weave fabrics consist of two sets of warp and weft threads, creating a double layer or double fabric [11]. Double fabrics are namely an extremely suitable textile substrate for 3D printing applications, as the materials for the top and bottom layers of the fabric can be different, thus creating different fabric functionalities [52]. In addition, a special thread can be inserted into the space between the layers to achieve specific characteristics of a fabric, e.g. temperature sensing [53]. The results of the research [11] showed remarkable differences between the two types of fabrics and emphasised the significant influence of the z-distance parameter on the adhesion force. This study highlights the complicated relationship between fabric structure, z-distance and adhesion strength in 3D printing applications on textiles. The study was performed on samples printed with two different z-distance settings. One part of the samples was printed with a constant z-distance (z1), which means that the height of the print head remained the same regardless of the thickness of the fabric, and was 0.2 mm. In this way, the nozzle was always positioned relatively deep into the fabric when printing the first layer. The other part was printed with a constant z-distance offset (z2) from the fabric surface, which means that the height of the nozzle varied and was adjusted to the fabric thickness. For each fabric sample, the nozzle was 0.1 mm below the surface when the first layer was printed. At constant z-distance, all samples showed higher adhesion strength than the samples printed at constant z-distance offset. When printing with a constant z-distance (z1), simple fabrics had weaker adhesion compared to thicker, double-layer fabrics, as print nozzle penetrates deeper into thicker fabric. Figure 2 above shows the cross-section of the (a) printed simple fabric and the (b) printed double fabric cut in warp direction. Both fabrics were printed with a z-distance of 0.25 mm. The images were taken with a scanning electron microscope. Figure 3 above shows the backs of the printed simple and double fabric samples. Both samples were printed with a z-distance of 0.25 mm. Numerous deposits of molten polymer can be seen on both samples, which penetrated through the pores of the fabric.

The printer nozzle penetrates deeper into a double weave fabric and the polymer penetrates through the pores of the upper layer into the lower layer, where it adheres to the yarns or fibres. In addition, double weaves have higher thread density; however, the threads are arranged in two layers and grouped according to the weave. As a result, the structure of the fabric is less compact, the specific surface area is larger, and thus, the adhesion is better.

Conclusion about textile properties influencing adhesive strength

The adhesion of materials to a textile in the context of 3D printing has been predominantly explained using the mechanical adhesion theory. This theory suggests that the adhesion strength is improved due to the roughness and porosity of textile surfaces. However, a comprehensive understanding of the adhesion properties of thermoplastic polymer layers deposited on textiles through 3D printing requires the integration of both diffusion and mechanical theories. By combining these two theories, a more complete understanding of adhesion mechanisms can be achieved, considering the interplay between surface roughness, porosity and molecular diffusion processes [43].

A review of research results revealed that the fabric construction parameter thickness appears to have a huge impact on the adhesion strength of the 3D printed polymer to the woven fabric.

Fabric thickness is determined by various factors, including yarn diameter, the degree of compression between interlaced threads and the presence of float sections within the weave repeat [54].

In other words, fabrics with different weaves, yarn count, thread density and raw material have different thickness; therefore, different adhesion forces can be expected. Consequently, the z-distance parameter must be optimised for each fabric regarding its thickness to print inside the substrate and to enhance the adhesion strength. It is important to note that some fabrics are more compressible that others [55]. Fabric thickness should hence be precisely measured before the printing process. In the research, fabric thickness was measured using textile thickness testers and the measurements were performed according to the standards [9, 11, 40]. Furthermore, a micrometre calliper was used to measure the thickness of a fabric with higher pressure, which can be compared to the nozzle pressure during 3D printing [9, 22].

Similarly, fabric roughness is influenced by the particular weave structure, the number of individual pores formed within the weave, as well as the densities of threads and any irregularities in the yarn [54]. Moreover, in the literature, fabric roughness was determined as a factor that positively correlates with the adhesion strength [13, 43]. The mean pore size also has a substantial influence on adhesion as found in the research by Eutionnat-Diffo et al. [43]. A higher mean flow pore size of the textile material could substantially enhance the adhesion strength.

Fabric parameters exert a significant influence on the maximum achievable adhesion forces between 3D printed polymers and textiles. However, the above presented parameters may not be adequate for accurately predicting adhesion forces for a particular fabric. In some cases, only a general trend can be discerned, highlighting the complexity and multifactorial nature of the adhesion process [17].

3.5 Improvement of adhesion with pre-treatment and after-treatment

The adhesion of 3D printing to a textile substrate can be increased by various pre- and after-treatment processes, as studies have shown. Polymer coatings on textiles can lead to a significant increase in adhesion [17]; various chemical pre-treatments can be successfully applied as well [51]. Kozior et al. [40] found that a glue stick in particular increased adhesion between cotton and PLA. Furthermore, other textile surface treatments to adjust the textile surface properties, e.g. hairiness or hydrophobicity, can improve adhesion. For example, washing the textile substrate [35] can result in a more hydrophilic surface, which confirms the statement of Korger et al. [45] that a hydrophilic surface of the textile substrate means a higher adhesion strength. A thermal treatment was researched as a possible after-treatment and in most cases confirmed to have a positive effect on adhesion strength, e.g. the research by Görmer et al., where ironing was performed [56].

4 Conclusion

Compared to knitted textile substrates, which are stretchable in several directions, and thus very flexible and more elastic than woven fabrics, the latter offer greater dimensional stability as well as the possibility of using stiffer yarns, which is advantageous in achieving certain properties in the production of protective clothing, technical textiles, decorative and apparel textiles etc., making them an ideal textile substrate for many different applications of 3D printing.

The literature review confirmed the fact that the influence of fabric construction on the adhesion of 3D printed polymers to a fabric is significant and must be constantly monitored and evaluated in the context of other parameters of 3D printing on textiles, e.g. the printing material used and the printing process itself. It was also found that the influence of the 3D printing process has been studied more, as changes can be made in a very controlled and systematic way, while this is usually difficult with fabric construction parameters. Therefore, the ability to produce fabrics for research, which was found only in few research papers, is of great value as the fabric construction parameters can be more precisely controlled in this way.

To achieve higher adhesion, it is necessary to design the textile substrate to have sufficient open area on which the molten polymer can adhere. In general, the improvement of adhesion is possible by increasing the roughness and porosity of a textile material. According to the research reviewed, such conditions can be achieved by increasing fabric thickness, double weave, lower thread density etc. Among other parameters which have a strong influence on adhesion and are not related to the construction of the fabric, the distance between the print head (nozzle) and the fabric is certainly the most important. Of course, more and more researchers are focusing on pre- and post-treatment, which also has a major impact on the adhesion of 3D printing to textiles; however, this was not the main focus of the review presented in this article.

In general, the adhesion force in 3D printing on textiles is primarily influenced by the properties of the textile substrate rather than the properties of the printing material; hence, the choice of a textile plays a crucial role in determining the adhesion force between the printed object and the fabric surface.

References

1. GIBSON, Ian, ROSEN, David, STUCKER, Brent. Additive manufacturing technologies: 3D printing, rapid prototyping, and direct digital manufacturing. New York : Springer, 2015, 1–18, doi: 10.1007/978-1-4939-2113-3_1.
2. AHRENDT, Dustin, ROMERO KARAM, Arturo. Development of a computer-aided engineering–supported process for the manufacturing of customized orthopaedic devices by three-dimensional printing onto textile surfaces. *Journal of Engineered Fibers and Fabrics,* 2020, **15**, 1–11, doi: 10.1177/1558925020917627.
3. PASRICHA, Anupama, GREENINGER, Rachel. Exploration of 3D printing to create zero-waste sustainable fashion notions and jewelry. *Fashion and Textiles*, 2018, **5**, 1–18, doi: 10.1186/s40691-018-0152-2.
4. SITOTAW Dereje, Berihun, AHRENDT, Dustin, KYOSEV, Yordan, KABISH, Abera, Kechi. Additive manufacturing and textiles - state of the art. *Applied Sciences*, 2020, **10**(15), 1–21, doi: 10.3390/app10155033.
5. GROTHE, Timo, BROCKHAGEN, Bennet, STORCK, Jan Lukas. Three-dimensional printing resin on different textile substrates using stereolithography: a proof of concept. *Journal of Engineered Fibers and Fabrics,* 2020, **15**, 1–7, doi: 10.1177/1558925020933440.
6. BARNES, Juliana. 3D printing: definition and development [online]. AATCC [accessed 3 July 2023]. Available on World Wide Web: <https://www.aatcc.org/aatccnews_06a>.
7. DAVE, Harshit, K. PATEL, Sandip,T. Introduction to fused deposition modeling based 3D printing process. In *Fused deposition modeling*

based 3D printing. Edited by Harshit K. Dave and J. Paulo Davim. Cham : Springer, 2021, 1–21.

8. TÜMER, Eda Hazal, ERBIL, Husnu Yildirim. Extrusion-based 3D printing applications of PLA composites: a review. *Coatings,* 2021, **11**(4), 1–42, doi: 10.3390/coatings11040390.
9. STÖRMER, Jannik, GÖRMER, Daniel, EHRMANN, Andrea. Influence of washing on the adhesion between 3D-printed TPU and woven fabrics. *Communications in Development and Assembling of Textile Products,* 2021, **2**(1), 34–39, doi: 10.25367/cdatp.2021.2.p34-39.
10. SILVESTRE, Rocio, GARCIA-BREIJO, Eduardo, FERRI, Josué, MONTAVA, Ignacio, BOU-BELDA, Eva. The influence of the structure of cotton fabrics on the adhesion of conductive polymer printed with 3D printing technology. *Polymers,* 2023, **15**(3), 1–14, doi: 10.3390/polym15030668.
11. ČUK, Marjeta, BIZJAK, Matejka, KOČEVAR, Tanja Nuša. Influence of simple and double-weave structures on the adhesive properties of 3D printed fabrics. *Polymers*, 2022, **14**(4), 1–18, doi: 10.3390/polym14040755.
12. MPOFU, Nonsikelelo Sheron, MWASIAGI, Josphat Igadwa, NKIWANE, Londiwe Cynthia, GITHINJI, David Njuguna. The use of statistical techniques to study the machine parameters affecting the properties of 3D printed cotton/polylactic acid fabrics. *Journal of Engineered Fibers and Fabrics,* 2020, **15**, 1–10, doi: 10.1177/1558925020928531.
13. MPOFU, Nonsikelelo Sheron, MWASIAGI, Josphat Igadwa, NKIWANE, Londiwe Cynthia, NJUGUNA, David. Use of regression to study the effect of fabric parameters on the adhesion of 3D printed PLA polymer onto woven fabrics. *Fashion and Textiles*, 2019, **6**, 1–12, doi: 10.1186/s40691-019-0180-6.
14. MUCK, Deja, KRIŽANOVSKIJ, Igor. *3D-Tisk*. Ljubljana: Pasadena, 2015.
15. SIN, Lee Tin, TUEEN, Bee Soo. Injection molding and three-dimensional printing of poly(lactic acid). In *Polylactic Acid.* Edited by Lee Tin Sin and Bee Soo Tueen. 2nd ed. Elsevier, 2019, 325–345.
16. AUMNATE, Chuanchom, PONGWISUTHIRUCHTE, Aphiwat, PATTANANUWAT, Prasit, POTIYARAJ, Pranut. Fabrication of ABS/graphene oxide composite filament for Fused Filament Fabrication (FFF) 3D printing. *Advances in Materials Science and Engineering*, 2018, **2018**, 1–10, doi: 10.1155/2018/2830437.
17. GRIMMELSMANN, Niels, KREUZIGER, Mirja, KORGER, Michael, MEISSNER, Hubert, EHRMANN, Andrea. Adhesion of 3D printed material on textile substrates. *Rapid Prototyping Journal,* 2018, **24**(1), 166–170, doi: 10.1108/RPJ-05-2016-0086.
18. MARTENS, Yasmin, EHRMANN, Andrea. Composites of 3D-Printed polymers and textile fabrics. *IOP Conference Series: Materials Science and Engineering*, 2017, **225**(1), 1–6, doi: 10.1088/1757-899X/225/1/012292.
19. PEI, Eujin, SHEN, Jinsong, WATLING, Jennifer. Direct 3D printing of polymers onto textiles: experimental studies and applications. *Rapid Prototyping Journal,* 2015, **21**(5), 556–571, doi: 10.1108/RPJ-09-2014-0126.
20. FENOLLOSA-ARTES, Felip, JORAND, Leo, TEJO-OTERO, Aitor, LUSTIG-GAINZA, Pamela, ROMERO-SABAT, Gulliem, MEDEL, Sandra, UCEDA, Roger. Soft 3D printing of thermoplastic polyurethane: preliminary study. *Proceedings of the Institution of Mechanical Engineers, Part B: Journal of Engineering Manufacture,* 2023, **237**(6-7), 1128–1135. doi: 10.1177/09544054221100077.
21. GONCU-BERK, Gozde, KARACAN, Burak, BALKIS, Ilke. Embedding 3D printed filaments with knitted textiles: investigation of bonding parameters. *Clothing and Textiles Research Journal,* 2022, **40**(3), 171–186. doi: 10.1177/0887302X20982927.
22. KORGER, Michael, GLOGOWSKY, Alexandra, SANDULOFF, Silke, STEINEM, Christine, HUYSMAN, Sofie, HORN, Bettina, ERNST, Michael, RABE, Maike. Testing thermoplastic

elastomers selected as flexible three-dimensional printing materials for functional garment and technical textile applications. *Journal of Engineered Fibers and Fabrics*, 2020, **15**, 1–10, doi: 10.1177/1558925020924599.

23. ERCEGOVIĆ RAŽIČ, Sanja, LUDAŠ, Anja, KAURIN, Tea, ZONJIĆ, Tin. Applicability of polymers printed on textiles with a 3D printer for possible use in car interior. *IOP Conference Series: Earth and Environmental Science,* 2023, **1128,** 1–8, doi: 10.1088/1755-1315/1128/1/012027.
24. STA. AGUEDA, Joseph Rey H., CHEN, Qiyi, MAALIHAN, Reymark, D., JINGBO, Ren, da SILVA, Italo G. M., DUGOS, Nathaniel P., CALDONA, Eugene B., ADVINCULA, Rigoberto C. 3D printing of biomedically relevant polymer materials and biocompatibility. *MRS Communications,* 2021, **11**, 197–212, doi: 10.1557/s43579-021-00038-8.
25. GÖKSAL, Erdem, EHRMAN, Andrea, GROTHE, Timo. Adhesion of new thermoplastic materials. *Tekstilec*, 2023, **66**(1), 57–63, doi: 10.14502/tekstilec.66.2023012.
26. SPAHIU, Tatjana, ZLATEV, Zlatin, IBRAHIMAJ, Elita, ILIEVA, Julieta, SHEHI, Ermira. Drape of composite structures made of textile and 3D printed geometries. *Machines,* 2022, **10**(7), 1–17, doi: 10.3390/machines10070587.
27. BURN, Kirstie, VETTESE, Sam, SHACKLETON, John. An exploration of the sustainable and aesthetic possibilities of 3D printing onto textiles as an alternative to traditional surface decoration. In *Circular Transitions Proceedings.* Edited by Rebecca Earley and Kate Goldsworthy. London : University of Arts, 2017, 141–154.
28. KOČEVAR, Tanja Nuša, DRUSANY, Manca. Designing a pattern with 3D printing on textiles. In *Book of proceedings: XVth International Izmir Textile and Apparel Symposium, Izmir, Turkey, 26–27 October 2021,* 233–239.
29. 3D Fashion by Stratasys: 3D fashion projects [online]. Stratasys [accessed 30. 6. 2023]. Available on World Wide Web: <https://3dprintedart.stratasys.com/portfolio-1>.
30. AGKATHIDIS, Asterios, BERDOS, Yorgos, BROWN, André. Active membranes: 3D printing of elastic fibre patterns on prestretched textiles. *International Journal of Architectural Computing,* 2019, **17**(1), 74–87, doi: 10.1177/1478077118800890.
31. RIVERA, Michael L, MOUKPERIAN, Melissa, ASHBROOK, Daniel, MANKOFF, Jennifer, HUDSON, Scott. E. Stretching the bounds of 3D printing with embedded textiles. In *CHI ,17: Proceedings of the 2017 CHI Conference on Human Factors in Computing Systems*. New York Association for Computing Machinery, 2017, 497–508, doi: 10.1145/3025453.3025460 0.
32. XIAO, Ya-Qian, KAN, Chi-Wai. Review on development and application of 3D-printing technology in textile and fashion design. *Coatings*, 2022, **12**(2), 1–13, doi: 10.3390/coatings12020267.
33. BISWAS, Manik Chandra, CHAKRABORTY, Samit, BHATTACHARJEE, Abhishek, MOHAMMED, Zaheeruddin. 4D printing of shape memory materials for textiles: mechanism, mathematical modeling, and challenges. *Advanced Functional Materials*, 2021, **31**(19), 1–25, doi: 10.1002/adfm.202100257.
34. AWAJA, Firas, GILBERT, Michael, KELLY, Georgina, FOX, Bronwyn Louise, PIGRAM, Paul. Adhesion of polymers. *Progress in Polymer Science*, 2009, **34**(9), 948–968, doi: 10.1016/j.progpolymsci.2009.04.007.
35. GORLACHOVA, Maryna, MAHLTIG, Boris. 3D-printing on textiles – an investigation on adhesion properties of the produced composite materials. *Journal of Polymer Research*, 2021, **28**, 1–10, doi: 10.1007/s10965-021-02567-1.
36. MALENGIER, Benny, HERTLEER, Carla, CARDON, L., VAN LANGENHOVE, L. 3d printing on textiles: testing of adhesion. *Journal of Fashion Technology & Textile Engineering,* 2018, S4:013, doi: 10.4172/2329-9568.S4-013.

37. UNGER, Lea, SCHEIDELER, Marvin, MEYER, Pia, GÖRZEN, Andreas, WORTMAN, Martin, DREYER, Axel, EHRMAN, Andrea. Increasing adhesion of 3D printing on textile fabrics by polymer coating. *Tekstilec,* 2018, **61**(4), 265–271, doi: 10.14502/Tekstilec2018.61.265-271.
38. SPAHIU, Tatjana, AL-ARABIYAT, M., MARTENS, Yasmin, EHRMAN, Andrea, PIPERI, Erald, SHEHI, E. Adhesion of 3D printing polymers on textile fabrics for garment production. *IOP Conference Series: Materials Science and Engineering,* 2019, **459,** 1–6, doi: 10.1088/1757-899X/459/1/012065.
39. SABANTINA, Lilia, KINZEL, Franziska, EHRMANN, Andrea, FINSTERBUSCH, Karin. Combining 3D printed forms with textile structures - mechanical and geometrical properties of multi-material systems. *IOP Conference Series: Materials Science and Engineering,* 2015, **87**, 1–6, doi: 10.1088/1757-899X/87/1/012005.
40. KOZIOR, Tomasz, DÖPKE, Christoph, GRIMMELSMANN, Nils, JUHÁSZ JUNGER, Irén, EHRMANN, Andrea. Influence of fabric pretreatment on adhesion of three-dimensional printed material on textile substrates. *Advances in Mechanical Engineering,* 2018, **10**(8), 1–8, doi: 10.1177/1687814018792316.
41. SPAHIU, Tatjana, GRIMMELSMANN, Nils, EHRMANN, Andrea, PIPERI, Erald, SHEHI, E. Effect of 3D printing on textile fabric. In *Proceedings. 1st International Conference Engineering and Entrepreneurship (ICEE), Tirana / Albania*, 2017, 1–7.
42. BEGUM, Most. Setara, MILAŠIUS, Rimvydas. Factors of weave estimation and the effect of weave structure on fabric properties: a review. *Fibers*, 2022, **10**(9), 1–22, doi: 10.3390/fib10090074.
43. EUTIONNAT-DIFFO, Prisca Aude, CHEN, Yan, GUAN, Jinpin, CAYLA, Aurélie, CAMPAGNE, Christine, ZENG, Xianyi, NIERSTRASZ, Vincent. Optimization of adhesion of poly lactic acid 3D printed onto polyethylene terephthalate woven fabrics through modelling using textile properties. *Rapid Prototyp Journal*, 2019, **26**(2), 390–401, doi: 10.1108/rpj-05-2019-0138.
44. ČUK, Marjeta, BIZJAK, Matejka, MUCK, Deja, KOČEVAR, Tanja Nuša. 3D printing and functionalization of textiles. In *10th International Symposium on Graphic Engineering and Design,* 2020, 499–506, doi: 10.24867/GRID-2020-p56.
45. KORGER, M., BERGSCHNEIDER, J., LUTZ, M., MAHLTIG, B., FINSTERBUSCH, K., RABE, M. Possible applications of 3D printing technology on textile substrates. *IOP Conference Series: Materials Science and Engineering,* 2016, **141**, 1–6, doi: 10.1088/1757-899X/141/1/012011.
46. EUTIONNAT-DIFFO, Prisca Aude, CHEN, Yan, GUAN, Jinpin, CAYLA, Aurelie, CAMPAGNE, Christine, ZENG, Xianyi, NIERSTRASZ, Vincent. Stress, strain and deformation of poly-lactic acid filament deposited onto polyethylene terephthalate woven fabric through 3D printing process. *Scientific Reports,* 2019, **9**, 1–18, doi: 10.1038/s41598-019-50832-7.
47. SANATGAR, Razieh Hashemi, CAMPAIGNE, Christine, NIERSTRASZ, Vincent. Investigation of the adhesion properties of direct 3D printing of polymers and nanocomposites on textiles: Effect of FDM printing process parameters. *Applied Surface Science,* 2017, **403**, 551–563, doi: 10.1016/j.apsusc.2017.01.112.
48. LEKECKAS, Kestutis, STIRBE, Julija, ANCUTIENE, Kristina, VALUSYTE, Ruta. Testing of 3D printing on textile fabrics for garments application within circular design. *International Journal of Clothing Science and Technology*, 2023, **35**(4), 627–647, doi: 10.1108/IJCST-06-2022-0080.
49. ČUK, Marjeta, GRAMC, Kristina, MUCK, Deja, BIZJAK, Matejka. Influence of fabric structure on the adhesion and functional properties of 3D printed polymers on the woven fabric. *Materials Science Forum,* 2022, **1063**, 25–33, doi: 10.4028/p-tg3e20.
50. MEYER, Pia, DÖPKE, Christoph, EHRMANN, Andrea. Improving adhesion of three-dimensional

printed objects on textile fabrics by polymer coating. *Journal of Engineered Fibers and Fabrics,* 2019, **14**, 1–7, doi: 10.1177/1558925019895257.

51. DEMIR, Murat, SEKI, Yasemin. Interfacial adhesion strength between FDM-printed PLA parts and surface-treated cellulosic-woven fabrics. *Rapid Prototyping Journal,* 2023, **29**(6), 1166–1174, doi: 10.1108/RPJ-10-2022-0369.
52. GE, Lan, TAN, Jeanne. Development of three-dimensional effects and stretch for polymeric optical fiber (POF) textiles with double weave structure containing spandex. *The Journal of The Textile Institute,* 2021, **112**(3), 398–405, doi: 10.1080/00405000.2020.1761679.
53. GU, Yiming, LI, Yanmei, SHAW, Andy. Development and performance of flexible temperature-sensing fabric. *The Journal of The Textile Institute,* 2022, **113**(12), 2770–2777, doi: 10.1080/00405000.2021.2013398.
54. KOLCAVOVA SIRKOVA, Brigita. Description of fabric thickness and roughness on the basis of fabric structure parameter. *Autex Research Journal,* 2012, **12**(2), 40–43, https://www.degruyter.com/document/doi/10.2478/v10304-012-0008-6/html.
55. POPESCU, Diana, CĂTĂLIN Gheorghe Amza. 3D Printing onto textiles: a systematic analysis of the adhesion studies. *3d Printing and Additive Manufacturing,* 2022, Ahead of Print, doi: 10.1089/3dp.2022.0100.
56. GÖRMER, Daniel, STÖRMER, Jannik, EHRMANN, Andrea. The influence of thermal after-treatment on the adhesion of 3D prints on textile fabrics. *Communications in development and assembling of textile products,* 2020, **1**(2), 104–110, doi: 10.25367/cdatp.2020.1.p 104–110.

Dominika Glažar, Barbara Simončič
University of Ljubljana, Faculty of Natural Sciences and Engineering, Department of Textiles, Graphic Arts and Design, Ljubljana, Snežniška 5, 1000 Ljubljana, Slovenia

TiO_2 and ZnO as Advanced Photocatalysts for Effective Dye Degradation in Textile Wastewater

TiO_2 in ZnO kot napredna fotokatalizatorja za učinkovito razgradnjo barvil v tekstilnih odpadnih vodah

***Scientific Review**/Pregledni znanstveni članek*

Corresponding author/*Korespondenčna avtorica:*
prof. dr. Barbara Simončič
E-mail: barbara.simoncic@ntf.uni-lj.si
ORCID: 0000-0002-6071-8829

Abstract

Textile wastewater, which consist of a complex mixture of synthetic dyes and other organic and inorganic compounds derived from various wet chemical textile processes, can have a harmful effect on the environment; therefore, it must be properly treated before being discharged into municipal wastewater treatment plants and natural water bodies. In this scientific review, the main physical, chemical and biological processes for the removal of dyes from textile wastewater are presented, focusing on photocatalysis, which is a promising advanced oxidation process. The mechanism of photocatalysis is described and the methods used to determine the efficiency of photocatalytic degradation of dyes are presented. Recent studies involving single photocatalytic treatments of real textile wastewaters in the presence of TiO_2 and ZnO as catalysts are presented. The advantages of combined processes of photocatalysis in conjunction with other chemical, physical and biological treatments to increase the efficiency of wastewater treatment are discussed. Accordingly, photocatalysis combined with H_2O_2, photocatalytic ozonation, a hybrid system of photocatalysis and membrane filtration, and coupled photocatalytic-biological processes are described.

Keywords: titanium dioxide, zinc oxide, photocatalysis, dye degradation, textile wastewater

Izvleček

Tekstilne odpadne vode, ki vključujejo kompleksno mešanico sintetičnih barvil in drugih organskih in anorganskih spojin, ki izhajajo iz različnih mokrih kemijskih tekstilnih postopkov, lahko škodljivo vplivajo na okolje, zato jih je potrebno pred izpustom v komunalne čistilne naprave in naravno vodno okolje ustrezno očistiti. V preglednem članku so predstavljeni najpomembnejši fizikalni, kemijski in biološki postopki za odstranitev barvil iz tekstilnih odpadnih vod s poudarkom na fotokatalizi, ki je obetavni napredni oksidacijski proces. Opisan je mehanizem fotokatalize in predstavljene so metode za določitev učinkovitosti fotokatalitske razgradnje barvil. Izpostavljene so najsodobnejše raziskave, ki vključujejo samostojno fotokatalitsko obdelavo realnih tekstilnih odpadnih voda v prisotnosti TiO_2 in ZnO kot fotokatalizatorjev. Predstavljene so prednosti kombiniranih postopkov, ki vključujejo fotokatalizo v povezavi z drugimi kemijskimi, fizikalnimi in biološkimi procesi. Med njimi so opisani fotokataliza v kombinaciji s H_2O_2, fotokatalitska ozonacija, hibridni sistem fotokatalize in membranske filtracije ter združeni fotokatalitski-biološki procesi.

Ključne besede: titanov dioksid, cinkov oksid, fotokataliza, razgradnja barvila, tekstilna odpadna voda

1 Introduction

The textile industry is considered one of the largest water pollutants and is responsible for about 20% of global clean water pollution from various wet chemical production processes [1–3]. Wastewaters from pretreatment, dyeing, printing and finishing processes are highly polluted by complex mixtures of synthetic dyes and pigments, finishing agents, auxiliaries, heavy metals, surfactants and other chemicals, which can result in harmful effluents in the environment [4–6]. Among the effluents, synthetic dyes are classified as one of the most hazardous pollutants as they are potentially toxic, non-biodegradable and persistent [7–9]. Due to light absorption, the presence of dyes in wastewater reduces sunlight penetration, which negatively affects flora and fauna [4, 8]. Accordingly, the removal/degradation of dyes from textile wastewater is a challenging research topic for which various physical, chemical and biological processes, and their combinations have been developed and introduced (Figure 1) [4–7, 9–12].

Physical methods for removing dyes from textile effluents primarily include adsorption and membrane filtration, in which dye removal is advantageously accomplished by forces such as electrical attraction, gravity, and Van der Waals forces or physical barriers [6]. In the adsorption method, numerous suitable adsorbents are used, the best known of which is activated carbon. In addition, polymer resins and low-cost agricultural and industrial by-products such as peat, chitin, clays and fly ash are used. Membrane filtration includes microfiltration, ultrafiltration, nanofiltration and reverse osmosis. Since nanofiltration is more effective than microfiltration and ultrafiltration, reverse osmosis is the most effective as it retains almost all substances from water [6].

Chemical methods include coagulation/flocculation, electrochemical processes, classical oxidation and advanced oxidation processes (AOP) [4, 6, 13]. Coagulation/flocculation is commonly used to destabilise particles with various coagulants such as inorganic coagulants, inorganic-organic double coagulants and synthetic polymer flocculants. A complete decolourisation is difficult to achieve with this method. Inorganic coagulants such as iron and aluminium salts are widely used in the treatment of textile wastewater; however, they have negative effects on the environment and human health [6, 14]. There are various electrochemical processes such as electrokinetic coagulation, electroflotation, electrodecantation and electrooxidation [15]. Electrons are used

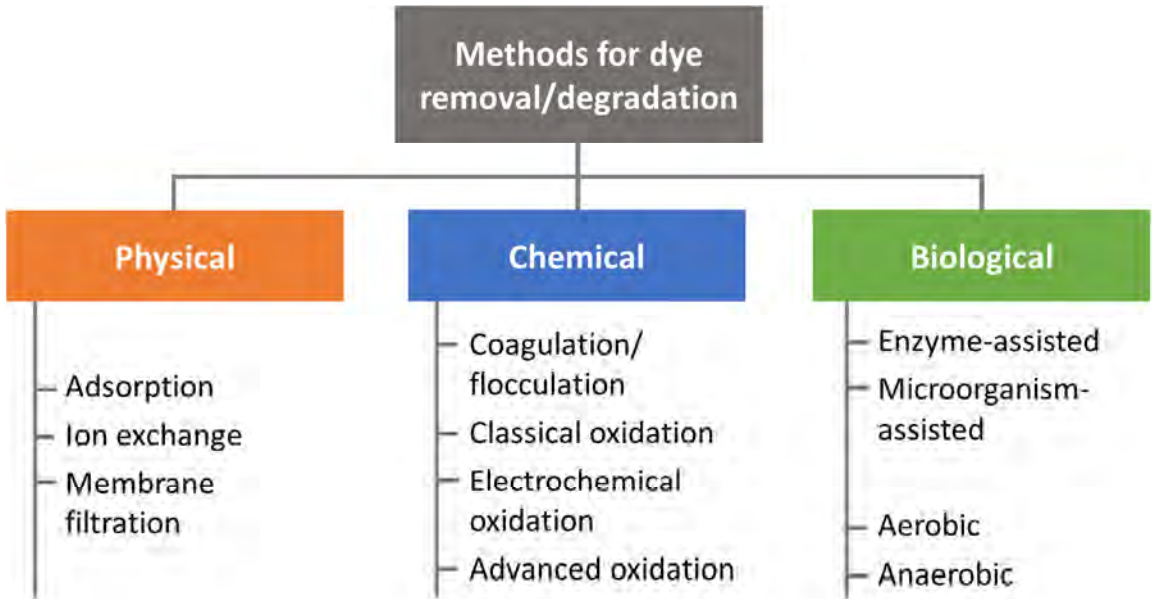

Figure 1: Methods for removal/degradation of dyes from textile wastewater

as "primary reagents," which are referred to as "clean reagents". In most cases, high concentrations of supporting electrolytes, especially NaCl, are required to achieve acceptable results; however, this leads to the generation of large amounts of environmentally harmful products [6, 15]. In the classical oxidation method, ozone (O_3), hydrogen peroxide (H_2O_2), potassium permanganate ($KMnO_4$), chlorine dioxide (ClO_2), chlorine (Cl_2), sodium hypochlorite (NaOCl) and oxygen (O_2) are used as oxidising agents that change the chemical composition of the compound [13]. In advanced oxidation processes (AOP), reactive oxygen species (ROS) such as hydroxyl radicals (•OH) and superoxide radicals ($•O_2^-$) are usually generated and utilised. These include various methods such as the photocatalytic ozonation, Fenton process, photo-, electro- and sono-Fenton processes, and photocatalysis [2, 6, 13, 16–19]. The best known advanced oxidation process is the Fenton process, which uses a mixture of ferrous iron (typically Fe(II)) and hydrogen peroxide (H_2O_2) to generate •OH in an acidic medium. However, the Fenton process can produce chemical sludges that must be properly disposed of. Compared to the Fenton process, the advantage of the photo-, electro- and sono-Fenton processes, which combine the Fenton reaction with light radiation, electrochemical processes and ultrasound, respectively, is a higher pollutant removal rate with a lower iron dose [19–24]. Photocatalysis is considered a sustainable treatment process for the degradation of dyes from textile wastewater in the presence of photocatalysts. In this process, high efficiency of photocatalytic degradation can be achieved under mild reaction conditions in the presence of oxygen and water from the atmosphere and UV/visible light radiation without the formation of secondary impurities as the dyes are degraded to carbon dioxide and water via intermediates [2, 25].

Biological processes use biomaterials such as industrial enzymes and microorganisms for dye degradation. They can be conducted under aerobic or anaerobic conditions. These processes consist of two main steps, i.e. adsorption of dyes onto biomaterials and their degradation to non-toxic products. While peroxidase and azo reductase are the most effective industrial enzymes, bacteria, fungi, algae and yeasts are used as microorganisms. Due to the high biodegradability of biomaterials and low operating costs, biological processes are considered the most promising treatment methods for textile wastewater from the environmental and economic perspective [4, 6, 11]. Despite many advantages of biological processes, there are still shortcomings, including the non-degradability of biomass-bound dyes and the difficult adsorption of some types of dyes such as azo and reactive dyes [6, 11].

2 Photocatalysis as AOP for synthetic dye degradation

Photocatalysis is a promising AOP that takes place in the presence of a photocatalyst, which is activated by light [16]. Due to its environmental friendliness and high efficiency, this process has attracted much attention in various scientific fields, including environmental remediation, where various organic and inorganic pollutants can be photocatalytically degraded. This also applies to dyes contained in textile wastewater. Various photocatalysts can be used in photocatalysis, including metal semiconductors such as TiO_2 and ZnO nanoparticles, which are very promising due to their excellent morphological, chemical and optical properties [26]. The efficiency of photocatalysis is directly influenced by the design of the photocatalyst, where the surface-to-volume ratio of the particles, their crystallinity, surface modifications and light absorption capacity play an important role.

2.1 Mechanism of semiconductor photocatalysis

The mechanism of semiconductor photocatalysis is shown in Figure 2 and can be explained as follows [27–29]: when a semiconductor absorbs a photon

with the energy equal to or higher than the bandgap energy (E_g) under irradiation with UV or visible light, the electrons in the valence band (VB) are excited into the vacant conduction band (CB), leaving holes in VB. The resulting free electrons and holes can migrate to the surface of the semiconductor, where they participate in the redox reactions. The electrons react with atmospheric oxygen to form $\bullet O_2^-$ in the reduction reaction and the holes react with absorbed water to form •OH in the oxidation reaction. Both reduction and oxidation take place when the edge of the semiconductor's conduction band is more negative and the edge of its valence band is more positive than the standard redox potential of the reactions. The formation of $\bullet O_2^-$ and •OH, which are the main ROS formed at the semiconductor surface, is crucial for the photocatalytic activity of the semiconductor since ROS can subsequently react with organic pollutants in the oxidation reaction and degrade them to carbon dioxide and water via intermediate compounds. At the same time, holes with a high oxidation potential can directly cause the oxidation of pollutants [25, 29–38]. Nevertheless, the recombination of electrons and holes that can occur during their migration to the semiconductor surface is an undesirable process as it reduces the photocatalytic efficiency of the semiconductor [38].

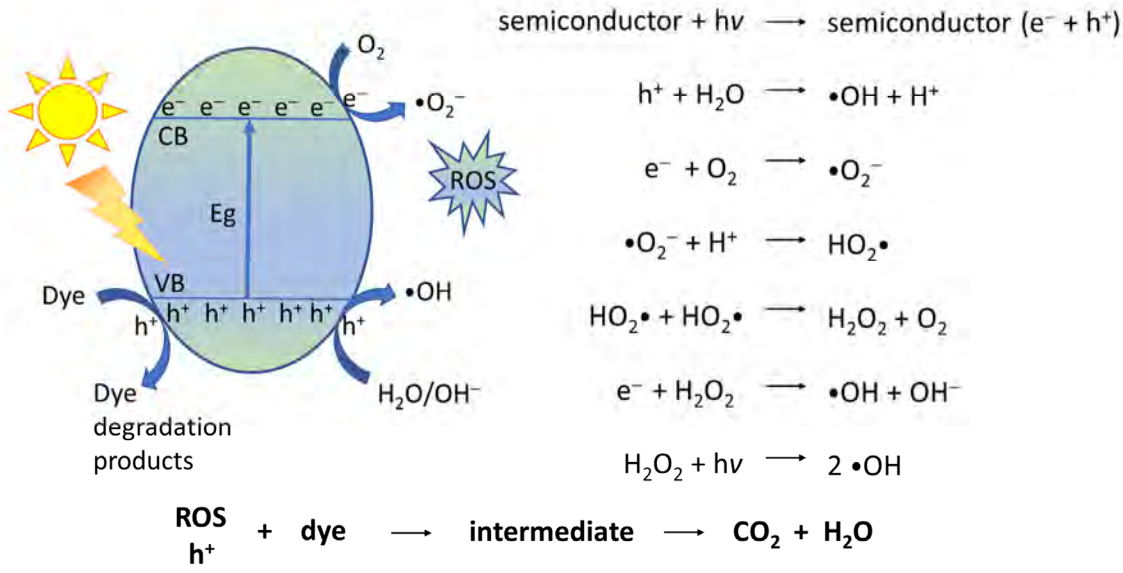

Figure 2: Schematic representation of fundamental mechanism of photocatalytic activity of semiconductors and proposed surface reactions; e^- is electron, h^+ is hole

To improve the separation of electrons and holes and thus the photocatalytic efficiency, semiconductors are doped with different metal and nonmetal ions, loaded with noble metals and coupled with other semiconductors to form heterojunctions [38, 39]. Doping with metal and nonmetal ions is based on the incorporation of host materials into the semiconductor crystal lattice to change the geometric and electronic structure and modulate the charge carrier density in the doped semiconductor. The doped ions introduce additional localised energy levels to trap electrons or holes that immobilise the charge carriers, hence reducing the recombination rate. As the dopant energy levels are formed above the VB or below the CB edge positions in the semiconductor, they decrease the bang gap energy and consequently increase the visible light absorption [40–42]. The loading of semiconductors with noble metals enables the formation of the Schottky-based heterojunction, typical of the semiconductor-metal system, where electrons are easily transferred from the CB of the semiconductor to the metal, which acts

as an electron trapper. By creating a Schottky barrier, the separation of photoinduced charge carriers is maximised and their recombination is prevented [38]. At the same time, visible light excites electrons in the metal, leading to surface plasmon resonance that further enhances photocatalytic activity [43]. The fabrication of semiconductor-semiconductor heterojunctions is one of the most effective strategies to enhance the photocatalytic performance under visible light. The mechanism of photogenerated charge transfer is very complex and depends on the design of the heterojunction. However, the most photocatalytically active heterojunctions are those in which the electrons and holes located in the CB and VB with lower redox power, respectively, are recombined, while ROS are formed in the more energetically favourable CB and VB of semiconductors [44].

2.2 Determination of photocatalytic degradation efficiency

The efficiency of the photocatalytic degradation of dyes can be determined from the degradation rate of the dye [20, 45–57], where the concentration ratio is calculated as follows:

$$\textit{Dye concentration ratio} = \frac{c_t}{c_0} \quad (1)$$

In Equation 1, c_t is the dye concentration at a given time of irradiation and c_0 is the initial dye concentration. The lower the dye concentration ratio at a given time, the higher the dye degradation.

The dye degradation efficiency can also be calculated as the percentage of dye degradation as follows [45–47, 49–51, 57, 58]:

$$\textit{Dye degradation percentage} = \frac{c_0 - c_t}{c_0} \times 100\ (\%) \quad (2)$$

The higher the dye degradation percentage, the higher the degradation efficiency.

The apparent rate constant, K_{app}, of the photocatalytic reaction can also be a measure of the efficiency of the photocatalytic degradation of dyes, where pseudo first-order kinetics is used as follows [46, 48, 50, 51, 58]:

$$ln\ \frac{c_t}{c_0} = -\ K_{app} \cdot t\ (\text{min}^{-1}) \quad (3)$$

In the treatment of real textile industry wastewater, the efficiency of dye removal/degradation is usually discussed based on the measurements of total organic carbon (TOC) and chemical oxygen demand (COD) measurements before and after wastewater treatment. In this case, the dye concentrations c_0 and c_t in Equation 2 are replaced with TOC_0 and TOC_t or COD_0 and COD_t, and the percentage of TOC or COD removal is calculated as a measure of the mineralisation efficiency of textile wastewater [12, 49, 52].

3 Titanium dioxide and zinc oxide as photocatalysts for dye degradation in real textile wastewater

In the field of textiles, titanium dioxide (TiO_2) and zinc oxide (ZnO) have emerged as the most important semiconductor nanomaterials with a variety of applications for the functionalisation of textile substrates as well as for the effective photocatalytic degradation of various dyes in an aqueous solution [3, 31, 32, 59–61]. The main advantages of TiO_2 and ZnO are their thermal, chemical and photochemical stability, non-toxicity, biocompatibility and low price [2, 32, 62–64].

TiO_2 and ZnO are n-type semiconductors with E_g of about 3.2 eV, which limits their photocatalytic activity to irradiation with UV light [65, 66]. Accordingly, surface modification of TiO_2 and ZnO by doping with metal and non-metal ions, loading with noble metals, such as Ag, coupling with other semiconductors, and dye sensitisation is of great importance to lower E_g and thus increase the photocatalytic activity in visible light [40, 67].

In the process of photocatalytic degradation of dyes in an aqueous solution, TiO_2- and ZnO-based nanomaterials were mostly used as photocatalysts in powder form, which were mixed into the dye solution under the study [22, 49, 50, 54, 68–75] and removed after the photocatalytic treatment usually with centrifugation [22, 49, 50, 71, 74, 75] or filtration [68–70, 72, 73]. In addition to powder form, TiO_2 was applied to various substrates such as transparent glass, glazed ceramic tile and stainless steel by doctor blade technique and used in photocatalytic reactors [45]. In another study, TiO_2 nanotubes were prepared on titanium foil by anodization at 48 V for 2 hours followed by iron doping with hydrothermal treatment at 150 °C for 3 hours and annealing at 550 °C for 1.5 hours [52]. In addition, TiO_2 and ZnO were incorporated into glass-ceramic materials with a conventional melting technique of glass batch followed by heat treatment at 450 °C for 10 hours and used in a batch reactor [76]. Ultra long nanofibers, including the $Bi_2Ti_4O_{11}/TiO_2$ heterojunction, were also produced via electrospinning and used as photocatalyst [77].

It should be noted that the efficiency of photocatalytic degradation of dye solutions is influenced not only by the structure of the photocatalyst, but also by the composition and quality of the wastewater [52]. A model dye solution containing a single synthetic dye at an appropriate concentration cannot simulate the real textile wastewater, which consists of a mixture of synthetic dyes of different chemical structure and several other organic and inorganic substances that can strongly influence the pH, TOC and COD of the wastewater; moreover, the parameters are highly variable [78]. In addition, these pollutants can significantly reduce the degradation rate of dyes by hindering the photocatalytic efficiency of semiconductors. Therefore, the study of photocatalysis as an AOP for the treatment of real textile wastewater from the textile industry is of great importance and represents a challenging research topic. The performance of TiO_2 and ZnO as photocatalysts in single AOP or in combination with other chemical, physical and biological processes for dye removal in real textile wastewater is summarised in Table 1.

Table 1: Treatment systems, photocatalysts, pollutants and experimental performance

Treatment system	Photocatalysts	Pollutant	Experimental performance	Ref.
Single photocatalysis	TiO_2, Al, F co-doped TiO_2 nanoparticles	Wastewater of textile factory, Erode, Tamilnadu, India	0.0125 mM catalyst in 10 ml wastewater, irradiation with visible light for 120 minutes	79
	Fe-doped TiO_2 nanotubes on titanium foil	Artificially compounded textile wastewater	2.5 × 5 cm^2 foil as photocatalyst in 5 mg/L Congo red dye in wastewater, irradiation with visible light for 180 minutes	52
	ZnO quantum dots of different size	Wastewater of dyehouse with pH in range of 6.9, Egypt	0.1 g catalyst in 100 ml wastewater, direct sunlight for 6 hours per day (9 am to 3 pm) for 6 months	81
Photocatalysis in combination with another AOP	TiO_2 nanoparticles	Wastewater from different textile industries in Ghaziabad and Gautam Buddha Nagar districts, Uttar Pradesh, India	TiO_2 at various concentrations (1.5 g/L to 20.0 g/L) in 100 mg/L Remazol Red in wastewater without and in presence of H_2O_2 of different concentrations, irradiation with UV light for 60 minutes	20
	Cd-doped ZnO nanoparticles	Wastewater from dyehouse near Erode, Tamilnadu, India	Cd-doped ZnO at different concentrations (0 to 1 g/L) and pH values (3 to 9) in 500 ml of wastewater irradiation with UV light for 240 minutes in presence of O_3 of different dose	18

Continuation of Table 1

Treatment system	Photocatalysts	Pollutant	Experimental performance	Ref.
Photocatalysis in combination with membrane filtration	Polyethylene glycol capped ZnO nanoparticles	Wastewater from textile factory performing dyeing, printing and finishing in Johor, Malaysia	Photocatalysis (0.08–0.30 g/L photocatalyst and pH of 4–13) for 240 minutes under UV irradiation followed by membrane ultrafiltration	83
Photocatalysis in combination with biological treatment	TiO_2, ZnO nanoparticles	Wastewater from dyehouse in Santa Catarina, Brazil	Photocatalysis under UV light irradiation for 120 minutes (150 mg of catalyst in 250 ml of wastewater) followed by aerobic bioprocess for 48 hours	22
	ZnO/polypyrrole nanocomposite	Wastewater from Gama S. A., textile industry in Mar del Plata, Argentina	Biological treatment for 96 hours followed by photocatalysis (0.5–2.0 g/L catalyst in 200 ml of wastewater) for 60 minutes	84

Table 1 shows that there are very few studies dealing with the photocatalysis of real textile wastewater. In these studies, TiO_2 and ZnO are used in a single AOP or in combination with other chemical, physical and biological processes. These processes are very complex and therefore difficult to compare as they differ in terms of chemical structure, morphology and concentration of the photocatalyst, the composition of the industrial wastewater and the experimental performances and conditions. They are presented in the following sections.

3.1 Photocatalysis as single AOP

Photocatalysis in the presence of TiO_2 and ZnO as semiconductor photocatalysts has already shown promise for photodegradation and mineralisation of real textile wastewater. The efficiency of photocatalysis is influenced by several factors, of which the structure of the photocatalyst and the composition of wastewater have been studied in detail.

3.1.1 TiO_2 versus Al and F co-doped TiO_2

Recently, the photocatalytic degradation of real textile wastewater (TEWW) compared to the dye methyl orange (MO) was studied using TiO_2 and aluminium (Al) and fluorine (F) co-doped TiO_2 (TAF10) nanoparticles under visible light irradiation (Figure 3) [79].

The results show that the absorbance of both the MO solution and TEWW decreased with increasing irradiation time, indicating an efficient decolourisation of the dye by both photocatalysts. It is also evident that the degradation efficiency is affected by both the dye solution and the structure of the photocatalyst. A comparison of the spectra in Figure 3a and Figure 3b shows that, as expected, the photocatalytic activity of TAF10 was higher than that of TiO_2 due to the co-doping of Al and F in TiO_2, resulting in an almost complete decolourisation of MO after 120 minutes of irradiation. This result was also confirmed by the calculated apparent rate constant of MO,

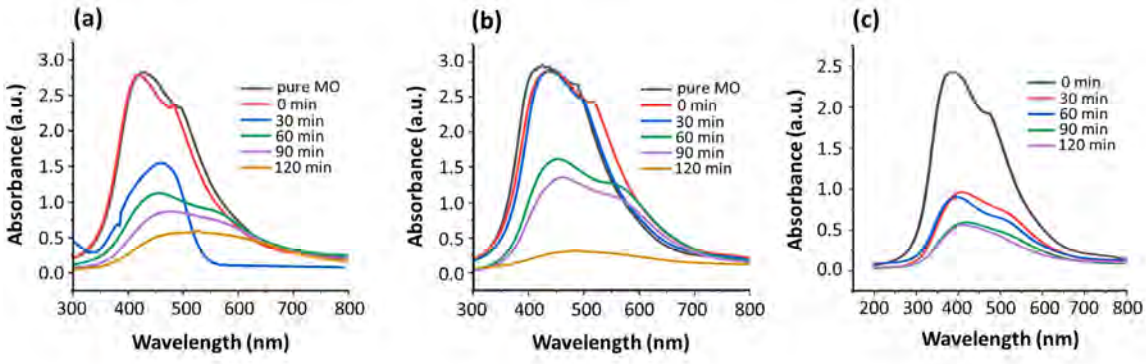

Figure 3: Photocatalytic degradation of MO dye with TiO_2 (a) and TAF10 (b) and of TEWW (c) with TAF10 (reprinted with permission from [79]; Copyright 2022, Elsevier)

which was higher for TAF10 (K_{app} = 0.0174 min^{-1}) than for TiO_2 (K_{app} = 0.0126 min^{-1}). Moreover, the efficiency of the TEWW degradation with TAF10 during the first hour of irradiation was much higher than that of MO; however, the efficiency decreased significantly during the second hour of irradiation (Figure 3c), resulting in the Kapp value of TEWW of 0.0134 min^{-1}, which is lower compared to the K_{app} value of MO obtained with the same photocatalyst.

3.1.2 Fe-doped TiO_2

To investigate the effect of chemical additives used in different steps of textile chemical processes on the photocatalytic removal and mineralisation efficiency of the dye Congo Red (CR), the real textile wastewater was imitated by adding glucose as a desizing and reducing agent, sodium carbonate as a scouring agent, ferric chloride as a colouring agent, magnesium sulphate as a printing agent and ammonium chloride as a finishing agent to the CR solution (Figure 4) [52]. For this purpose, iron-doped titanium dioxide nanotubes (Fe–TiO_2) were used as the photocatalyst and the batch experiments were carried out in the laboratory photoreactor under visible light irradiation for 180 minutes after the adsorption-desorption equilibrium was reached in the dark. The

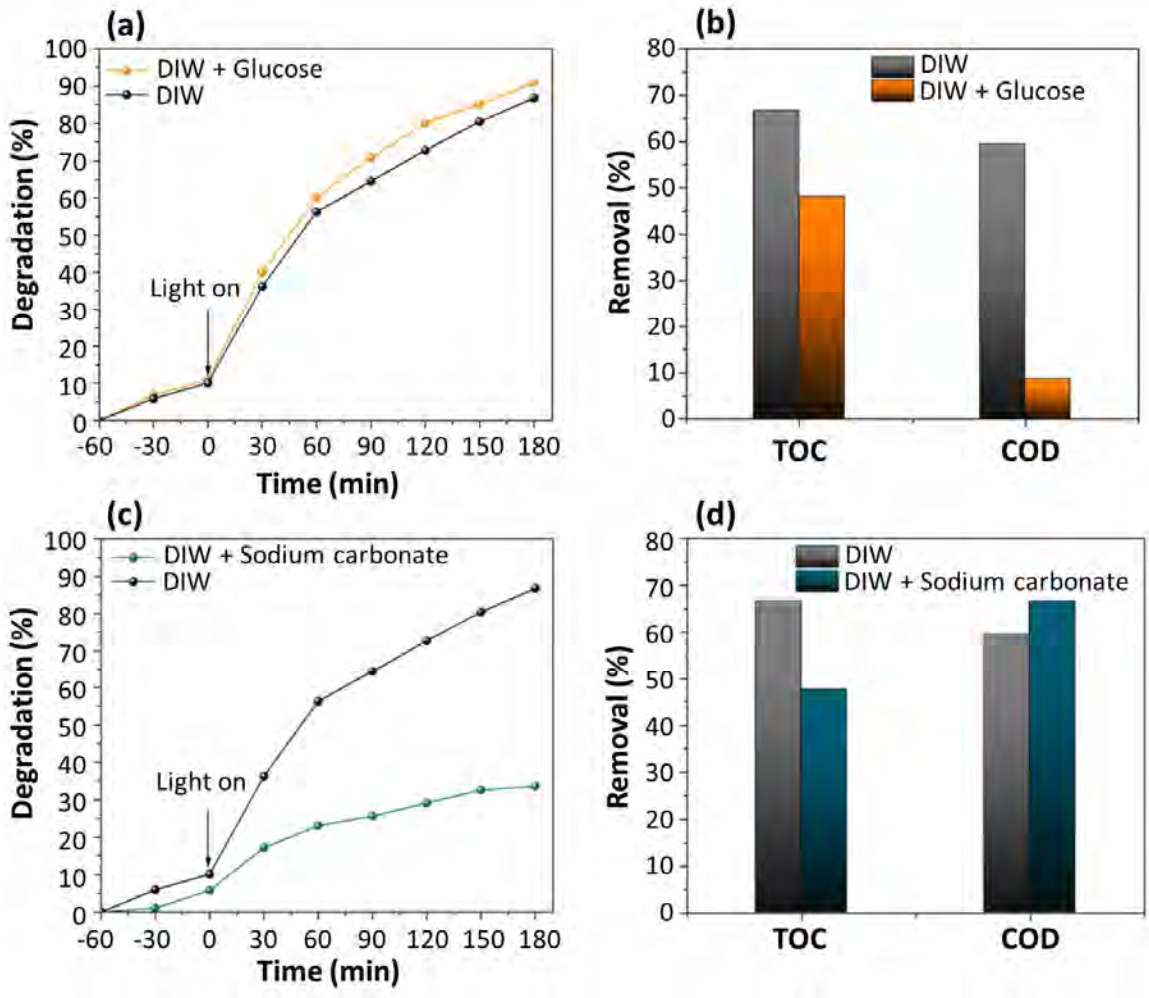

Figure 4: Impacts of glucose on dye degradation efficiency of CR (a) and removal efficiency of TOC and COD (b); impacts of sodium carbonate on degradation efficiency of CR (c) and removal efficiency of TOC and COD (d) (concentrations: CR = 5 mg/L, Glucose = 500 mg/L Sodium carbonate = 500 mg/L); DIW stands for deionised water (reprinted with permission from [52]; Copyright 2021, Elsevier)

results show that the degree of the CR photodegradation increased with the irradiation time and that the structure of the additives directly affected the photodegradation efficiency.

For example, the addition of a small amount of glucose to the CR solution did not hinder the efficiency of the photocatalytic degradation of CR, it even improved it (Figure 4a). The most reasonable explanation for this phenomenon was that glucose acts as a co-substrate that undergoes the oxidation reaction and thus affects the degradation of CR. It is believed that glucose acts as a scavenger of the photoinduced holes during the photocatalytic reaction and prevents the recombination of electron-hole pairs on the Fe–TiO_2 nanotubes. At the same time, the oxidation of glucose by holes did not hinder the photodegradation of CR, since the main ROS for the oxidation of CR was •OH, as shown by the results of the degradation mechanism. In contrast, the addition of glucose to the CR solution did not positively affect the removal of TOC and COD, as the presence of glucose decreased TOC removal by 19% and COD removal by 50% (Figure 4b).

The presence of sodium carbonate in the CR solution significantly delayed the photodegradation of CR, which dropped from 86% to 34% after 180 minutes of irradiation (Figure 4c). The reason for this phenomenon was attributed to the combination of the ability of carbonate ions to scavenge •OH and the competitive adsorption of carbonate ions on the catalyst surface and blocking of the active sites [52, 80]. The effect of sodium carbonate on TOC and COD removal efficiency was opposite. While TOC removal decreased with the addition of sodium carbonate, COD removal increased (Figure 4d). The decrease in the TOC removal efficiency was related to the lower CR degradation in the presence of sodium carbonate. However, the concomitant increase in COD removal suggests that sodium carbonate triggered the decomposition of inorganic compounds in the solution, resulting in a decrease in COD, but not TOC [52].

3.1.3 ZnO of different morphologies

To investigate the photodegradation efficiency of a real industrial wastewater from an Egyptian dye factory under sunlight irradiation, four ZnO samples of different morphologies and sizes were used for the experiment, including two ZnO quantum dots (QD) with the average sizes of 7.1 nm and 9.8 nm, and two ZnO nanoparticles (Nano) with the average sizes of 13.5 nm and 34 nm (Figure 5) [81]. Commercial ZnO powder was used as a reference. The experiments were conducted for 6 hours (from 9 am to 3 pm) on different study days from May to October 2018, and the solar photocatalytic activity of the ZnO samples was investigated by determining COD before and after the degradation experiment.

The results show that the COD values of real industrial wastewater before the photocatalytic experiments ranged from 4985 mg/L to 6867 mg/L, regardless of the study date, and that the COD values decreased in the presence of ZnO samples after 6 hours of irradiation (Figure 5a). It is also evident that the COD removal increased with the decrease of the ZnO particle size, indicating the effectiveness of the size effect of ZnO QDs on the photodegradation processes. The reusability of ZnO QDs and Nano ZnO for 8 times in the photodegradation process of wastewater resulted in a decrease in the photodegradation rate, and only the mineralisation efficiency achieved by ZnO QDs with the particle size of 7.1 nm stayed below the COD limit after the 8th recycling process (Figure 5b). It is assumed that the size of the photocatalyst increases during the recycling process, which is a consequence of the accumulation of photocatalysts with repeated use.

Research shows that doping TiO_2 with metal and non-metal ions and reducing ZnO particle size significantly increase the efficiency of the wastewater photodegradation process. It is also obvious that the photocatalytic degradation of wastewater is directly affected by the chemical additives present. If the additive ions can scavenge ROS, the photocatalytic process will be significantly hindered.

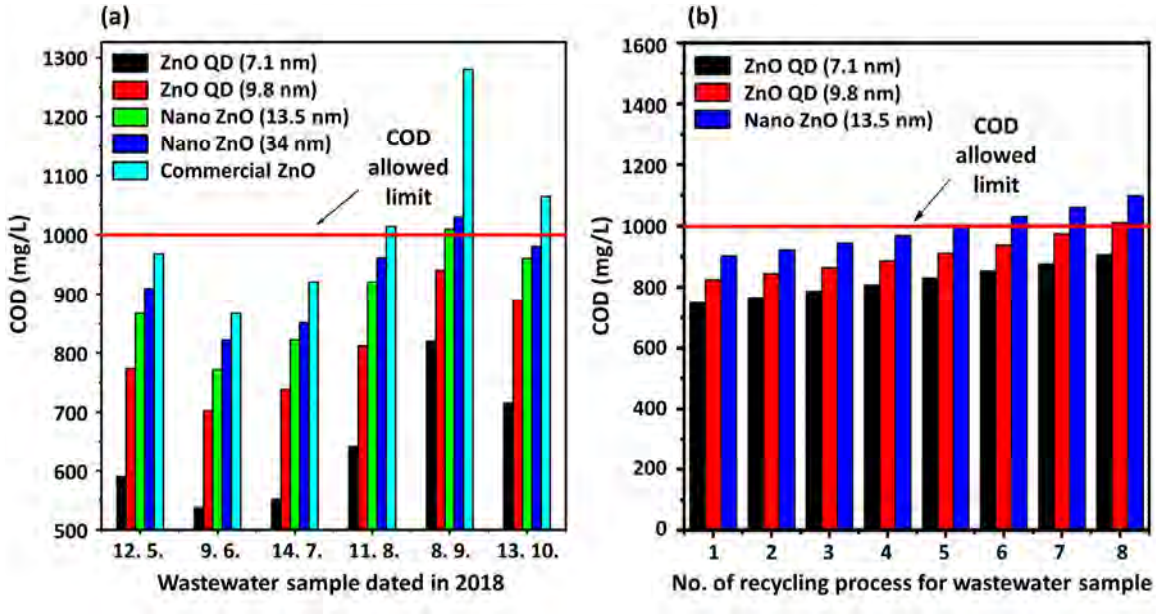

Figure 5: COD limits and situation of real industrial wastewater for six months using ZnO QDs, Nano ZnO and commercial ZnO during photocatalysis by sunlight (a); COD limits for recycling process of real industrial wastewater in October 2019 in presence of ZnO NDs and Nano ZnO during photocatalysis by sunlight (b) (reprinted with permission from [81]; Copyright 2020, Elsevier)

3.2 Photocatalysis in combination with other chemical, physical and biological processes

To increase the efficiency of wastewater treatment, photocatalysis has already been advantageously combined with other chemical, physical and biological processes. A combination of different processes for wastewater treatment offers several advantages over single treatments, as certain process combinations, their proper integration and optimisation can create the synergistic effect in their performance that is critical for efficient, versatile, scalable, cost-effective and environmentally sound wastewater treatment.

3.2.1 TiO_2 in combination with H_2O_2 versus photo-Fenton

To study the photodegradation activity of the dye Remazol Red (RR) in textile industry wastewater, a nanosized TiO_2 photocatalyst was used in combination with H_2O_2 under UV irradiation, and the results were compared with the photo-Fenton process as a rapid and cost-effective AOP [20]. The degree of dye degradation was calculated based on the initial and final TOC values and presented as TOC removal (Figure 6).

The results show that the presence of 5 mM H_2O_2 increased the photocatalytic activity of TiO_2 compared with that obtained in the absence of H_2O_2 and that the photocatalytic activity also increased when the concentration of TiO_2 increased from 0.20 g/L to 0.50 g/L (Figure 6a). This resulted in an RR dye degradation efficiency of 90% in 210 minutes in the presence of 0.5 g/L TiO_2 and 5 mM H_2O_2. UV irradiation is thought to cause photolysis of H_2O_2, generating additional •OH radicals that have a synergistic effect on the photocatalytic activity of TiO_2 and consequently on the photodegradation of the RR dye. A further increase in the TiO_2 concentration to 1.0 g/L increased the rate of dye degradation and resulted in an almost complete degradation (≈ 98%) in 60 minutes. However, a comparison of these results with the RR dye degradation in the photo-Fenton treatment revealed that a complete dye degradation (100%)

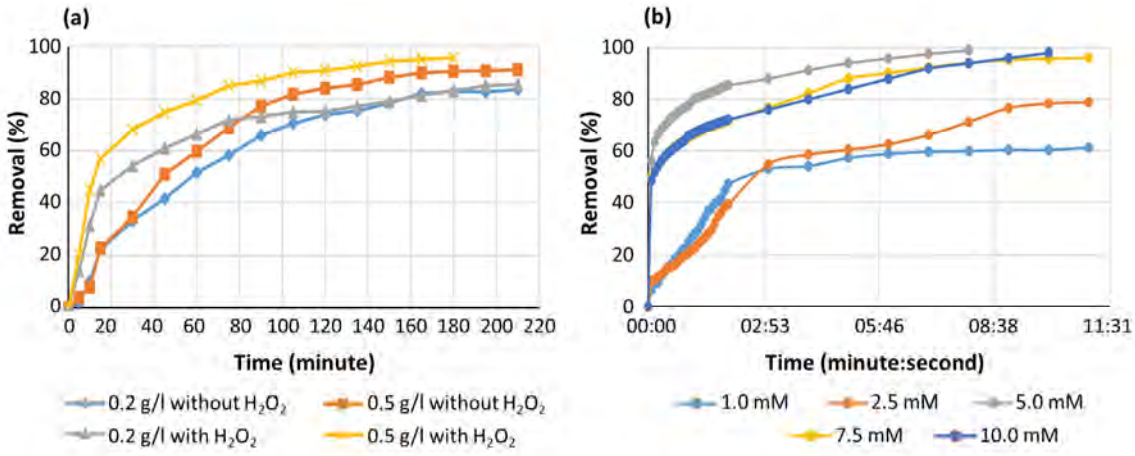

Figure 6: Photocatalytic degradation of RR dye with TiO_2 in presence and absence of H_2O_2 (a); photo-Fenton treatment of RR dye at Fe^{2+} concentration varying H_2O_2 concentration (mM) and pH 3.0 (b) (reprinted with permission from [20]; Copyright 2021, Springer)

was achieved in the experiment with 0.5 mM Fe^{2+} and 5.0 mM H_2O_2 at pH 3 in only 8 minutes (Figure 6b). An economic comparison of the two processes also shows that the photo-Fenton process is not only faster, but also less expensive.

3.2.2 Cd-doped ZnO in combination with O_3

In another study, photocatalytic ozonation (PCO), which integrates photocatalysis in the presence of ozonation, was described as an effective approach for the degradation of real textile wastewater under UV irradiation (Figure 7) [18]. For this purpose, ZnO nanocatalyst doped with cadmium (Cd–ZnO) was synthesised and used in a photoreactor connected to an ozone (O_3) generator. The operating parameters such as O_3 dose, pH, and Cd–ZnO amount were studied to achieve the optimal conditions for PCO, i.e. O_3 dose of 0.44 g/h, pH of 7 and 0.2 g/L Cd–ZnO. The efficiency of the mineralisation of textile wastewater with PCO (Cd–ZnO/UV/O_3) was determined based on COD determination at different times of wastewater treatment and compared with that of separate photocatalysis (Cd–ZnO/UV) and ozonation (O_3/UV) processes (Figure 7a).

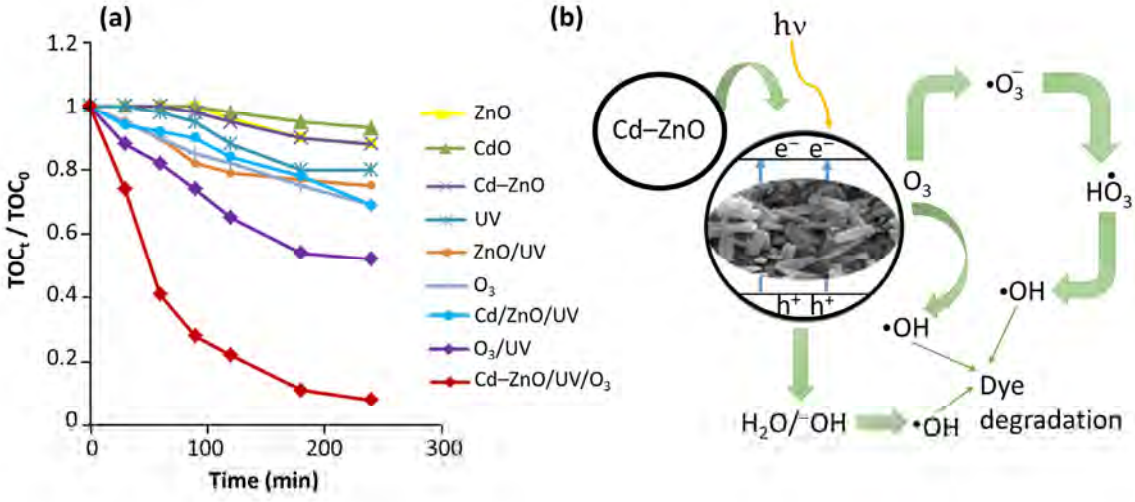

Figure 7: Mineralisation of textile wastewater with different processes (a); mechanism of Cd–ZnO/UV/O_3 for degradation of textile wastewater (b) (reprinted with permission from [18]; Copyright 2019, OIP Publishing)

The results show that the mineralisation rate observed with Cd–ZnO/UV/O_3 was by 4.2 times and 3.5 times higher than that of Cd–ZnO/UV and O_3/UV, respectively, indicating a synergistic effect between O_3 and Cd–ZnO/UV in PCO. This was due to the efficient trapping of generated electrons with O_3, resulting in the formation of ozonide radical anions ($\bullet O_3^-$). The radicals react rapidly with protons in the solution to form perhydroxyl radicals ($HO_3\bullet$), which then contribute to the formation of •OH (Figure 7b). Due to the more efficient trapping of photogenerated electrons with O_3, a recombination between holes and electrons is minimised, leading to the formation of a larger number of •OH, which accelerates the photocatalytic reaction [82].

3.2.3 Polyethylene glycol capped ZnO in combination with membrane filtration

A membrane photocatalytic reactor (MPR) (Figure 8a), which is a hybrid system of photocatalysis process and membrane filtration system, was used as an environmentally friendly approach for industrial textile wastewater treatment [83]. In MPR, the photocatalytic degradation of the wastewater was performed under UV-C irradiation in the photocatalytic reactor in the presence of polyethylene glycol capped ZnO (ZnO-PEG) nanoparticles as the initial treatment, followed by filtration through the polypiperazine-amide (PPA) tight ultrafiltration membrane (UF-PPA). The photocatalytic efficiency of the ZnO-PEG nanoparticles was estimated by analysing the flux decline during membrane filtration, where the normalised flux was calculated as the ratio between wastewater flux and pure water flux.

The results show that a photocatalytic degradation of wastewater with ZnO-PEG significantly reduced the pollutants filtered by the UF-PPA membrane, which prevented pore plugging of the

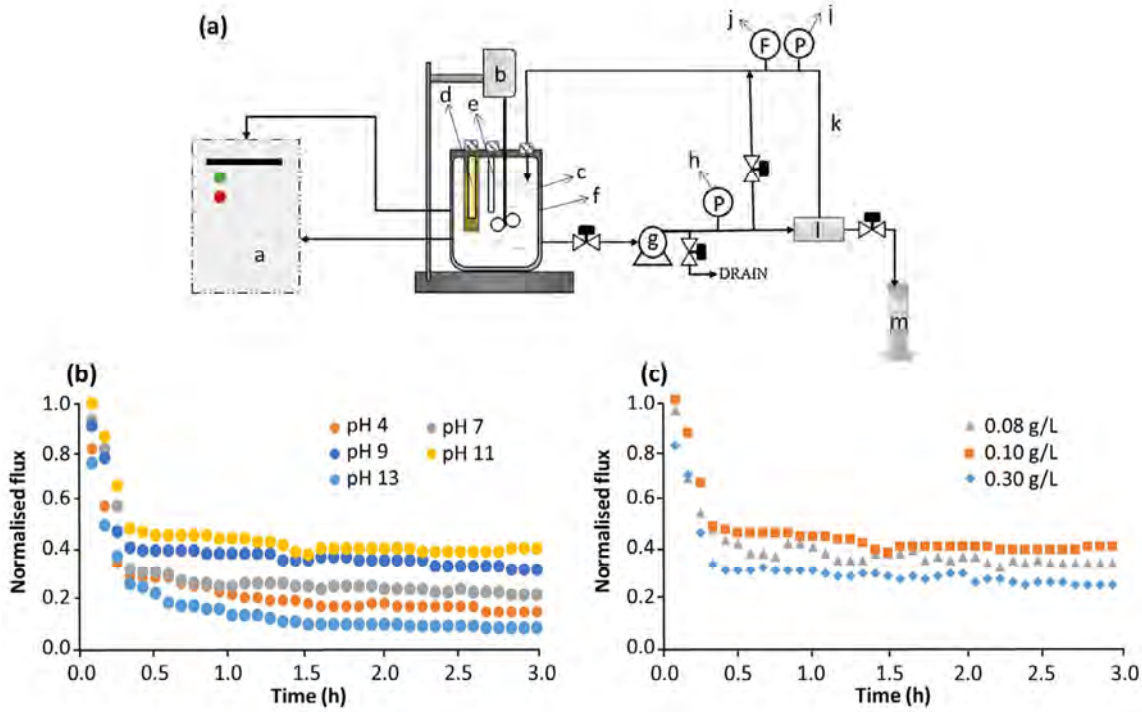

Figure 8: Schematic diagram of MPR (a) (Legend: a – water chiller, b – overhead stirrer with stand, c – photocatalytic reactor, d – UV lamp, e – feed, f – cooling jacket, g – pump, h, i – pressure gauge, j – flow meter, k – recycle flow, l – membrane filtration system, m – measuring cylinder); normalised flux of UF-PPA membrane against time under different pH of industrial wastewater at loading of ZnO-PEG = 0.10 g/L (b); normalised flux of UF-PPA membrane against time under different loading of ZnO-PEG nanoparticles at pH = 11 (c); reaction conditions: dilution of wastewater = 75%, pressure = 6 bars (reprinted with permission from [83]; Copyright 2019, Elsevier)

membrane for its permeability to be maintained and permeate flux through it sustained. The influence of the initial wastewater pH and the ZnO-PEG loading on the process performance was investigated, and the optimal operating conditions of ZnO-PEG in the MPR system were determined at pH 11 (Figure 8b), 0.10 g/L ZnO-PEG nanoparticles (Figure 8c), and 75% dilution of the textile wastewater. Under these conditions, the presence of ZnO-PEG nanoparticles as a photocatalyst significantly improved the effectiveness of the MPR system, resulting in maximal photocatalytic degradation efficiency and minimal membrane fouling.

3.2.4 TiO_2 and ZnO in combination with biological system

The coupled photocatalytic and biological process was applied to the treatment of industrial textile wastewater, including photocatalytic degradation of wastewater in the presence of ZnO or TiO_2 as photocatalysts under UV irradiation, followed by an aerobic bioprocess using sludge microorganisms acclimated to textile wastewater (Figure 9) [22]. The photocatalytic process was performed in the reactor for 2 hours and the biological test was performed in the incubator under suitable conditions for 12, 24 and 28 hours.

The results show that the absorption peak of the wastewater decreased significantly during the UV-assisted photocatalysis in the presence of TiO_2, resulting in a 44% decolourisation of the wastewater and that the subsequent bioprocess additionally contributed to the decolourisation of the wastewater, resulting in an 88% colour removal after 12 hours and a nearly complete decolourisation of 97% within 48 hours of biological treatment (Figure 9a). These results indicate that the combined TiO_2/UV and biological system is suitable for the decolourisation of real textile wastewater. In contrast to TiO_2, photocatalysis with ZnO was much less effective and caused virtually no changes in the absorption spectrum after 2 hours of photocatalysis (Figure 9b). The lower photocatalytic efficiency of ZnO compared to TiO_2 was attributed to the lower surface area of ZnO particles. The subsequent biological process did not contribute to the efficiency of the combined process; hance, only 48% of the colour was removed after 48 hours of treatment. These results demonstrate the importance of photocatalysis for the decolourisation efficiency of the combined photocatalytic-biological process.

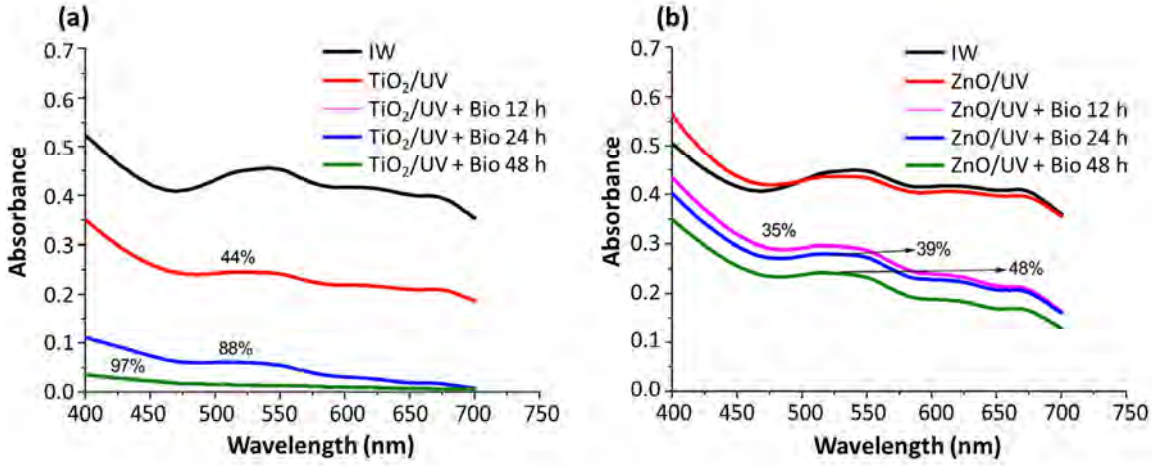

Figure 9: Absorption spectra of industrial wastewater before (IW) and after photocatalytic treatment (TiO_2/UV and ZnO/UV) and combined photocatalytic-biological treatment (TiO_2/UV + Bio and ZnO/UV + Bio), including percentage of colour removal after each treatment step; photocatalysis with TiO_2 (a), and ZnO (b) (reprinted with permission from [22]; Copyright 2019, John Wiley and Sons

3.2.5 ZnO/polypyrrole in combination with biological system

In another proposed coupled photocatalytic-biological process, biological treatment of textile wastewater was conducted as a pretreatment and photocatalysis as a subsequent process using a ZnO/polypyrrole (ZnO/PPy) composite [84]. Previously, the bacterial consortium was collected from the inspection chamber of the factory sewer and enriched for the biological treatment, and the optimal amount of ZnO/PPy photocatalyst and its recyclability were determined for photocatalysis. In the combined process, real textile wastewater containing the azo dye Direct Black 22 was pretreated with a bacterial consortium for 96 hours and then photodegraded in the presence of ZnO/PPy for one hour under UV irradiation (Figure 10a). The time dependence of Direct Black 22 was observed in both treatments. The results show that when the two process steps were applied separately, the biological treatment resulted in 71.3% decolourisation of the dye and 80.0% removal of TOC, while the photocatalysis resulted in 83.6% decolourisation of the dye and 88.4% removal of TOC (Figure 10b). Coupling the two treatment processes resulted in a much higher decolourisation efficiency of 95.7%, while the final TOC removal reached remarkable 99.9% (Figure 10b).

The presented combined processes have proved the importance of their performance for wastewater treatment. It is obvious that the efficiency of photocatalysis is significantly increased in the presence of oxidants such as H_2O_2 and O_3. In fact, the addition of H_2O_2 was found to have a synergistic effect on the photocatalytic activity of nanosized TiO_2, as H_2O_2 generates additional •OH radicals under UV irradiation. The synergistic effect between the ZnO-based nanocomposite and O_3 was attributed to the efficient capture of the generated electrons by O_3, leading to the formation of $•O_3^-$ and $HO_3•$, which then contribute to the formation of •OH. In a hybrid system of photocatalysis and membrane filtration, the initial photocatalytic treatment of wastewater with ZnO under UV-C irradiation significantly improved the efficiency of the ultrafiltration membrane system, resulting in maximum photocatalytic degradation efficiency and minimal membrane fouling. The coupled photocatalytic and biological processes also proved to be promising treatment methods, with photocatalysis performed as a pretreatment or as a subsequent process. The coupling of the two processes resulted in significantly higher decolourisation efficiency and TOC removal compared to the processes performed separately.

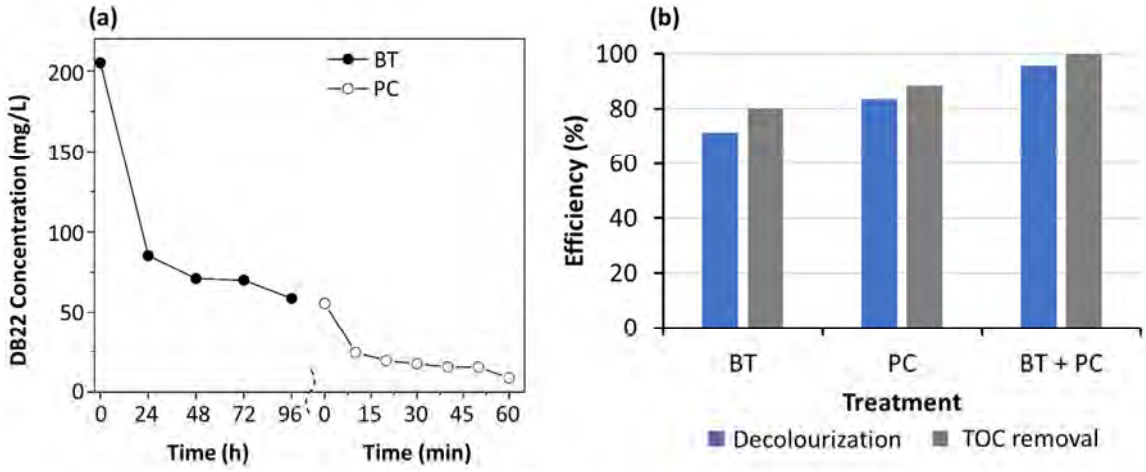

Figure 10: Sequential biological treatment and photocatalysis of real textile wastewater containing azo dye Direct Black 22 (a); decolorisation and TOC removal efficiencies of individual steps of separately applied treatments and coupled treatment (b); DB22 stands for Direct Black 22, BT stands for biological treatment, PC stands for photocatalytic treatment (reprinted with permission from [84]; Copyright 2020, Elsevier)

4 Conclusion

The treatment of real textile wastewater to remove synthetic dyes prior to disposal to the municipal wastewater treatment plant or the environment remains a major challenge. Various physical, chemical and biological processes have been used for this purpose, among which photocatalysis has already established itself as one of the most challenging ones.

Both TiO_2- and ZnO-based photocatalysis have unique advantages that make them an important AOP for textile wastewater treatment. One of the key advantages is environmental sustainability, as TiO_2 and ZnO are recognised as biocompatible, non-toxic, and chemically inert nanomaterials on the one hand, and the ability of photocatalysis to degrade the pollutants to water and carbon dioxide without hazardous by-products on the other hand. It should be emphasised that photocatalysis can be used in a variety of environmental remediation processes to convert toxic pollutants into harmless products, which would not be possible with conventional wastewater treatment processes. However, in addition to the advantages, there are also some limitations of photocatalysis. One of them is its narrow spectral response, mostly in the UV range, which limits its ability to utilise a broader spectrum of sunlight. In addition, the introduction of photocatalysis for large-scale applications is still a challenging research topic as it is usually studied under ideal laboratory conditions. To improve the applicability of photosynthesis in real-world scenarios and to ensure the long-term stability of the photocatalysis system, further research and development efforts are needed for a careful construction and design of large-scale photocatalytic reactors.

In addition to single photocatalytic processes, combined processes in which photocatalysis is coupled with other chemical, physical and biological processes have attracted a considerable interest due to their synergistic effects in wastewater treatment. Photocatalysis has been successfully performed in the presence of other oxidants such as H_2O_2 and O_3, and in combination with ultrafiltration and biological processes. In these studies, a proper system design and determination of optimal treatment parameters are of great importance to take advantage of each process and maximise treatment performance. The complementation of the coupled processes and the creation of a synergistic effect resulted in more efficient comprehensive and diverse pollutant removal compared to a single wastewater treatment. When photocatalysis is coupled with membrane filtration as pretreatment, fouling can be reduced, which improves and stabilises filtration performance. By combining photocatalysis as a pretreatment with a biological process, organic load is reduced, which lowers energy consumption and operational costs.

Acknowledgments

The research was conducted as part of the course Environmental Aspects in Textiles and Graphics within the doctoral study programme Textile Engineering, Graphic Communication and Textile Design at the University of Ljubljana, Faculty of Natural Science and Engineering, Department of Textiles, Graphic Arts and Design. The authors sincerely thank the programme coordinator Prof. Dr. Petra Forte Tavčer for her constructive comments and guidance during the research work.

Funding

This research was funded by the Slovenian Research Agency, Slovenia (Programme P2-0213 Textiles and Ecology, Infrastructural Centre RIC UL-NTF, and a grant for the doctoral student D.G.).

References

1. KANT, R. Textile dyeing industry an environmental hazard. *Natural Science,* 2012, **4**(1), 22–26, doi: 10.4236/ns.2012.41004.
2. DIHOM, H.R., AL-SHAIBANI, M.M., RADIN MOHAMED, R.M.S., AL-GHEETHI, A.A., SHARMA, A., BIN KHAMIDUN, M.H. Photocatalytic degradation of disperse azo dyes in textile wastewater using green zinc oxide

nanoparticles synthesized in plant extract: a critical review. *Journal of Water Process Engineering*, 2022, **47**, 1–12, doi: 10.1016/j.jwpe.2022.102705.

3. NUR, A.S.M., SULTANA, M., MONDAL, A., ISLAM, S., ROBEL, F.N., ISLAM, A., SUMI, MST.S.A. A review on the development of elemental and codoped TiO_2 photocatalysts for enhanced dye degradation under UV–Vis irradiation. *Journal of Water Process Engineering*, 2022, **47**, 1–17, doi: 10.1016/j.jwpe.2022.102728.
4. AL-TOHAMY, R., ALI, S.S., LI, F., OKASHA, K.M., MAHMOUD, Y.A.G., ELSAMAHY, T., JIAO, H., FU, Y., SUN, J. A critical review on the treatment of dye-containing wastewater: ecotoxicological and health concerns of textile dyes and possible remediation approaches for environmental safety. *Ecotoxicol and Environmental Safety*, 2022, **231**, 1–17, doi: 10.1016/j.ecoenv.2021.113160.
5. DHRUV PATEL, D., BHATT, S. Environmental pollution, toxicity profile, and physico-chemical and biotechnological approaches for treatment of textile wastewater. *Biotechnology and Genetic Engineering Reviews*, 2022, **38**(1), 33–86, doi: 10.1080/02648725.2022.2048434.
6. WANG, X., JIANG, J., GAO, W. Reviewing textile wastewater produced by industries: characteristics, environmental impacts, and treatment strategies. *Water Science & Technology*, 2022, **85**(7), 2076–2096, doi: 10.2166/wst.2022.088.
7. VANDEVIVERE, P.C., BIANCHI, R., VERSTRAETE, W. Review: Treatment and reuse of wastewater from the textile wet-processing industry: review of emerging technologies. *Journal of Chemical Technology & Biotechnology*, 1998, **72**(4), 289–302, doi: 10.1002/(SICI)1097-4660(199808)72:4<289::AID-JCTB905>3.0.CO;2-%23.
8. SARATALE, R.G., SARATALE, G.D., KALYANI, D.C., CHANG, J.S., GOVINDWAR, S.P. Enhanced decolorization and biodegradation of textile azo dye Scarlet R by using developed microbial consortium-GR. *Bioresour Technol*, 2009, **100**(9), 2493–2500, doi: 10.1016/j.biortech.2008.12.013.
9. SELVARAJ, V., SWARNA KARTHIKA, T., MANSIYA, C., ALAGAR, M. An over review on recently developed techniques, mechanisms and intermediate involved in the advanced azo dye degradation for industrial applications. *Journal of Molecular Structure*, 2021, **1224**, 1–15, doi: 10.1016/j.molstruc.2020.129195.
10. HOLKAR, C.R., JADHAV, A.J., PINJARI, D. V., MAHAMUNI, N.M., PANDIT, A.B. A critical review on textile wastewater treatments: possible approaches. *Journal of Environmental Management*, 2016, **182**, 351–366, doi: 10.1016/j.jenvman.2016.07.090.
11. BHATIA, D., SHARMA, N.R., SINGH, J., KANWAR, R.S. Biological methods for textile dye removal from wastewater: a review. *Critical Reviews in Environmental Science and Technology*, 2017, **47**(19), 1836–1876, doi: 10.1080/10643389.2017.1393263.
12. YASEEN, D.A., SCHOLZ, M. Textile dye wastewater characteristics and constituents of synthetic effluents: a critical review. *International Journal of Environmental Science and Technology*, 2019, **16**, 1193–1226, doi: 10.1007/s13762-018-2130-z.
13. ROŠ, M. *Sodobni postopki čiščenja odpadnih vod*. Celje : Fit media, 2015, 87–107.
14. HUANG, X., BO, X., ZHAO, Y., GAO, B., WANG, Y., SUN, S., YUE, Q., LI, Q. Effects of compound bioflocculant on coagulation performance and floc properties for dye removal. *Bioresource Technology*, 2014, **165**, 116–121, doi: 10.1016/j.biortech.2014.02.125.
15. BRILLAS, E., MARTÍNEZ-HUITLE, C.A. Decontamination of wastewaters containing synthetic organic dyes by electrochemical methods. An updated review. *Applied Catalysis B: Environmental,* 2015, **166–167**, 603–643, doi: 10.1016/j.apcatb.2014.11.016.
16. LIU, H., WANG, C., WANG, G. Photocatalytic advanced oxidation processes for water treatment: Recent advances and perspective. *Chemistry – An Asian Journal*, 2020, **15**(20), 3239–3253, doi: 10.1002/asia.202000895.

17. HASSAAN, M.A., EL NEMR, A. Advanced oxidation processes for textile wastewater treatment. *International Journal of Photochemistry and Photobiology*, 2017, **2**(3), 85–93, doi: 10.11648/j.ijpp.20170203.13.
18. PANDIAN, L., RAJASEKARAN, R., GOVINDAN, P. Synergistic effect of ozone on cadmium doped zinc oxide nanocatalyst for the degradation of textile dyeing wastewater. *Materials Research Express*, 2019, **6**, 1–8, doi: 10.1088/2053-1591/ab1da6.
19. XU, M., WU, C., ZHOU, Y. Advancements in the Fenton process for wastewater treatment. In *Advanced Oxidation Processes*. Edited by C. Bustillo-Lecompte. Rijeka : IntechOpen, 2020, p. 1–17. doi: 10.5772/intechopen.90256.
20. PIPIL, H., YADAV, S., CHAWLA, H., TANEJA, S., VERMA, M., SINGLA, N., HARITASH, A.K. Comparison of TiO_2 catalysis and Fenton's treatment for rapid degradation of Remazol Red dye in textile industry effluent. *Rendiconti Lincei. Scienze Fisiche e Naturali*, 2022, **33**, 105–114, doi: 10.1007/s12210-021-01040-x.
21. LI, S., ZHANG, C., LI, F., HUA, T., ZHOU, Q., HO, S.-H. Technologies towards antibiotic resistance genes (ARGs) removal from aquatic environment: A critical review. *Journal of Hazardous Materials*, 2021, **411**, 1–13, doi: 10.1016/j.jhazmat.2021.125148.
22. DA SILVA, L.S., GONÇALVES, M.M.M., RADDI DE ARAUJO, L.R. Combined photocatalytic and biological process for textile wastewater treatments. *Water Environment Research*, 2019, **91**(11), 1490–1497, doi: 10.1002/wer.1143.
23. KAYA, Ş., AŞÇI, Y. Evaluation of color and COD removal by Fenton and photo-Fenton processes from industrial paper wastewater. *Journal of the Institute of Science and Technology*, 2019, **9**(3), 1539–1550, doi: 10.21597/jist.507181.
24. MACHULEK, A., QUINA, F., GOZZI, F., SILVA, V., FRIEDRICH, L., MORAES, J. Fundamental mechanistic studies of the photo-Fenton reaction for the degradation of organic pollutants. In *Organic Pollutants Ten Years After the Stockholm Convention - Environmental and Analytical Update*. Edited by T. Puzyn, A. Mostrag. London : IntechOpen, 2012, 271–292, doi: 10.5772/30995.
25. GUO, R., WANG, J., BI, Z. XU, CHEN, X., HU, X., PAN, W. Recent advances and perspectives of g–C_3N_4–based materials for photocatalytic dyes degradation. *Chemosphere*, 2022, **295**, 1–17, doi: 10.1016/j.chemosphere.2022.133834.
26. WANG, L., ZHAO, J., LIU, H., HUANG, J. Design, modification and application of semiconductor photocatalysts. *Journal of the Taiwan Institute of Chemical Engineers*, 2018, **93**, 590–602, doi: 10.1016/j.jtice.2018.09.004.
27. CARP, O., HUISMAN, C.L., RELLER, A. Photoinduced reactivity of titanium dioxide. *Progress in Solid State Chemistry*, 2004, **32**(1–2), 33–177, doi: 10.1016/j.progsolidstchem.2004.08.001.
28. SCHNEIDER, J., MATSUOKA, M., TAKEUCHI, M., ZHANG, J., HORIUCHI, Y., ANPO, M., BAHNEMANN, D.W. Understanding TiO_2 photocatalysis: mechanisms and materials. *Chemical Reviews*, 2014, **114**(19), 9919–9986, doi: 10.1021/cr5001892.
29. NAM, Y., LIM, J.H., KO, K.C., LEE, J.Y. Photocatalytic activity of TiO_2 nanoparticles: a theoretical aspect. *Journal of Materials Chemistry A*, 2019, **7**, 13833–13859, doi: 10.1039/c9ta03385h.
30. KOE, W.S., LEE, J.W., CHONG, W.C., PANG, Y.L., SIM, L.C. An overview of photocatalytic degradation: photocatalysts, mechanisms, and development of photocatalytic membrane. *Environmental Science and Pollution Research*, 2020, **27**, 2522–2565, doi: 10.1007/s11356-019-07193-5.
31. RASHID, M.M., SIMONČIČ, B., TOMŠIČ, B. Recent advances in TiO_2-functionalized textile surfaces. *Surfaces and Interfaces*, 2021, **22**, 1–33, doi: 10.1016/j.surfin.2020.100890.
32. VERBIČ, A., GORJANC, M., SIMONČIČ, B. Zinc oxide for functional textile coatings: recent advances. *Coatings*, 2019, **9**(9), 1–26, doi: 10.3390/coatings9090550.

33. FU, J., CHEN, Z., WANG, M., LIU, S., ZHANG, J., ZHANG, J., HAN, R., XU, Q. Adsorption of methylene blue by a high-efficiency adsorbent (polydopamine microspheres): kinetics, isotherm, thermodynamics and mechanism analysis. *Chemical Engineering Journal*, 2015, **259**, 53–61, doi: 10.1016/j.cej.2014.07.101.
34. GHAFOOR, S., INAYAT, A., AFTAB, F., DURAN, H., KIRCHHOFF, K., WASEEM, S., ARSHAD, S.N. TiO_2 nanofibers embedded with g-C_3N_4 nanosheets and decorated with Ag nanoparticles as Z-scheme photocatalysts for environmental remediation. *J Environ Chem Eng*, 2019, **7**(6), 1–10, doi: 10.1016/j.jece.2019.103452.
35. LIU, Y., REN, M., ZHANG, X., YANG, G., QIN, L., MENG, J., GUO, Y. Supramolecule self-assembly approach to direct Z-scheme TiO_2/g-C_3N_4 heterojunctions for efficient photocatalytic degradation of emerging phenolic pollutants. *Applied Surface Science*, 2022, **593**, 1–15, doi: 10.1016/j.apsusc.2022.153401.
36. ISARI, A.A., PAYAN, A., FATTAHI, M., JORFI, S., KAKAVANDI, B. Photocatalytic degradation of rhodamine B and real textile wastewater using Fe-doped TiO_2 anchored on reduced graphene oxide (Fe-TiO_2/rGO): characterization and feasibility, mechanism and pathway studies. *Applied Surface Science*, 2018, **462**, 549–564, doi: 10.1016/j.apsusc.2018.08.133.
37. YE, Z., KONG, L., CHEN, F., CHEN, Z., LIN, Y., LIU, C. A comparative study of photocatalytic activity of ZnS photocatalyst for degradation of various dyes. *Optik (Stuttg)*, 2018, **164**, 345–354, doi: 10.1016/j.ijleo.2018.03.030.
38. SHEN, R., JIANG, C., XIANG, Q., XIE, J., LI, X. Surface and interface engineering of hierarchical photocatalysts. *Applied Surface Science*, 2019, **471**, 43–87, doi: 10.1016/j.apsusc.2018.11.205.
39. ETACHERI, V., DI VALENTIN, C., SCHNEIDER, J., BAHNEMANN, D., PILLAI, S.C. Visible-light activation of TiO_2 photocatalysts: Advances in theory and experiments. *Journal of Photochemistry and Photobiology C: Photochemistry Reviews*, 2015, **25**, 1–29, doi: 10.1016/j.jphotochemrev.2015.08.003.
40. KUMAR, S.G., RAO, K.S.R.K. Comparison of modification strategies towards enhanced charge carrier separation and photocatalytic degradation activity of metal oxide semiconductors (TiO_2 , WO_3 and ZnO). *Applied Surface Science*, 2017, **391**, 124–148, doi: 10.1016/j.apsusc.2016.07.081.
41. CHANG, S-MIN, LIU, W-SZU. The roles of surface-doped metal ions (V, Mn, Fe, Cu, Ce, and W) in the interfacial behavior of TiO_2 photocatalysts. *Appl Catal B*, 2014, **156–157**, 466–475, doi: 10.1016/j.apcatb.2014.03.044.
42. BLOH, J.Z., DILLERT, R., BAHNEMANN, D.W. Designing optimal metal-doped photocatalysts: Correlation between photocatalytic activity, doping ratio, and particle size. *Journal of Physical Chemistry C*, 2012, **116**(48), 25558–25562, doi: 10.1021/jp307313z.
43. KHAN, M.R., CHUAN, T.W., YOUSUF, A., CHOWDHURY, M.N.K., CHENG, C.K. Schottky barrier and surface plasmonic resonance phenomena towards the photocatalytic reaction: study of their mechanisms to enhance photocatalytic activity. *Catalysis Science & Technology,* 2015, **5**, 2522–2531, doi: 10.1039/C4CY01545B.
44. XU, Q., ZHANG, L., YU, J., WAGEH, S., AL-GHAMDI, A.A., JARONIEC, M. Direct Z-scheme photocatalysts: principles, synthesis, and applications. *Materials Today,* 2018, **21**(10), 1042–1063, doi: 10.1016/j.mattod.2018.04.008.
45. SIRIRERKRATANA, K., KEMACHEEVAKUL, P., CHUANGCHOTE, S. Color removal from wastewater by photocatalytic process using titanium dioxide-coated glass, ceramic tile, and stainless steel sheets. *Journal of Cleaner Production*, 2019, **215**, 123–130, doi: 10.1016/j.jclepro.2019.01.037.
46. SHI, X., ZHANG, Y., LIU, X., JIN, H., LV, H., HE, S., HAO, H., LI, C. A mild in-situ method to construct Fe-doped cauliflower-like rutile TiO_2

photocatalysts for degradation of organic dye in wastewater. *Catalysts*, 2019, **9**(5), 1–17, doi: 10.3390/catal9050426.

47. RAJAGOPAL, S., PARAMASIVAM, B., MUNIYASAMY, K. Photocatalytic removal of cationic and anionic dyes in the textile wastewater by H_2O_2 assisted TiO_2 and micro-cellulose composites. *Separation and Purification Technology*, 2020, **252**, 1–11, doi: 10.1016/j.seppur.2020.117444.
48. NEZHADALI, A., SHAPOURI, M.R., AMOLI-DIVA, M. Laser and solar light-induced degradation of pollutant dyes using bi-plasmonic Ag-Au nanoparticles-decorated magnetic TiO_2 for textile wastewater treatment. *Journal of Nanostructures*, 2022, **12**(1), 45–61, doi: 10.22052/JNS.2022.01.006.
49. HELMY, E.T., NEMR, A. EL, ARAFA, E., EL-DAFRAWY, S., MOUSA, M. Photocatalytic degradation of textile dyeing wastewater under visible light irradiation using green synthesized mesoporous non-metal-doped TiO_2. *Bulletin of Materials Science*, 2021, **44**, 1–11, doi: 10.1007/s12034-020-02322-0.
50. CRUZ, D., ORTIZ-OLIVEROS, H.B., FLORES-ESPINOSA, R.M., ÁVILA PÉREZ, P., RUIZ-LÓPEZ, I.I., QUIROZ-ESTRADA, K.F. Synthesis of Ag/TiO_2 composites by combustion modified and subsequent use in the photocatalytic degradation of dyes. *J King Saud Univ Sci*, 2022, **34**(4), 1–8, doi: 10.1016/j.jksus.2022.101966.
51. SHAFIQUE, M., MAHR, M.S., YASEEN, M., BHATTI, H.N. CQD/TiO_2 nanocomposite photocatalyst for efficient visible light-driven purification of wastewater containing methyl orange dye. *Materials Chemistry and Physics*, 2022, **278**, 1–14, doi: 10.1016/j.matchemphys.2021.125583.
52. ZAFAR, Z., FATIMA, R., KIM, J.-O. Experimental studies on water matrix and influence of textile effluents on photocatalytic degradation of organic wastewater using Fe–TiO_2 nanotubes: Towards commercial application. *Environmental Research*, 2021, **197**, 1–10, doi: 10.1016/j.envres.2021.111120.
53. PONCE, J., PEÑA, J., ROMÁN, J., PASTOR, J.M. Recyclable photocatalytic composites based on natural hydrogels for dye degradation in wastewaters. *Separation and Purification Technology*, 2022, **299**, 1–10, doi: 10.1016/j.seppur.2022.121759.
54. AHMAD, M.N., MASOOD UL HASSAN, M., NAWAZ, F., ANJUM, M.N., IQBAL, S.Z., HUSSAIN, T., MUJAHID, A., FARID, M.F. Synthesis and characterization of poly(o-chloroaniline)/TiO_2 nanocomposites for photocatalytic degradation of direct yellow 50 dye in textile wastewater. *Global NEST Journal*, 2022, **24**(1), 53–58, doi: 10.30955/gnj.004205.
55. MIN, K.S., MANIVANNAN, R., SON, Y.-A. Porphyrin dye/TiO_2 imbedded PET to improve visible-light photocatalytic activity and organosilicon attachment to enrich hydrophobicity to attain an efficient self-cleaning material. *Dyes and Pigments*, 2019, **162**, 8–17, doi: 10.1016/j.dyepig.2018.10.014.
56. ZHOU, S., XIA, L., ZHANG, K., FU, Z., WANG, Y., ZHANG, Q., ZHAI, L., MAO, Y., XU, W. Titanium dioxide decorated natural cellulosic juncus effusus fiber for highly efficient photodegradation towards dyes. *Carbohydrate Polymers*, 2020, **232**, 1–9, doi: 10.1016/j.carbpol.2020.115830.
57. CHANDAN, M.R., GOYAL, S., RIZWAN, M., IMRAN, M., SHAIK, A.H. Removal of textile dye from synthetic wastewater using microporous polymer nanocomposite. *Bulletin of Materials Science*, 2021, **44**, 1–11, doi: 10.1007/s12034-021-02559-3.
58. MESGARI, Z., GHARAGOZLOU, M., KHOSRAVI, A., GHARANJIG, K. SYNTHESIS. Characterization and evaluation of efficiency of new hybrid Pc/Fe-TiO_2 nanocomposite as photocatalyst for decolorization of methyl orange using visible light irradiation. *Applied Catalysis A: General*, 2012, **411–412**, 139–145, doi: 10.1016/j.apcata.2011.10.031.

59. AKPAN, U.G., HAMEED, B.H. Parameters affecting the photocatalytic degradation of dyes using TiO_2-based photocatalysts: A review. *Journal of Hazardous Materials*, 2009, **170**(2-3), 520–529, doi: 10.1016/j.jhazmat.2009.05.039.
60. KHATAEE, A.R., KASIRI, M.B. Photocatalytic degradation of organic dyes in the presence of nanostructured titanium dioxide: Influence of the chemical structure of dyes. *Journal of Molecular Catalysis A: Chemical*, 2010, **328**(1–2), 8–26, doi: 10.1016/j.molcata.2010.05.023.
61. MAHLAULE-GLORY, L.M., HINTSHO-MBITA, N.C. Green derived zinc oxide (ZnO) for the degradation of dyes from wastewater and their antimicrobial activity: a review. *Catalysts*, 2022, **12**(8), 1–25, doi: 10.3390/catal12080833.
62. TANWAR, N., DHIMAN, V., KUMAR, S., KONDAL, N. Plant extract mediated ZnO-NPs as photocatalyst for dye degradation: an overview. *Materials Today: Proceedings*, 2022, **48**(5), 1401–1406, doi: 10.1016/j.matpr.2021.09.186.
63. AL-BURIAHI, A.K., AL-GHEETHI, A.A., SENTHIL KUMAR, P., RADIN MOHAMED, R.M.S., YUSOF, H., ALSHALIF, A.F., KHALIFA, N.A. Elimination of rhodamine B from textile wastewater using nanoparticle photocatalysts: a review for sustainable approaches. *Chemosphere*, 2022, **287**, 1–14, doi: 10.1016/j.chemosphere.2021.132162.
64. RAHMAN, A., HARUNSANI, M.H., TAN, A.L., KHAN, M.M. Zinc oxide and zinc oxide-based nanostructures: Biogenic and phytogenic synthesis, properties and applications. *Bioprocess and Biosystems Engineering*, 2021, **44**, 1333–1372, doi: 10.1007/s00449-021-02530-w.
65. SÁENZ-TREVIZO, A., AMÉZAGA-MADRID, P., PIZÁ-RUIZ, P., ANTÚNEZ-FLORES, W., MIKI-YOSHIDA, M. Optical band gap estimation of ZnO nanorods. *Materials Research*, 2016, **19**, 33–38, doi: 10.1590/1980-5373-MR-2015-0612.
66. TALESHI, F. The effect of carbon nanotube on band gap energy of TiO_2 nanoparticles. *Journal of Applied Spectroscopy*, 2015, **82**, 303–306, doi: 10.1007/s10812-015-0102-3.
67. PARK, H., PARK, Y., KIM, W., CHOI, W. Surface modification of TiO_2 photocatalyst for environmental applications. *Journal of Photochemistry and Photobiology, C: Photochemistry Reviews*, 2013, **15**, 1–20, doi: 10.1016/j.jphotochemrev.2012.10.001.
68. KURNIAWAN, T.A., MENGTING, Z., FU, D., YEAP, S.K., OTHMAN, M.H.D., AVTAR, R., OUYANG, T. Functionalizing TiO_2 with graphene oxide for enhancing photocatalytic degradation of methylene blue (MB) in contaminated wastewater. *Journal of Environmental Management*, 2020, **270**, 1–8, doi: 10.1016/j.jenvman.2020.110871.
69. POOLWONG, J., KIATBOONYARIT, T., ACHIWAWANICH, S., BUTBUREE, T., KHEMTHONG, P., KITYAKARN, S. Three-dimensional hierarchical porous TiO_2 for enhanced adsorption and photocatalytic degradation of Remazol dye. *Nanomaterials*, 2021, **11**(7), 1–11, doi: 10.3390/nano11071715.
70. KABIR, R., SAIFULLAH, MD.A.K., AHMED, A.Z., MASUM, S.MD., MOLLA, MD.A.I. Synthesis of N-doped ZnO nanocomposites for sunlight photocatalytic degradation of textile dye pollutants. *Journal of Composites Science*, 2020, **4**(2), 1–10, doi: 10.3390/jcs4020049.
71. BOUTRA, B., SEBTI, A., TRARI, M. Photocatalytic treatment of synthetic and real textile wastewater using zinc oxide under the action of sunlight. *Theoretical and Experimental Chemistry*, 2021, **57**, 226–236, doi: 10.1007/s11237-021-09692-4.
72. ELBADAWY, H.A., SADIK, W.A., ELHUSSEINY, A.F., HUSSEIN, S.M. Design of economic photocatalytic system with low energy consumption, and high quantum yield, for the degradation of Acid Red 37 textile dye. *Process Safety and Environmental Protection*, 2021, **148**, 1191–1206, doi: 10.1016/j.psep.2021.02.036.
73. FAZIL, A.A., NARAYANAN, S., BEGUM, M.S., MANIKANDAN, G., YUVASHREE, M. Green

synthesis strategy for producing doped and undoped ZnO nanoparticles: Their photocatalytic studies for industrial dye degradation. *Water Science and Technology*, 2021, **84**(10–11), 2958–2967, doi: 10.2166/wst.2021.308.

74. YASHNI, G., AL-GHEETHI, A., RADIN MOHAMED, R.M.S., DAI-VIET, N.V., AL-KAHTANI, A.A., AL-SAHARI, M., NOR HAZHAR, N.J., NOMAN, E., ALKHADHER, S. Bio-inspired ZnO NPs synthesized from *Citrus Sinensis* peels extract for Congo red removal from textile wastewater via photocatalysis: Optimization, mechanisms, techno-economic analysis. *Chemosphere*, 2021, **281**, 1–12, doi: 10.1016/j.chemosphere.2021.130661.
75. SHARMA, M., SONDHI, H., KRISHNA, R., SANJEEV KUMAR, S., RAJPUT, P., NIGAM, S., JOSHI, M. Assessment of GO/ZnO nanocomposite for solar-assisted photocatalytic degradation of industrial dye and textile effluent. *Environmental Science and Pollution Research*, 2020, **27**, 32076–32087, doi: 10.1007/s11356-020-08849-3.
76. ABDEL-WAHED, M.S., ABDEL-KARIM, A., MARGHA, F.H., GAD-ALLAH, T.A. UV sensitive ZnO and TiO_2-ZnO nanocrystalline transparent glass-ceramic materials for photocatalytic decontamination of surface water and textile industry wastewater. *Environmental Progress & Sustainable Energy*, 2021, **40**(5), 1–11, doi: 10.1002/ep.13653.
77. JUAY, J., YANG, J.C.E., BAI, H., SUN, D.D. Novel ultralong and photoactive $Bi_2Ti_4O_{11}/TiO_2$ heterojunction nanofibers toward efficient textile wastewater treatment. *RSC Adv*ances, 2022, **12**(39), 25449–25456, doi: 10.1039/d2ra02181a.
78. PAŹDZIOR, K., BILIŃSKA, L. Microscopic analysis of activated sludge in industrial textile wastewater treatment plant. *Autex Research Journal*, 2022, **22**(3), 358–364, doi: 10.2478/aut-2020-0050.
79. ANCY, K., BINDHU, M.R., BAI, J.S., GATASHEH, M.K., HATAMLEH, A.A., ILAVENIL, S. Photocatalytic degradation of organic synthetic dyes and textile dyeing waste water by Al and F co-doped TiO_2 nanoparticles. *Environmental Research*, 2022, **206**, 1–9, doi: 10.1016/j.envres.2021.112492.
80. WANG, Y., LU, K., FENG, C. Influence of inorganic anions and organic additives on photocatalytic degradation of methyl orange with supported polyoxometalates as photocatalyst. *Journal of Rare Earths*, 2013, **31**(4), 360–365, doi: 10.1016/S1002-0721(12)60286-5.
81. MOHAMED, W.A.A., IBRAHEM, I.A., EL-SAYED, A.M., GALAL, H.R., HANDAL, H., MOUSA, H.A., LABIB, A.A. Zinc oxide quantum dots for textile dyes and real industrial wastewater treatment: Solar photocatalytic activity, photoluminescence properties and recycling process. *Advanced Powder Technology*, 2020, **31**(6), 2555–2565, doi: 10.1016/j.apt.2020.04.017.
82. AGUSTINA, T.E., ANG, H.M., VAREEK, V.K. A review of synergistic effect of photocatalysis and ozonation on wastewater treatment. *Journal of Photochemistry and Photobiology C: Photochemistry Reviews*, 2005, **6**(4), 264–273, doi: 10.1016/j.jphotochemrev.2005.12.003.
83. DESA, A.L., HAIROM, N.H.H., NG, L.Y., NG, C.Y., AHMAD, M.K., MOHAMMAD, A.W. Industrial textile wastewater treatment via membrane photocatalytic reactor (mpr) in the presence of ZnO-PEG nanoparticles and tight ultrafiltration. *Journal of Water Process Engineering*, 2019, **31**, 1–11, doi: 10.1016/j.jwpe.2019.100872.
84. CERETTA, M.B., VIEIRA, Y., WOLSKI, E.A., FOLETTO, E.L., SILVESTRI, S. Biological degradation coupled to photocatalysis by ZnO/polypyrrole composite for the treatment of real textile wastewater. *Journal of Water Process Engineering*, 2020, **35**, doi: 10.1016/j.jwpe.2020.101230.

S. Natarajan, V. Ramesh Babu, S. Ariharasudhan, P. Chandrasekaran, S. Sundaresan
Kumaraguru College of Technology, Department of Textile Technology,
Coimbatore, 641049, India

Investigating the Effect of Knot Configuration and Suture Diameter on the Knot Performance of Silk Sutures

Raziskava vpliva konfiguracije vozla in premera šiva na učinkovitost svilenih šivov

Original scientific article/*Izvirni znanstveni članek*
Received/Prispelo 10-2022 • Accepted/Sprejeto 7-2023

Corresponding author/*Korespondenčni avtor:*
Assist Prof S. Natarajan
E-mail: natarajan.s.txt@kct.ac.in
Phone: +91 98435 23479
ORCID: 0000-0002-8759-3704

Abstract

Knot configurations serve as the foundation for postoperative tissue repair. Loosening surgical knots during or after tying might lead to an unsuccessful suture and compromise the outcome. This investigation was carried out to study the mechanical properties of knotted silk sutures that are made from braided structures with three different diameters. A maximum tensile strength (33.24 N) and minimum breaking elongation (15%) of dry suture, maximum tensile strength (22.6 N) and minimum breaking elongation (13.6%) of wet suture were achieved with five throws and a diameter of 0.3 mm with surgeon's square knot.
Keywords: knot configurations, tensile strength

Izvleček

Konfiguracije vozlov so osnova za pooperativno obnovo tkiva. Razrahljanje kirurških vozlov med zavezovanjem ali po njem lahko privede do neuspešnega šivanja in ogrozi izid. Raziskava je bila izvedena z namenom proučiti mehanske lastnosti vozlastih svilenih šivov, izdelanih iz pletenih struktur treh različnih premerov. Najvišja natezna trdnost 33,24 N in najnižji pretržni raztezek 15 odstotkov v suhem ter natezna trdnost 22,6 N in najnižji pretržni raztezek 13,6 odstotka v mokrem so bili doseženi z uporabo kirurškega kvadratnega vozla s petimi zavozljaji in premerom šiva 0,302 mm.
Ključne besede: oblike vozlov, natezna trdnost

1 Introduction

The mechanical property of a suture, such as its tensile and knot strength, is often correlated to its success. Sutures require knotting in order to achieve optimal tissue closure strength. The knot also represents a large amount of material in the body that could cause discomfort [1].

Suture security is the ability of a knot to uphold tissue approximation during recovery without slippage, unravelling and breaking. When a suture loop that surrounds an artery is dislodged, bleeding can

occur. To reduce suture slippage, more throws can be introduced. However, these additional throws are more time-consuming, which increases the duration of an operative procedure. Additional throws also reduce the resistance of a wound to infection. Thus, surgeons prefer to make a secure knot with the fewest number of throws. It is important for a surgeon to understand available quantitative information related to the performance of a surgical suture during wound closure [2, 3].

Brent [4] studied the effect of suture type and size on knot performance and concluded that the type of knot used in wound closure affects knot security. Sutures size also plays an important role in knot performance, especially in monofilament sutures.

Frictional force holds a knot together, and resistance can be attributed to suture material deformation. Bending and contraction are two types of deformation. Because braided sutures have a lower bending stiffness than monofilament sutures, the handling characteristics of braided sutures are mostly due to surface friction. However, with monofilament sutures, the impacts of suture bending stiffness and plasticity cannot be overlooked [5].

A knot-secured loop with a set perimeter is one component of a suture used to connect injured tissue. By retaining the tissue within the loop, it compresses the adjoining surfaces. A knot holds tissues together. After it has been secured, more throws can be added to ensure knot security and minimise bleeding. As a result, the knot is made up of multiple throws that are close together. The ears are the clipped ends of the suture that help to keep the loop from unravelling owing to slippage [6].

The surface characteristics of a suture material affect knot performance. The coefficient of friction for a braided construction is higher because the threads are mobile, which enhances the knot-holding ability. Knot untying does not occur after knot failure in braided constructions, which have strong mechanical qualities and knot security with only two-throw knots. Thus, more throws are not required to improve knot strength [7, 8].

Braid angle also affect the breaking load and elongation of a suture. The knot in a suture decreases the breaking load and rupture occurs consistently at the knot region. Flexural, frictional and compressive force are the three main forces developed inside a knot when a knotted suture is subjected to longitudinal pull [9].

Ben Abdessalem [10] investigated the effect of suture friction on knot performance, and his findings revealed that increasing the suture-to-suture coefficient of friction results in good knot security but increases resistance to the motion of strands contributing to the knot, making it difficult to control the sliding of sutures. The bending rigidity of a suture is proportional to the knot tie-down.

The results of this study provide insight into the effect of suture size, knot configuration and the number of throws per knot on the mechanical performance of a knotted suture.

2 Materials and methods

2.1 Materials

Mulberry silk filaments from United States Pharmacopoeia (USP), sizes 0, 2/0 and 3/0, which are a set of standardised sizes used in medicine to describe the thickness or diameter of surgical sutures, were chosen. The filaments were braided into three different diameters of 0.23 mm, 0.30 mm and 0.37 mm. The diameter was determined through trial and error by adjusting the machine's take-off speed. The suture was pre-soaked in a normal saline solution at room temperature for at least five minutes for the purpose of measuring wet strength. A braid structure of 1/2 was selected as result of optimised results from previous work.

A circular braiding with 14 carriers and bobbins with a size of 48 mm x180 mm was used to produce a braided structure. The machine used operates at a speed of 360 rpm, which allows for the creation of braids with different colours, textures and thicknesses.

2.2 Knot configuration

In this study, a surgeon's square knot, square knot and granny knot were chosen, as shown in Figure 1. In a surgeon's knot, a double wrap throw is followed by a single throw. In a granny knot, the right ear and loop cross or escape on opposite sides of the knot. In a square knot, the right ear and loop of a two-throw knot exit on the same side of the knot and are parallel to each other. Sutures were knotted around a stainless-steel mandrel with a 34 mm diameter to maintain the standard loop length of all knots created [11].

A surgeon must complete two steps to tie a knot. The initial step is to use a one-throw or two-throw knot on the wound surface to achieve the precise approximation of the wound boundaries. The surgeon obtains a preview of the final fixation of the wound margins once the throw or throws contact the wound. The second stage of knot tying is to complete the knot with additional throws, which will secure the wound edges together and promote healing. The number of additional throws required will depend on the type of suture material used and the thickness of the tissue being sutured. Once the knot is complete, the surgeon trims any excess suture material and closes the skin or tissue layers above the knot to finish the procedure [12]. The additional throws are made to enhance the security and stability of a knot. Here, throws are meant for additional throws over the base knot. The granny knot is rarely used by surgeons. However, understanding its properties helps assess knot security in surgery. Surgeons choose knots based on tissue type, tension, and desired security.

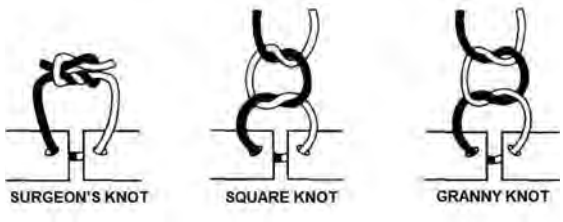

Figure 1: Knot configurations [12]

2.3 Experimental design

Design Expert Software uses a Response Surface Methodology (RSM) to determine the optimum point in Central Composite Design optimisation. RSM is a statistical technique that uses mathematical models to represent the relationship between the input variables (factors) and the output variable (response). The software fits a mathematical model to the experimental data and subsequently employs this model to predict the response at any combination of the input variables.

The effects of knot configuration and number of throws on tensile strength and elongation under wet and dry conditions were studied. Since the response surface approach provides a good coefficient approximation to identify the relation between parameters and response, they were studied using Central Composite Design (CCD) [13]. CCD is a statistical technique used in experimental design to optimise a process for non-numerical or categorical input. It involves systematically varying input variables in a series of experiments and analysing the data to identify the optimal input values for the desired output. To use CCD for non-numerical variables, they are first converted into categorical variables and assigned numerical values for analysis. This method can then be used in the same way as for numerical input variables. Design Expert 13 programme was employed for regression, graphical analysis and optimisation.

This is a complete factorial design enhanced with a second-order fractional factorial design, centre points, and axial points. There are three sorts of design points in a central composite design: factorial, axial and centre points. The number of experimental runs in this study was 11, equivalent to four factorial points, four axial points of each numerical factor and three centre point replications for one level of categorical component. As a result, the total number of experimental runs for three level categorical factors was 33. The numerical components were the number of throws and suture size. Knot configuration is the categorical factor.

The knot configurations used in this study are given in Table 1. The experimental table is created

using these boundary ranges and the Central Composite Design (CCD) to get tensile strength and breaking under wet and dry conditions (Table 2).

ANOVA was used to validate the equations, and a result of $p < 0.05$ was declared statistically significant. The coefficient of determination R^2 and expected R^2 transferred the nature of the fitted quadratic model (Pred-R^2). The response surface was utilised to determine the test variable's individual, and interaction impacts on the handling attributes.

Table 1: Experimental range of independent variables

Variable	Variable type	Levels		
		-1	0	1
No. of throws (X1)	Numerical	3	4	5
Suture diameter (mm) (X2)		0.23	0.30	0.37
Knot configuration (X3)	Categorical	Surgeon's knot (SS)	Square knot (S)	Granny knot (G)

2.4 Evaluation of tensile and knot performance braided silk suture

The mechanical performance of a knot was determined by measuring knot break force. A Dak-universal testing instrument was used to assess straight-pull tensile strength and knot-pull tensile strength. The gauge length was maintained at 150 mm, while the rate of extension was kept constant at 90 mm/min. Each sample was analysed five times. To assess the tensile strength and knot security of sutures with distinct structures, all samples were examined at the same gauge length[14]. An adjustable dynamometer grip was used to capture the top end suture for longitudinal traction. All tests were conducted at a temperature of 21°C and a relative humidity of 65%.

Table 2: Experimental design for independent variables and their response values

Sample	Factors			Responses/Test condition			
				Dry		Wet	
	No. of throws (X_1)	**Suture diameter (X_2)**	**Knot configuration (X_3)**	**Tensile strength (N)**	**Breaking elongation (%)**	**Tensile strength (N)**	**Breaking elongation (%)**
1	3	0.23	SS	28.0	18	20.2	16
2	5	0.23	SS	33.0	16	23.4	15
3	3	0.37	SS	29.2	21	21.3	19
4	5	0.37	SS	35.9	20	25.7	17
5	3	0.30	SS	29.0	17	20.5	15
6	5	0.30	SS	34.0	15	23.4	13
7	4	0.23	SS	31.0	18	22.2	16
8	4	0.37	SS	34.0	20	24.6	17
9	4	0.30	SS	29.0	16	20.4	14
10	4	0.30	SS	28.5	16	20.5	15
11	4	0.30	SS	29.0	16	20.7	14
12	3	0.23	S	25.5	19	18.4	17
13	5	0.23	S	29.7	17	21.0	15
14	3	0.37	S	26.3	23	18.3	21
15	5	0.37	S	32.3	21	22.4	19

Continuation of Table 2.

16	3	0.30	S	26.1	21	18.6	18
17	5	0.30	S	30.6	18	21.4	15
18	4	0.23	S	27.9	19	20.3	16
19	4	0.37	S	30.6	21	21.4	18
20	4	0.30	S	26.0	18	18.2	15
21	4	0.30	S	24.5	18	17.6	16
22	4	0.30	S	26.1	18	18.1	16
23	3	0.23	G	24.0	16	17.7	14
24	5	0.23	G	26.7	15	19.2	13
25	3	0.37	G	23.7	19	17.1	18
26	5	0.37	G	29.1	17	20.4	14
27	3	0.30	G	23.5	16	16.6	15
28	5	0.30	G	27.5	13	19.7	11
29	4	0.23	G	25.1	17	18.3	16
30	4	0.37	G	27.5	18	19.0	16
31	4	0.30	G	23.5	14	17.4	12
32	4	0.30	G	23.0	15	16.1	12
33	4	0.30	G	23.5	15	16.0	12
Standard deviation				3.3	2.3	2.4	2.3

3 Results and discussion

3.1 Effect of knot configuration and suture size on tensile strength of dry suture

It is evident from the contour plot that increasing the number of throws and suture diameter generally leads to an increase in tensile strength. The contour plot also shows that the knot configuration has a significant effect on tensile strength.

Equations 1–3 express the coefficients of the response surface models of tensile strength for each suture.

The contour lines for different knot configurations are not parallel, indicating that the effect of the number of throws and suture diameter on tensile strength depends on knot configuration. Specifically, the highest tensile strength is observed for the surgeon's knot configuration, followed by the square knot (S) knot and granny knot (G) configurations, respectively. The highest value of tensile strength of dry suture, 34 N, was obtained at five throws, a suture diameter of 0.30 mm and a surgeon's knot, as shown in Figure 2a.

Figure 2b shows the contour plot for the effect of the number of throws and suture diameter on the tensile strength of dry suture of a square knot. The increase in number of throws results in an increase in tensile strength of dry suture at all levels. Figure 2c illustrates the contour plot for the effect of the number of throws and suture diameter on the tensile strength of dry suture of a granny knot.

The mean tensile strength of dry suture was 28 N, while the mean tensile strength of wet suture was 20 N. This suggests that exposure to moisture has a negative effect on the tensile strength of the material. The standard deviation for the tensile strength of dry suture was 3.4 N, while the standard deviation for the tensile strength of wet suture was 2.4 N. This indicates that there is some variability in strength measurements within each condition.

Surgeon's knot (1)

$$\textit{Tensile strenght of dry suture (N)} = +67.11 - 6.02\,x_1/mm - 224.06\,x_2/mm + 7.47\,x_1x_2/mm - 0.820\,x_1^2 + 351.83\,x_1^2/mm^2$$

Square knot (2)

$$\textit{Tensile strenght of dry suture (N)} = +65.96 - 6.35\,x_1/mm - 226.46\,x_2/mm + 7.47\,x_1x_2/mm - 0.820\,x_1^2 + 351.83\,x_1^2/mm^2$$

Granny knot (3)

$$\textit{Tensile strenght of dry suture (N)} = +65.25 - 6.77\,x_1/mm - 230.42\,x_2/mm + 7.47\,x_1x_2/mm - 0.820\,x_1^2 + 351.83\,x_1^2/mm^2$$

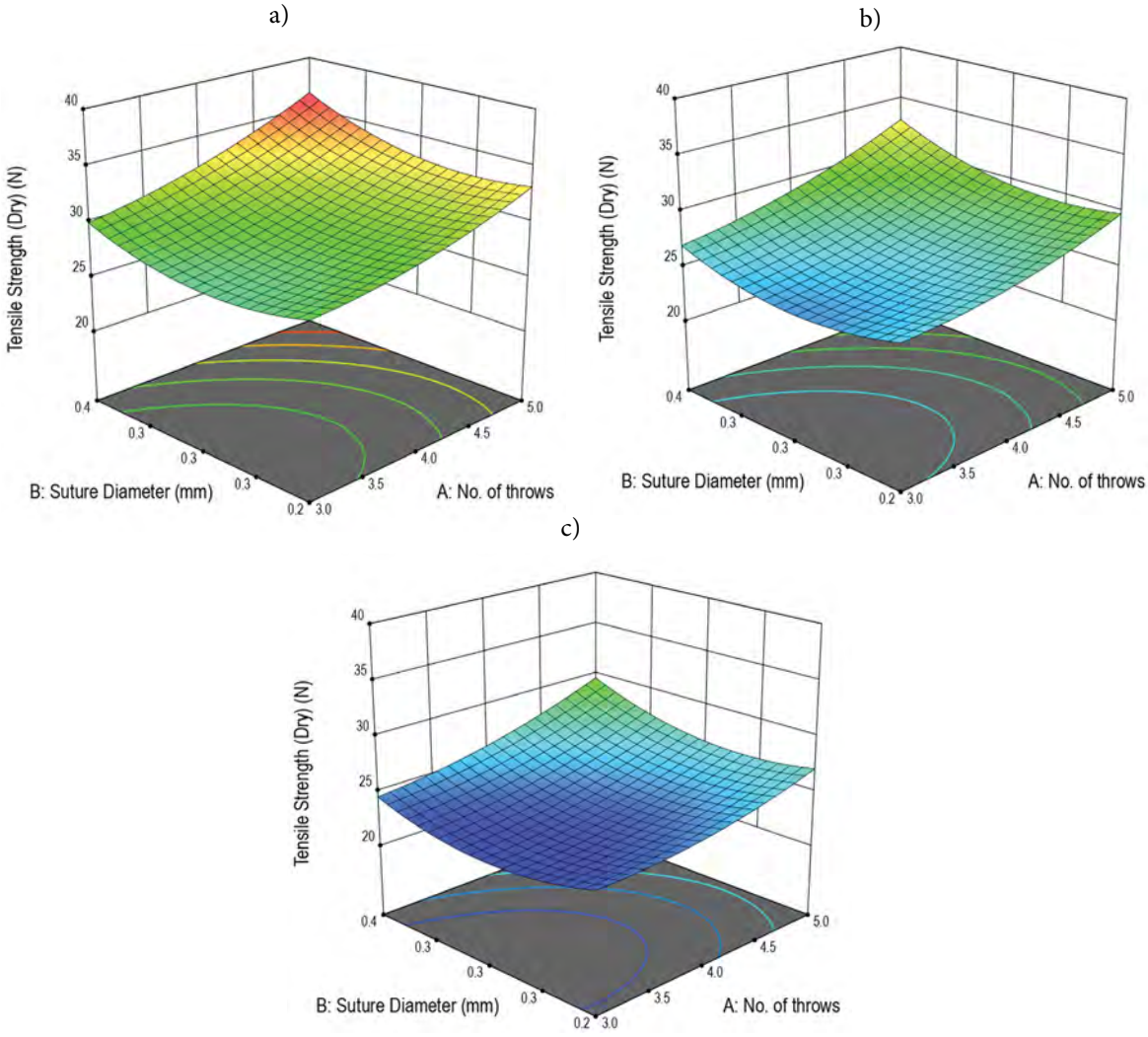

Figure 2: Effect of number of throws and suture diameter on tensile strength of (a) surgeon's knot, (b) square knot and (c) granny knot

3.2 Effect of knot configuration and suture size on elongation of dry suture

The coefficients of the response surface models of elongation for each braided structure are expressed in Equations 4–6. It is evident from Figure 3a that breaking elongation decreases as the number of throws increases. This may be because the number of throws increased at a higher level made the suture more rigid. The highest value of elongation of dry suture (23%) was obtained at three throws, a suture diameter of 0.37 mm and a square knot. Figure 3b illustrates the effect of the number of throws and

suture diameter of a square knot on breaking elongation. Figure 3c illustrates the effect of the number of throws and suture diameter on the elongation of dry suture of a granny knot. The difference between loop and knot security is that a suture material with a large elastic elongation can stretch, resulting in a loose loop, even if the knot is completely secure. The ideal knot would be easy to tie and reproducible, and would not slide back or extend before the tissue healed [15].

Surgeon's knot (4)

$$\textit{Elongation of dry suture (\%)} = +47.82 - 0.85\,x_1 - 344.09\,x_2/mm + 3.57\,x_1x_2/mm - 0.131\,x_1^2 + 585.39\,x_1^2/mm^2$$

Square knot (5)

$$\textit{Elongation of dry suture (\%)} = +49.44 - 6.55\,x_1 - 124.41\,x_2/mm + 8.98\,x_1x_2/mm - 0.71\,x_1^2 + 247.04\,x_1^2/mm^2$$

Granny knot (6)

$$\textit{Elongation of dry suture (\%)} = +49.04 - 3.86\,x_1 - 280.77\,x_2/mm + 3.57\,x_1x_2/mm - 0.47\,x_1^2 + 515.57\,x_1^2/mm^2$$

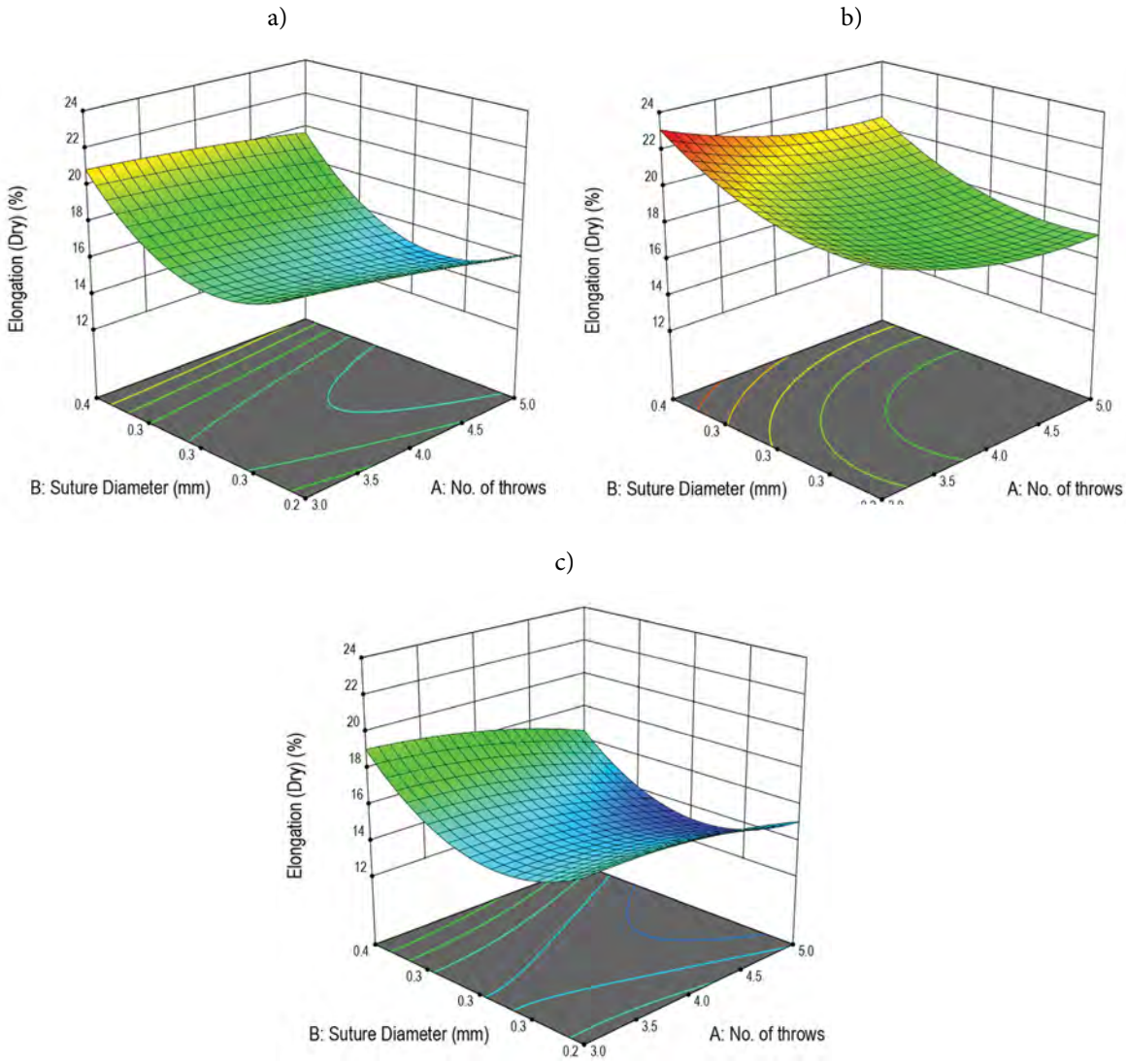

Figure 3: Effect of number of throws and suture diameter on elongation of (a) surgeon's knot, (b) square knot and (c) granny knot in dry state

3.3 Effect of knot configuration and suture size on tensile strength of wet suture

In terms of p-values, the number of throws (X_1), suture diameter (X_2), knot configuration (X_3) and their squared values Size USP (X_2) have significant effects (p-valuee less than 0.0500) on tensile strength of wet suture. The coefficients of the response surface models of tensile strength of wet suture for each knot are expressed in Equations 8–10.

Surgeon's knot (7)

$$\textit{Tensile strenght of wet suture (N)} = +49.9 - 2.63\,x_1/mm - 194.6\,x_2/mm + 3.5\,x_1x_2/mm - 0.4\,x_1^2 + 320.4\,x_1^2/mm^2$$

Square knot (8)

$$\textit{Tensile strenght of wet suture (N)} = +49.6 - 2.63\,x_1/mm - 201.7\,x_2/mm + 3.5\,x_1x_2/mm - 0.4\,x_1^2 + 320.4\,x_1^2/mm^2$$

Granny knot (9)

$$\textit{Tensile strenght of wet suture (N)} = +49.3 - 2.9\,x_1/mm - 201.7\,x_2/mm + 3.5\,x_1x_2/mm - 0.4\,x_1^2 + 320.4\,x_1^2/mm^2$$

a) b)

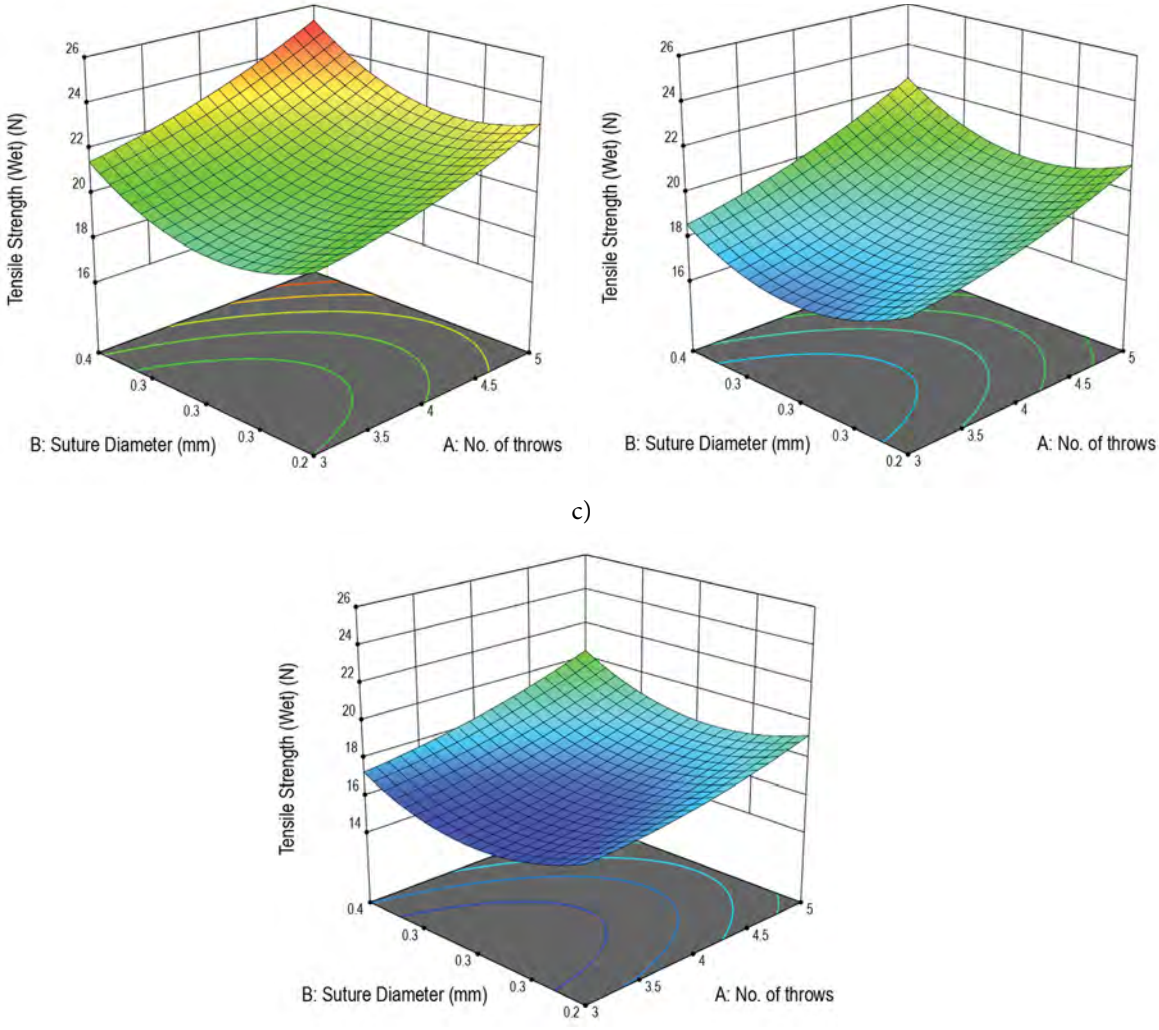

Figure 4: Effect of number of throws and suture diameter on tensile strength of (a) a surgeon's knot, (b) a square knot and (c) a granny knot in wet state

Figure 4a illustrates the contour plot for the effect of the number of throws and suture diameter on the tensile strength of wet suture of a surgeon's knot. The highest value of tensile strength of wet suture, 25.7 N, was obtained at five throws, a suture diameter of 0.37 mm and a surgeon's knot. The results show that an increase in suture diameter results in an increase in tensile strength.

Figure 4b illustrates the contour plot for the effect of the number of throws and suture diameter on the tensile strength of wet suture of a square knot. The increase in number of throws results in increase in tensile strength of wet suture at all levels. Figure 4c illustrates the contour plot for the effect of the number of throws and suture diameter on the tensile strength of wet suture of a granny knot.

3.4 Effect of knot configuration and suture size on elongation of wet suture

The coefficients of the response surface models of elongation for each braid structure are expressed in Equations 10–12. It is evident from Figure 5a that breaking elongation decreases as the number of throws increases. This may be because the number of throws increased at a higher level made

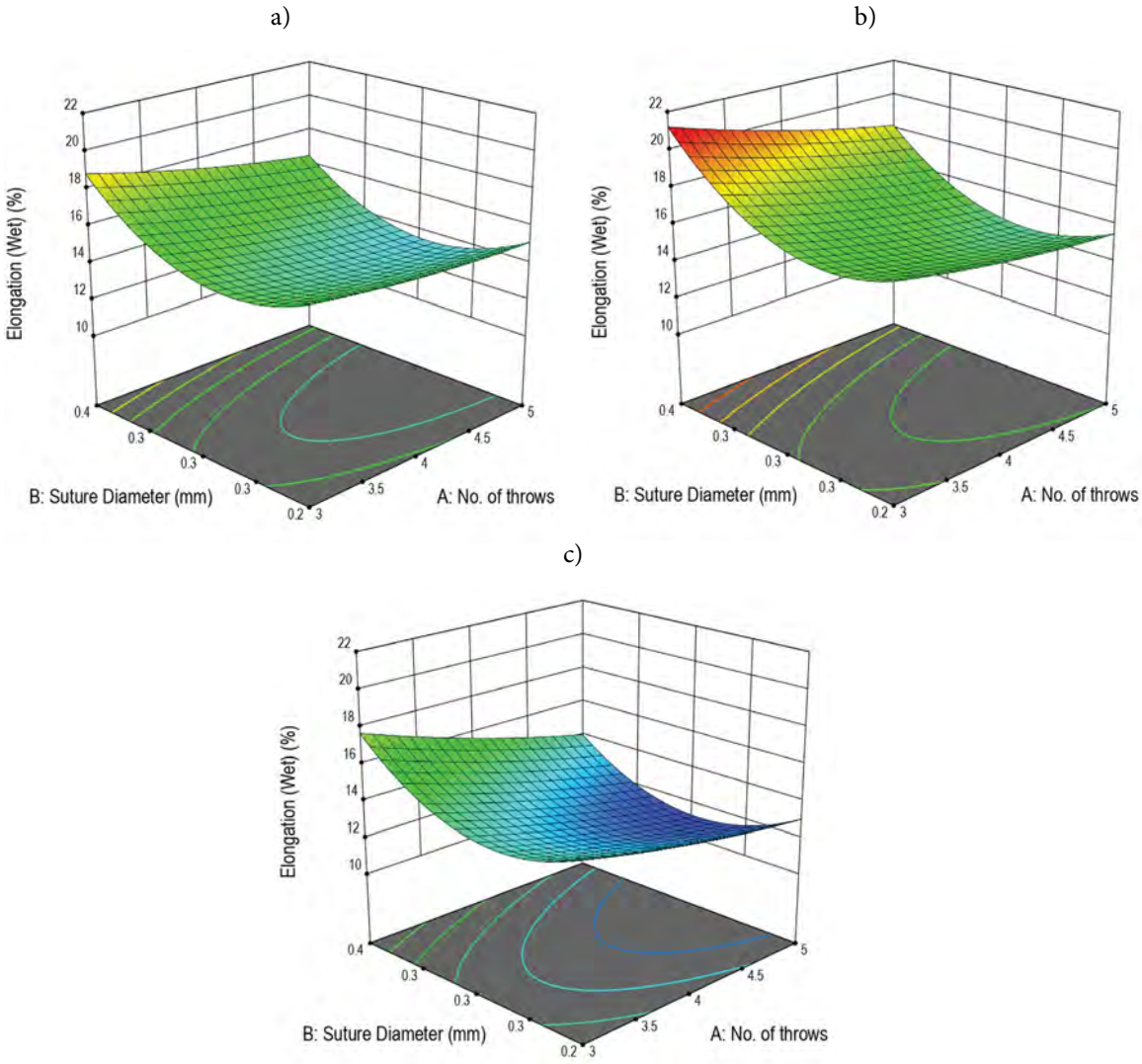

Figure 5: Effect of number of throws and suture diameter on elongation of (a) a surgeon's knot, (b) a square knot and (c) a granny knot in wet state

Surgeon's knot (10)

$$\textit{Elongation of wet suture (\%)} = +52.4 - 1.2\,x_1 - 240.5\,x_2/mm - 4.7\,x_1x_2/mm + 0.23\,x_1^2 + 456.4\,x_1^2/mm^2$$

Square knot (11)

$$\textit{Elongation of wet suture (\%)} = +52.2 - 1.6\,x_1 - 231.1\,x_2/mm - 4.7\,x_1x_2/mm + 0.23\,x_1^2 + 456.4\,x_1^2/mm^2$$

Granny knot (12)

$$\textit{Elongation of wet suture (\%)} = +54.1 - 1.9\,x_1 - 242.9\,x_2/mm - 4.7\,x_1x_2/mm + 0.23\,x_1^2 + 456.4\,x_1^2/mm^2$$

the suture more rigid. The highest value of elongation of wet suture (21%) was obtained at three throws, a suture diameter of 0.37 mm and a square knot. Figure 5b illustrates the effect of the number of throws and suture diameter of a square knot on breaking elongation. Figure 5c illustrates the effect of the number of throws and suture diameter on the elongation of wet suture of a granny knot.

3.5 Effect of wet condition on tensile strength of knot

During surgical procedures, sutures are exposed to bodily fluids, such as blood, which would compromise the strength of the knot. By evaluating the knot strength in wet conditions, surgeons can get a more accurate representation of how the suture will perform post-surgery. In this study, tensile strength of dry suture had a mean of 28 N with a standard deviation of 3.4, while tensile strength of wet suture had a mean of 20 N with a standard deviation of 2.4.

A t-test was performed to compare the means of dry and tensile strength of wet suture. The critical value for a two-tailed test at a significance level of 0.05 was 2.0 using a t-table with 64 degrees of freedom (33 + 33 - 2). Since the calculated t-value of 11.11 is greater than the critical value of 2.0, the null hypothesis can be rejected, and it was concluded that there is a significant difference between the mean tensile strength of dry suture and the mean tensile strength of wet suture. Under wet conditions, the knot's tensile strength decreases by 28%.

3.6 Optimisation of handling characteristics

Design Expert Software was used to generate optimised values of independent variables for the analysis of braided suture knot performance. The purpose of this optimisation process was to achieve a determined response that satisfies all variables properties. The goals were set as shown in Table 3. It is important to note that a loose suture will not hold tissue in place [16]. As a result, the goal for suture elongation

Table 3: Constraints used for optimisation

Response	Goal	Lower limit	Upper limit
Tensile strength of dry suture (N)	Maximum	23.0	35.9
Elongation of dry suture (%)	Minimum	13	23
Tensile strength of wet suture (N)	Maximum	16.0	25.7
Elongation of wet suture (%)	Minimum	11	21

Table 4: Forecasted values given by the model

Independent variables	Values	Dependent variables	Predicted values
No. of throws (X_1)	5	Tensile strength of dry suture (N)	33.240
Suture diameter (mm) (X_2)	0.3	Elongation of dry suture (%)	15
Knot configuration, (X_3)	Surgeon's knot (SS)	Tensile strength of wet suture (N)	22.6
		Elongation of wet suture (%)	13.6

Table 5: Experimental results conducted at optimum parameters

S. no.	No. of throws (X_1)	Suture diameter (mm) (X_2)	Knot configuration (X_3)	Tensile strength of dry suture (N)			Elongation of dry suture (%)			Tensile strength of wet suture (N)			Elongation of wet suture (%)		
				PV[a]	EV[b]	Error (%)	PV	EV	Error (%)	PV	EV	Error (%)	PV	EV	Error (%)
1	5	0.3	SS	33.25	34.2	-2.86	15.14	14.85	1.92	22.67	23	-3.71	13.62	13.2	3.08
2	5	0.3	SS	33.21	33.85	-1.93	15.16	15.2	-0.26	22.67	23	-1.46	13.63	13.4	1.69
3	5	0.3	SS	33.26	33.75	-1.47	15.12	15	0.79	22.67	23	-2.47	13.61	13.8	-1.4

[a] Predicted values; [b] Experimental values

in dry and wet conditions was kept at a minimum.

Based on the results, it can be concluded that the knot performance of a suture was not dependent on a single factor. Table 4 presents the forecasted values of the number of throws, suture diameter and knot configuration given by the model. Table 5 shows the error percent between the predicted and experimental values, which were conducted as repeated runs based on optimisation process parameters.

4 Conclusion

The effect of suture diameters (0.23 mm, 0.30 mm and 0.37 mm) and knot configuration with the following configuration: surgeon's square knot, square knot and granny knot, number of throws analysed for their mechanical properties during wet and dry state comparisons. The optimum independent variables for the maximum tensile strength (33.24 N) and minimum breaking elongation (15%) of dry suture, maximum tensile strength (22.6 N) and minimum breaking elongation (13.6%) of wet suture were achieved with five throws and a diameter of 0.3 mm with surgeon's square knot.

References

1. ALTMAN, Gregory H., DIAZ, Frank, JAKUBA, Caroline, CALABRO, Tara, HORAN, Rebecca L., CHEN, Jingsong, LU, Helen, RICHMOND, John, KAPLAN, David L. Silk-based biomaterials. *Biomaterials*, 2003, **24**(3), 401–416, doi: 10.1016/S0142-9612(02)00353-8.
2. ERGÜN, Selim, AKGÜN, Umut, KARAHAN, Mustafa. The effect of loop size on loop security and elongation of a knot. *Orthopaedics & Traumatology: Surgery & Research,* 2020, **106**(1), 35–38, doi:10.1016/J.OTSR.2019.10.008.
3. DEBBABI, Faten, ABDESSALEM, Saber B. New approach for appreciating the surgeon's satisfaction of braided sutures. *Journal of Industrial Textiles*, 2015, **46**(6), 1319–1341, doi: 10.1177/1528083715622426.
4. FAULKNER, Brent C., TRIBBLE, Curtis G., THACKER, John G., RODEHEAVER, George T., EDLICH, Richard F. Knot performance of polypropylene sutures. *Journal of Biomedical Materials Research*, 1996, **33**(3), 187–192, doi: 10.1002/(SICI)1097-4636(199623)33:3<187::AID-JBM8>3.0.CO;2-M.
5. TOMITA, N., TAMAI, S., MORIHARA, T., IKEUCHI, K., IKADA, Y. Handling characteristics of braided suture materials for tight tying. *Journal of Applied Biomaterials*, 1993, **4**(1), 61–65, doi: 10.1002/JAB.770040108.
6. IVY, Joseph J., UNGER, James B., HURT, Jason, MUKHERJEE, Debi. The effect of number of throws on knot security with nonidentical sliding knots. *American Journal of Obstetrics and Gynecology*, 2004, **191**(5), 1618–1620, doi: 10.1016/J.AJOG.2004.05.029.
7. KIM, Jin-Cheol, LEE, Yong-Keun, LIM, Bum-Soon, RHEE Sang-Hoon, YANG, Hyeong-Cheol. Comparison of tensile and knot se-

curity properties of surgical sutures. *Journal of Materials Science. Materials in Medicine*, 2007, **18**(12), 2363–2369, doi: 10.1007/S10856-007-3114-6.

8. BAYRAKTAR, E. Karaca, HOCKENBERGER, A. Şengönül. Investigating the knot performance of silk, polyamide, polyester, and polypropylene sutures. *Textile Research Journal,* 2016, **71**(5), 435–440, doi: 10.1177/004051750107100511.
9. HRISTOV, Krasimira, ARMSTRONG-CARROLL, Eileen, DUNN, Matt, PASTORE, Christopher, GOWAYED, Yasser. Mechanical behavior of circular hybrid braids under tensile loads. *Textile Research Journal*, 2016, **74**(1), 20–26, doi: 10.1177/004051750407400104.
10. BEN ABDESSALEM, Saber, DEBBABI, Faten, JEDDA, Hanen, ELMARZOUGUI, Saber, MOKHTAR, Sofiene. Tensile and knot performance of polyester braided sutures. *Textile Research Journal,* 2009, **79**(3), 247–252, doi: 10.1177/0040517508094090.
11. IM, Jung Nam, KIM, Jeong Kyung, KIM, Hyun Kyoon, LEE, Kuen Yong, PARK, Won Ho. Effect of tying conditions on the knot security of suture materials. *Journal of Applied Polymer Science,* 2008, **109**(2), 918–922, doi: 10.1002/APP.28109.
12. SILVER, E., WU, R., GRADY, J., SONG, L. Knot security-how is it affected by suture technique, material, size, and number of throws? *Journal of Oral and Maxillofacial Surgery,* 2016, **74**(7), 1304–1312, doi: 10.1016/j.joms.2016.02.004.
13. WASEEM, Muhammad, SALAH, Bashir, HABIB, Tufail, SALEEM, Waqas, ABAS, Muhammad, KHAN, Razaullah, GHANI, Usman, SIDDIQI, Muftooh Ur Rehman. Multi-response optimization of tensile creep behavior of PLA 3D printed parts using categorical response surface methodology. *Polymers*, 2020, **12**(12), 1–16, doi: 10.3390/POLYM12122962.
14. ZIMMER, Christopher A., THACKER, John G., POWELL, David M., BELLIAN, Kenneth T., BECKER, Daniel G., RODEHEAVER, George T., EDLICH, Richard F. Influence of knot configuration and tying technique on the mechanical performance of sutures. *Journal of Emergency Medicine*, 1991, **9**(3), 107–113, doi: 10.1016/0736-4679(91)90313-5.
15. LIVERMORE, Ryan W., CHONG, Alexander C.M., PROHASKA, Daniel J., COOKE, Francis W., JONES, Teresa L. Knot security, loop security, and elongation of braided polyblend sutures used for arthroscopic knots. *American Journal of Orthopedics (Belle Mead, NJ)*, 2010, **39**(12), 569–576.
16. MISHRA, Dev K., CANNON, W. Dilworth, LUCAS, Duncan J., BELZER, John P. Elongation of arthroscopically tied knots. *American Journal of Sports Medicine*, 1997, **25**(1), 113–117, doi: 10.1177/036354659702500122.

Siver Cakar, Andrea Ehrmann
Faculty of Engineering and Mathematics, Bielefeld University of Applied Sciences and Arts, 33619 Bielefeld, Germany

Adhesion and Stab-resistant Properties of FDM-printed Polymer/Textile Composites

Adhezija in odpornost pri vbodu kompozitov, izdelanih s tehnologijo FDM tiskanja polimera na tekstilijo

***Original scientific article**/Izvirni znanstveni članek*
Received/*Prispelo* 6-2023 • Accepted/*Sprejeto* 8-2023

Corresponding author/*Korespondenčna avtorica*:
Prof. Dr. Dr. Andrea Ehrmann
E-mail: andrea.ehrmann@hsbi.de
ORCID: 0000-0003-0695-3905

Abstract

Stab-resistant clothing has been used for centuries by soldiers. Today, it is also used by policemen and other people in dangerous jobs or situations. While chain-mail or metal inserts in protective vests are heavy and uncomfortable, lightweight and bendable alternatives are currently the subject of investigation. Special textile fabrics offer a certain level of stab-resistance that can be improved by different coatings. In this study, we investigated composites of different flexible 3D printing materials, used for the fused deposition modelling (FDM) technique, on woven fabrics. Besides the adhesion between both parts of these composites, the quasi-static stab-resistant properties were investigated and compared with those of pure textile fabrics and 3D prints, respectively.

Keywords: 3D printing, fused deposition modelling (FDM), flexible polymer, stab-resistance, VPAM-KDIW

Izvleček

Proti vbodom odporna oblačila že stoletja uporabljajo vojaki, danes pa tudi policisti in ljudje na nevarnih delovnih mestih ali v nevarnih okoliščinah. Žična pletiva ali kovinski vložki v zaščitnih jopičih so težki in neudobni, zato dandanes raziskujejo lahke in upogljive alternativne materiale. Specialnim tkaninam lahko izboljšajo odpornost proti vbodom z različnimi premazi. V tej raziskavi so bili izdelani tekstilni kompoziti s pomočjo različno upogibljivih polimernih materialov za 3D-tiskanje, ki jih uporabljajo pri modeliranju s spajanjem slojev (FDM). Poleg adhezije med komponentama polimer-tekstilija je bila raziskana tudi odpornost tekstilnih kompozitov proti kvazistatičnim vbodom in izvedena primerjava z lastnostmi tkanin oziroma 3D-tiskanin.

Ključne besede: 3D-tisk, modeliranje s spajanjem slojev, FDM, upogibljiv polimer, odpornost proti vbodu, Združenje testnih centrov za materiale in proti napadom odporne konstrukcije (VPAM), smernice za testiranje »zaščite pred vbodi in udarci« (KDIW)

1 Introduction

Stab-resistant garments are gaining importance due to the increasing amount of fatal stabbing injuries [1]. To avoid heavy and uncomfortable body armour, especially in the case of the long-term use of stab-resistant clothes, today's textiles and other polymer-based stab-resistant garments, which enable drapability, air and water vapor permeability combined with low thermal resistance, are the subject of investigation [2–4].

Textile fabrics for stab-resistance are often prepared from *p*-aramids or ultra-high molecular weight polyethylene (UHMWPE), and sometimes from other technical yarns, such as carbon or S-glass, and are typically used as woven or needle-punched fabrics [5-8]. Ceramic coatings can be applied to improve fibre-fibre friction, hardness and wear resistance [9,10], while coatings with shear-thickening fluids stiffen at the moment of an impact and have practically no effect on fabric drapability [11, 12]. Reinforced polymers and composites, on the other hand, can often absorb more energy, but are usually more rigid [13–15].

Recently, 3D printed stab-resistant body armour has received increasing interest [16–18]. Tests of these samples often show fractures along the printing orientation in the case of fused deposition modelling (FDM) printing [16], which suggests that combining them with textile fabrics would improve in-plane strength.

This approach is reported here, combining woven fabrics with different elastic FDM-printed materials, to investigate the textile/3D-printed composite compared with both single materials. One important parameter required for the formation of a proper stab-resistant composite using 3D printing on a textile fabric is the adhesion between both parts, which is largely influenced by the stand-off distance (commonly referred to as the z-distance) between the nozzle and fabric during printing [19–21]. Stab-resistance itself can be investigated, for example, using dynamic tests, such as the German VPAM-KDIW 2004 [22], the British HOSDB (Home Office Scientific Development Branch) [23] or NIJ standard 0115.00 of the National Institute of Justice of the USA [24, 25]. Quasi-static tests are also defined, e.g. by ASTM F1342 [26], and are performed on universal test machines, where the upper clamp holds a standardized knife, and instead of a lower clamp, a sample holder or a backing with plasticine or foams is applied, and the load-displacement curves are recorded [27]. Quasi-static tests using plasticine and a standardized VPAM-KDIW blade were applied in this study.

2 Materials and methods

All samples were 3D-printed on a plain-woven fabric (thickness 0.45 mm) from Dynel/viscose (70%/30%), with a water contact angle of 64°, i.e. hydrophilic, which may be supportive for the adhesion of a 3D-printed polymer [28].

A Creality CR-10S Pro FDM printer with a nozzle size of 0.4 mm was used to prepare the samples, applying a layer height of 0.2 mm. All materials were printed with a nozzle temperature of 245 °C on an unheated printing bed at a speed of 30 mm/s, an infill density of 100%, applying a rectilinear infill (orientation ±45°), and a flow rate of 110%. The z-distance between the sample surface and nozzle was varied (-0.5 mm, -0.7 mm and -0.8 mm, where negative values denote printing "inside" the sample to improve adhesion).

Three elastic filaments from thermoplastic polyurethane (TPU) were used with a shore hardness of 98 A, 85 A and 82 A, respectively, with the latter being the most elastic.

For adhesion tests, strips measuring 150 mm in length and 25 mm in width were printed on the textile fabric (three samples per material and z-distance). Samples for stab-resistance tests measured 100 mm in length and 100 mm in width, respectively. All samples had a height of 0.4 mm, i.e. 2 layers.

Adhesion tests according to DIN 53530 were performed using a Sauter TVM-N (Kern & Sohn GmbH, Balingen-Frommern, Germany) universal

test machine and evaluated according to ISO 6133, procedure B (recommended for less than twenty peaks per measurement).

For quasi-static stab-resistance tests, a blade according to VPAM-KDIW [22] was inserted into the upper clamp of the universal test machine, while the lower clamp was replaced by a box with plasticine (from Carl Weible KG, Schorndorf, Germany) on which the samples were placed. The plasticity of the plasticine is defined in VPAM-KDIW as follows: a steel ball (diameter of 63.5 mm and a mass of 1039 g) falling on the plasticine from a height of 2.00 m results in an indentation depth of 20 mm ± 2 mm. The tip of the blade stabbed the sample with a constant velocity of 16 mm/min, while force and displacement were measured.

A Camcolms2 digital microscope was used to take microscopic images of the samples.

3 Results and discussion

As an example, Figure 1 depicts a typical measurement of the force-displacement curve during an adhesion test. Such a structure, with many small peaks, is typical for the adhesion of a 3D-printed layer on a woven fabric, since the distance between nozzle and sample surface alternates, and the pores in the woven fabric will not always be identical, so that the imprinted polymer can penetrate more or less, resulting in a variation of the form-locking adhesion between both parts of such a composite.

The results of all adhesion measurements are compared in Figure 2. Generally, a z-distance of -0.7 mm is advantageous, especially for the softest filament with a shore hardness of 82 A. It is well-known from previous investigations that the optimum z-distance is where the polymer is sufficiently pressed into the textile substrate, before the nozzle is clogged, as occurs for lower z-distances [19]. Clogging starts here at a z-distance of -0.8 mm, as shown by optical inspection during the printing process. For this reason, the corresponding adhesion forces are lower than those measured for z = -0.7 mm.

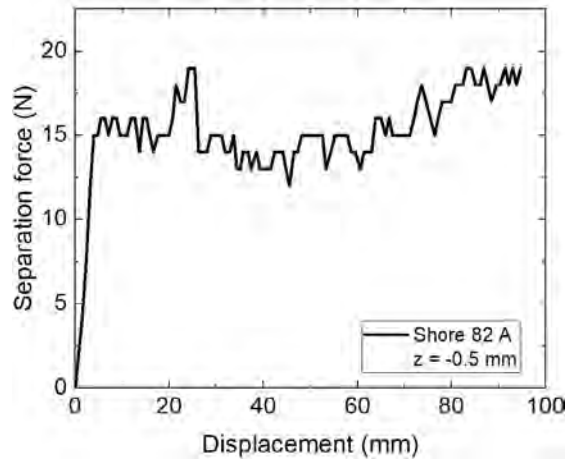

Figure 1: Sample measurement of the adhesion forces of the softest TPU (shore hardness of 82 A) on the woven textile fabric, shown here with the highest z-distance of -0.5 mm

On the other hand, softer materials typically show a higher adhesion than harder materials, which is also visible here, when comparing the results for the optimum distance of -0.7 mm. Generally, a maximum adhesion force of approximately 50 N or, normalized by the sample width of 25 mm, of 20 N/cm, which was found for the softest TPU under ideal printing conditions in this study, corresponds well with a previous study of another group with similar materials [29].

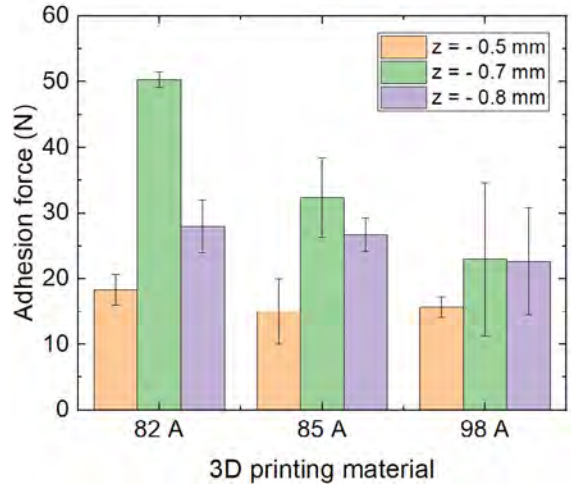

Figure 2: Average adhesion forces of samples under investigation, with error bars showing standard deviations

The adhesion, however, is only one factor that leads to improvement in stab-resistance due to the polymer printed on the textile fabric, compared with textile fabric alone. Figure 3a depicts sample force-displacement curves for a composite (two layers of TPU with a shore hardness of 85 A printed on the woven fabric) and a pure textile fabric. The force necessary to penetrate the composite with the blade is clearly higher than that for the pure textile fabric.

The average cutting forces are depicted in Figure 3b. Here, it is clearly evident that the TPU with a shore hardness of 82 A only leads to a small improvement in the cutting force, while both harder TPUs can better withstand a penetrating blade, leading to the enhancement of the cutting forces by a factor of approximately 3–4. No significant difference between the TPUs with a shore hardness of 85 A and a shore hardness of 98 A is evident ($t = 0.74$ in the Welsh-test, i.e. smaller than the critical t-value of 3.60 for the 95% double-sided confidence interval). On the contrary, the differences between the pure textile or the 82 A sample, respectively, and both 85 A and 98 A samples are significant for a 99% double-sided confidence interval, which is also valid for the difference between the pure textile and 82 A composite.

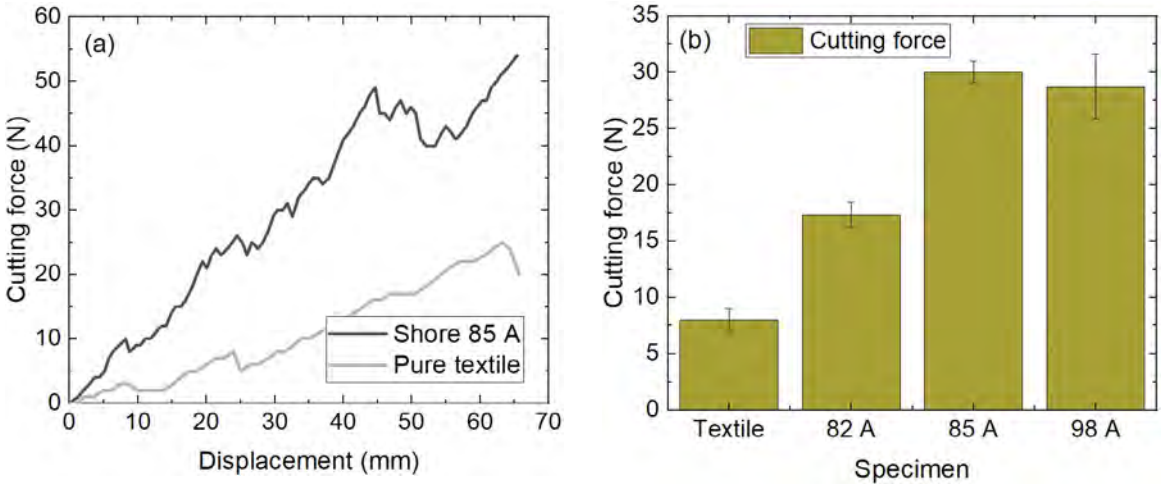

Figure 3: a) Sample measurement of the cutting forces through the TPU with a shore hardness of 85 A on the woven fabric; b) average cutting forces for the pure textile fabric and polymer/textile composites

This behaviour is reflected by the microscopic images of the composites after the stabbing test, as shown in Figure 4. While the softest material (82 A) demonstrates a mixture of bending and cutting, the strands of both harder materials are clearly cut. This suggests combining materials of different elasticity to absorb more energy than possible with only one of these mechanisms.

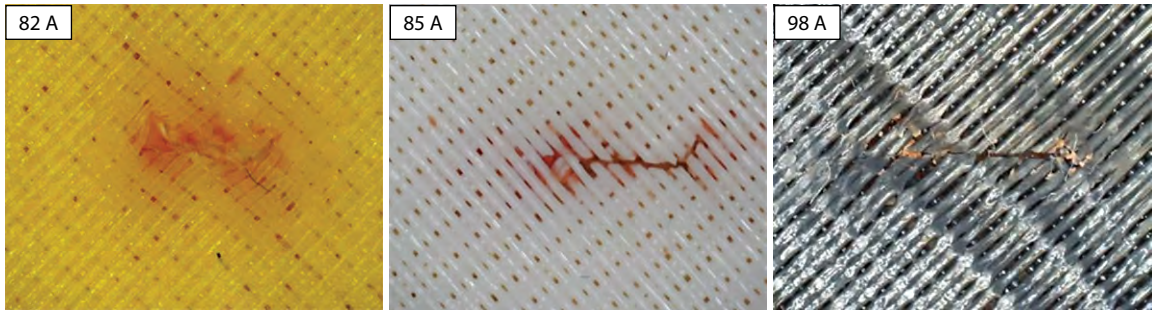

Figure 4: Microscopic images of composite samples after the quasi-static stabbing test

It should be mentioned that, in spite of the increased flow rate, neighbouring strands are still not fully connected, indicating that even higher cutting forces can be achieved with an enhanced 3D printer whose settings enable a continuous connection of neighbouring strands without air voids between them.

4 Conclusion and outlook

Three TPU filaments were FDM-printed on a woven fabric and investigated with respect to the adhesion between both parts and to the quasi-static stab-resistance of these composites. While the softest TPU (shore hardness of 82 A) showed the best adhesion, both composites with harder TPUs necessitated higher stabbing forces. Combinations of different materials, e.g. with the softest TPU printed on the textile fabric and covered by one of the harder TPUs, can be expected to result in better adhesion throughout the composite and to combine different energy absorption modes, thus increasing the stab-resistance of such lightweight, bendable composites for the use as body armour.

Acknowledgments

The study was partly funded by the German Federal Ministry for Economic Affairs and Climate Action via the AiF, based on a resolution of the German Bundestag, grant number KK5129708TA1.

References

1. LATOURRETTE, Tom. The life-saving effectiveness of body armor for police officers. *Journal of Occupational and Environmental Hygiene,* 2010, **7**(10), 557–562, doi: 10.1080/15459624.2010.489798.
2. RICCIARDI, Richard, DEUSTER, Patricia A., TALBOT, Laura A. Metabolic demands of body armor on physical performance in simulated conditions. *Military Medicine,* 2008, **173**(9), 817–824, doi: 10.7205/MILMED.173.9.817.
3. MATUSIAK, M. Thermal comfort index as a method of assessing the thermal comfort of textile materials. *Fibres & Textiles in Eastern Europe*, 2010, **18**(2), 45–50.
4. NAYAK, Rajkishore, KANESALINGAM, Sinnappoo, WANG, Lijing, PADHYE, Rajiv. Stab resistance and thermophysiological comfort properties of boron carbide coated aramid and ballistic nylon fabrics. *The Journal of The Textile Institute,* 2019, **110**(8), 1159–1168, doi: 10.1080/00405000.2018.1548800.
5. MAYO, J.B., Jr., WETZEL, E.D. Cut resistance and failure of high-performance single fibers. *Textile Research Journal,* 2014, **84**(2), 1233–1246, doi: 10.1177/0040517513517966.
6. LI, Ting-Ting, WANG, Zhike, ZHANG, Xiayun, WU, Liwei, LOU, Ching-Wen, LIN, Jia-Horng. Dynamic cushion, quasi-static stab resistance, and acoustic absorption analyses of flexible multifunctional inter-/intra-bonded sandwich-structured composites. *The Journal of The Textile Institute,* 2021, **112**(1), 47–55, doi: 10.1080/00405000.2020.1747676.
7. ZHANG, Xiayun, LI, Ting-Ting, SUN, Fei, PENG, Hao-Kai, WANG, Zhike, LIN, Jia-Horng, LOU, Ching-Wen. Stab/puncture resistance performance of needle punched nonwoven fabrics: effects of filament reinforcement and thermal bonding. *Fibers and Polymers,* 2022, **23**, 2330–2339, doi: 10.1007/s12221-022-3968-8.
8. TIAN, Luxin, SHI, Juanjuan, CHEN, Hongxia, HUANG, Xiaomei, CAO, Haijian. Cut-resistant performance of Kevlar and UHMWPE covered yarn fabrics with different structures. *The Journal of The Textile Institute,* 2022, **113**(7), 1457–1463, doi: 10.1080/00405000.2021.1933327.
9. GADOW, Rainer, VON NIESSEN, Konstantin. Ceramic coatings on fiber woven fabrics. In *26th Annual Conference on Composites, Advanced Ceramics, Materials, and Structures: A: Ceramic Engineering and Science Proceedings*. Edited by Hua-Tay Lin, Mrityunjay Singh. Hoboken : John Wiley & Sons, 277–285.

10. GADOW, Rainer., VON NIESSEN, Konstantin. lightweight ballistic with additional stab protection made of thermally sprayed ceramic and cermet coatings on aramide fabrics. *International Journal of Applied Ceramic Technology,* 2006, **3**(4), 284–292, doi: 10.1111/j.1744-7402.2006.02088.x.
11. LEE, Young S., WETZEL, E.D., WAGNER, N.J. The ballistic impact characteristics of Kevlar woven fabrics impregnated with a colloidal shear thickening fluid. *Journal of Materials Science,* 2003, **38**, 2825–2833, doi: 10.1023/A:1024424200221.
12. DECKER, M.J., HALBACH, C.J., NAM, C.H., WAGNER, N.J., WETZEL, E.D. Stab resistance of shear thickening fluid (STF)-treated fabrics. *Composites Science and Technology,* 2007, **67**(3–4), 565–578, doi: 10.1016/j.compscitech.2006.08.007.
13. MAYO, Jessie B., Jr., WETZEL, Eric D., HOSUR, Mahesh V., JEELANI, Shaik. Stab and puncture characterization of thermoplastic-impregnated aramid fabrics. *International Journal of Impact Engineering,* 2009, **36**(9), 1095–1105, doi: 10.1016/j.ijimpeng.2009.03.006.
14. STOJANOVIC, Dusica B., ZRILIC, Milorad, JANCIC-HEINEMANN, Radmila, ZIVKOVIC, Irena, KOJOVIC, Aleksandar, USKOKOVIC, Peter S., ALEKSIC, Radoslav. Mechanical and antistabbing properties of modified thermoplastic polymers impregnated multiaxial *p*-aramid fabrics. *Polymers for Advanced Technologies,* 2013, **24**(8), 772–776, doi: 10.1002/pat.3141.
15. CHEON, Jinsil, LEE, Minwook, KIM, Minkook. Study on the stab resistance mechanism and performance of the carbon, glass and aramid fiber reinforced polymer and hybrid composites. *Composite Structures,* 2020, **234**, 111690, doi: 10.1016/j.compstruct.2019.111690.
16. CICEK, Umur Ibrahim, SOUTHEE, Darren John, JOHNSON, Andrew Allan. Assessing the stab resistive performance of material extruded body armour specimens. *International Journal of Protective Structures,* 2022, **14**(3), 335–356, doi: 10.1177/20414196221112148.
17. MAIDIN, S., CHONG, S.Y., HEING, T.K., ABDULLAH, Z., ALKAHARI, R. Stab resistant analysis of body armour design features manufactured via fused deposition modelling process. In *Textile Manufacturing Processes.* Edited by F. Uddin. London : IntechOpen, 2019, 69–83.
18. JIANG, J.H., YUAN, M.Q., JI, T.C. Investigations on laser sintered textiles for stab-resistant application. In *Proceedings of the 26th Annual International Solid Freeform Fabrication Symposium - An Additive Manufacturing Conference*, Austin, TX, USA, 10–12 August 2015, 2155–2164.
19. GRIMMELSMANN, Nils, KREUZIGER, Mirja, KORGER, Michael, MEISSNER, Hubert, EHRMANN, Andrea. Adhesion of 3D printed material on textile substrates. *Rapid Prototyping Journal,* 2018, **24**(1), 166–170, doi: 10.1108/RPJ-05-2016-0086.
20. SANATGAR, Razieh Hashemi, CAMPAGNE, Christine, NIERSTRASZ, Vincent. Investigation of the adhesion properties of direct 3D printing of polymers and nanocomposites on textiles: effect of FDM printing process parameters. *Applied Surface Science,* 2017, **403**, 551–563, doi: 10.1016/j.apsusc.2017.01.112.
21. ERDEM, Göksal, GROTHE, Timo, EHRMANN, Andrea. Adhesion of new thermoplastic materials printed on textile fabrics. *Tekstilec,* 2023, **66**(1), 57–63, doi: 10.14502/tekstilec.66.2023012.
22. KDIW 2004 [online]. VPAM [accessed 23 August 2023]. Available on World Wide Web: <https://www.vpam.eu/pruefrichtlinien/aktuell/kdiw-2004/>.
23. Home Office Body Armor Standard 2017 (knife and spike) [online]. Protection Group Denmark [accessed 23 August 2023]. Available on World Wide Web: <https://protectiongroupdenmark.com/articles/14-home-office-body-armor-standard-2017-knife-and-spike/>.
24. NIJ Standard–0115.00. Stab resistance of personal body armor. Washington : National Institute of Justice, 2000.

25. NIJ Standard–0115.01: draft. Stab resistance of personal body armor. Gaithersburg : National Institute of Standards and Technology, 2020.
26. ASTMF1342/F1342M-05(2022). Standard test method for protective clothing material resistance to puncture. West Conshohocken : ASTM International, 2022, https://www.astm.org/f1342_f1342m-05r22.html.
27. PANNEKE, Niklas, EHRMANN, Andrea. Stab-resistant polymers – recent developments in materials and structures. *Polymers,* 2023, **15**(4), 1–22, doi: 10.3390/polym15040983.
28. KOZIOR, Tomasz., DÖPKE, Christoph, GRIMMELSMANN, Nils, JUHÁSZ JUNGER, Irén, EHRMANN, Andrea. Influence of fabric pretreatment on adhesion of 3D printed material on textile substrates. *Advances in Mechanical Engineering,* 2018**,** **10**(8)**,** 1–8, doi: 10.1177/1687814018792316.
29. KORGER, M., GLOGOWSKY, A., SANDULOFF, S., STEINEM, C., HUYSMAN, S., HORN, B., ERNST, M., RABE, M. Testing thermoplastic elastomers selected as flexible three-dimensional printing materials for functional garment and technical textile applications. *Journal of Engineered Fibers and Fabrics,* 2020, **15**, 1–10, doi: 10.1177/1558925020924599.

Mohammad Ehsan Momeni Heravi
Department of Textile and Fashion Design, Mashhad Branch,
Islamic Azad University, Mashhad, Iran

Industrial Design of Yarn Speed Monitoring System in Positive Feed Circular Knitting Machine

Industrijska zasnova sistema za spremljanje hitrosti preje na krožnem pletilniku s pozitivnim dovajanjem preje

***Original scientific article**/Izvirni znanstveni članek*
Received/*Prispelo* 4-2023 • Accepted/*Sprejeto* 8-2023

Corresponding author/*Korespondenčni avtor:*
Mohammad Ehsan Momeni Heravi
E-mail: momeni5892@mshdiau.ac.ir
ORCID: 0000-0003-3473-2165

Abstract

As constant yarn feeding tension is essential in the formation of uniform stitches, the lack of a monitoring system in a circular weft knitting machine capable of measuring the uniformity of the yarn feeding speed in different driven belts and comparing the feeding rate during the knitting process has led to the use of experimental methods which are dependent on skilled operators. Additionally, in the case of any defects, the equalisation is done by the operator using the trial-and-error method, which consequently increases the risk of human error. Considering the importance of a uniform adjustment of yarn feeding speed on the quality of final fabrics, a monitoring system for measuring and reporting yarn feeding speed was designed. Following its installation on a circular weft knitting machine, the performance of the system in an industrial environment was evaluated. A comparison with the traditional system proved the functionality of the designed automation process. The current study highlights the characteristics of an appropriate sensor, the applicable installation place and direct data reception without intermediaries.

Keywords: circular weft knitting machine, positive yarn feeding system, automation, measuring system

Izvleček

Konstantna napetost dovajanja preje je bistvenega pomena pri oblikovanju enakomernih zank. Ker ni bilo nadzornega sistema na krožnem votkovnem pletilniku, ki bi bil zmožen meriti enakomernost hitrosti dovajanja preje pri različnih gnanih jermenih in primerjati hitrost dovajanja med postopkom pletenja, so se začele uporabljati eksperimentalne metode, odvisne od usposobljenosti upravljavcev pletilnikov. Poleg tega pri kakršnih koli okvarah upravljavec stroja lahko izravnava hitrost po metodi poskusov in napak, a se s tem poveča tveganje za napake. Glede na pomen nastavitve enakomerne dovajalne hitrosti preje za kakovost končnih pletiv je bil zasnovan nadzorni sistem za merjenje in beleženje dovajalne hitrosti preje. Po namestitvi na krožni pletilnik je bila ocenjena učinkovitost

sistema v industrijskem okolju. Primerjava s tradicionalnim sistemom je dokazala učinkovitost zasnovanega procesa avtomatizacije. V študiji so navedene značilnosti ustreznega senzorja, primerno mesto namestitve in neposredno zajemanje podatkov brez posrednikov.

Ključne besede: krožni pletilnik, pozitivni sistem dovajanja preje, avtomatizacija, merilni sistem

1 Introduction

A positive feed device is a knitted loop-shape and loop-length control device which employs small pulleys moved by belts, gears etc. to exactly control the yarn feeding speed, keeping it constant.

Positive feed devices are designed to overcome loop-shape and loop-length variation by positively supplying yarn at the correct rate under low yarn tension to the knitting point instead of allowing the latch needles or loop-forming sinkers to draw loops the length of which could be affected by varying yarn input tension. In such systems, the presence of a continuous toothed belt, which is driven by a pulley, ensures the uniform and uninterrupted provision of yarn to each feeding unit. The tape speed is altered by adjusting the scrolled segments of the drive pulley (V.D.Q pulley) to produce a larger or smaller driving circumference.

The difference in feeding speeds in the pulleys of the positive feeding system causes a change in the tension of the yarn being fed and ultimately a difference in the length of loops and knitting dynamics [1–3].

The difference in the length of stitches makes the structure of knitted fabrics heterogeneous, which affects the appearance of the fabric in terms of its surface uniformity. Moreover, this unevenness is also visible on the surface of the final garment produced [4–6]. Additionally, the difference in the feeding speed of yarns prevents the yarns to be finished simultaneously in the creels, and as the operator has to change the yarn, it is time-consuming.

In a study conducted by Zhao et al., it was shown that the control of yarn tension fluctuations improves the uniformity of the fabric surface effectively [7].

In similar research, Catarino and his colleagues proved that the tension of the yarn provides useful insight into how to better control the circular knitting process in the machines. A change in the yarn feeding speed will increase or decrease the tension of the yarn, which can be recognised by the change in the vibration of the tension force [8–9].

The effect of machine speed on yarn input tension and course length was observed by Kobir [10].

Extensive research has been conducted on the automation of the yarn feeding mechanism in weaving machines and warp knitting machines, and several researchers have tried to equip these machines with control tools to increase production efficiency and improve the quality of the final product.

In their research, Jeddi et al. [11] measured the fluctuation and tension changes of warp yarn and were able to increase the efficiency of the weaving machine to obtain uniformity in the properties of the produced fabric.

Dayik and others [12] designed a program based on gene expression programming to control the yarn opening mechanism in the weaving machine. The application of this control system reduced warp tearing and increased the weaving efficiency.

Nosraty et al. [13] controlled the tension changes of weft yarns in the air jet weaving machine using an online system with a closed-loop control system and showed that by controlling tension in weft, the coefficient of variation belonging to the mechanical and physical properties of the produced fabrics significantly reduced.

In a circular weft knitting machine with a positive feeding mechanism, it is not easy to measure and compare the uniformity of the yarn feeding speed in different driven belts during the knitting process and it is usually conducted experimentally by a skilled operator. In the case of non-uniformity between the feeding speed of yarns, the equalisation is achieved

by a skilled operator via the trial-and-error method, which is highly associated with human error.

Accordingly, the importance of yarn feeding speed uniformity in the quality of the final fabric in knitting machines with a positive feeding mechanism has required the design of condition monitoring systems in these machines.

2 System design and construction

In processes where measurements are taken without standard systems and they only rely on the operator, the possibility of human error increases. These errors not only occur while taking the measurements, but they also happen during decision-making and result analysis. Errors can have an impact on quality, quantity, production efficiency, and safety and can sometimes cause life-threatening conditions.

The best results are obtained when the operator only has the supervisory and complementary role, while the measuring, processing, decision-making and result analysis are done under an integrated system. In an integrated and fully automatic system, the operator does not have an active role in system control and the measurement is taken online by the installed sensors. The output of the measurements is processed by the values that can be defined either by the operator or the system itself; the results, displayed on the screen, are sent to the operators and later modifications, if necessary, can be applied.

The fluctuations of key parameters in any mechanical system indicate the prevailing conditions of that system; consequently, it is necessary to be informed of such changes in order to monitor the state of the system and prevent the occurrence of defects or the creation of inconsistencies [14]. While designing and constructing the system, the choice of the right sensor is of particular importance. The sensor must have a timely response and provide the necessary outputs for processing. Additionally, noises and harmonics should not disturb its performance.

After examining and studying different types of sensors, it is critical to consider the superior property of proximity sensors, i.e. the ability to be used without causing mechanical interference, longer life span and lack of disruption. The usage of such sensors in the construction of the yarn feeding speed measuring system has also been taken into consideration.

At the same time, optical proximity sensors are also considered suitable candidates. However, since environmental pollution, e.g. dust, lint and vibrations, which are the byproduct of manufacturing, or the pollutions that occur during the cleaning, repairs, adjustments, are frequent in the production site, the possibility of disruption is high in these environments, which makes proximity sensors preferable over the optical type.

Activated by the presence of ferromagnetic material, inductive proximity sensors are minorly affected by environmental pollution. Additionally, the economical and cost-effective equipment is preferable for the speed-measuring system of positive yarn feeding.

2.1 Sensor installation location

In addition to not causing any disturbance in the normal function of the circular weft knitting machine, the efficient performance of the sensor should be guaranteed while designing the system. Investigations have proven that the bottom feed wheel of the positive yarn feeder is the best place to install the sensor, where the input coefficient of the yarn feeding speed can be measured directly.

A special base was needed for the installation of the sensor, which facilitated the installation on the feeder and also provided the possibility of adjusting the distance of the sensor. Figure 1 shows the view of the knitting machine. The positive yarn feeding mechanism is shown in Figure 2. Moreover, Figure 3 shows the installation location of the base on the industrial circular weft knitting machine as well as the installation location of the sensor on a positive feeder.

Figure 1: Circular weft knitting machine [15]

Figure 2: Mechanism of positive yarn feeding [15]

a)

b)

Figure 3: Industrial circular weft knitting machine: a) location of base on positive yarn feeder in industrial circular weft knitting machine, b) location of sensor on base and positive yarn feeder

The system was designed and installed in a way that the assembly does not affect the structure of the knitting machine and no additional part disturbs the yarn flow while feeding. The sensor can be installed on any positive feeding unit in the knitting machine and can directly monitor the yarn feeding speed.

2.2 Data processing and display

Most circular weft knitting machines have a central control panel that acts as the human-machine interface. The control parameters of this panel include manual controls, e.g. turning the machine on and off, controlling the inverter and machine speed, controlling the brightness and operation of the fans, controlling air compression, and automatic panel controls, including stopping the machine in case of yarn breakage, stopping the machine in case of increase in temperature and oil pressure, stopping the machine when the main door of the machine is opened and stopping the machine at the end of the fabric take up.

The central electronic board of the system, capable of measuring and displaying the yarn feeding speed, is responsible for receiving and processing sensor signals, displaying the speed of yarns, receiving operator commands and generating alarm signals. The board includes a microcontroller programmed for the aforementioned purposes, a sensor isolator, speed display, setting input and an alarm driver.

The signal produced by the sensors is transferred to the central board of the device, which can by applying the necessary coefficients measure the speed of yarn feeding and display it on the screen in real time with the ability to select common speed units. In the Pulse Width Modulation (PWM) section of the microcontroller, the lack of speed coordination in different feeders can be detected and the amount will be displayed, which is accompanied by sound alarms to inform the operator.

The central electronic board uses a AVR ATmega32 microcontroller, which has a counter with PWM capability and is used to detect the lack of speed coordination. Moreover, this microcontroller has an internal memory of FLASH type with the capability of storing the speed mismatch values. The FLASH memory has the ability to retain information even in the event of a power cut.

In order to connect the display, the remote device uses the standard RS485 serial communication of the microcontroller. In addition to applicability in long distances, RS485 communication is less effective against environmental noise, which makes it a better choice for industrial use. Furthermore, to minimise the effect of environmental noise on the performance of the central electronic board, an optocoupler is used to isolate the signals. The signal transmission from input to output is achieved by infrared radiation in optocouplers with no electrical connection, which eliminates the possibility of noise emission. Figure 4 shows the block diagram of the system and the central electronic board. Figure 5 shows the display panel of the monitoring system of the yarn feeding speed in a knitting machine.

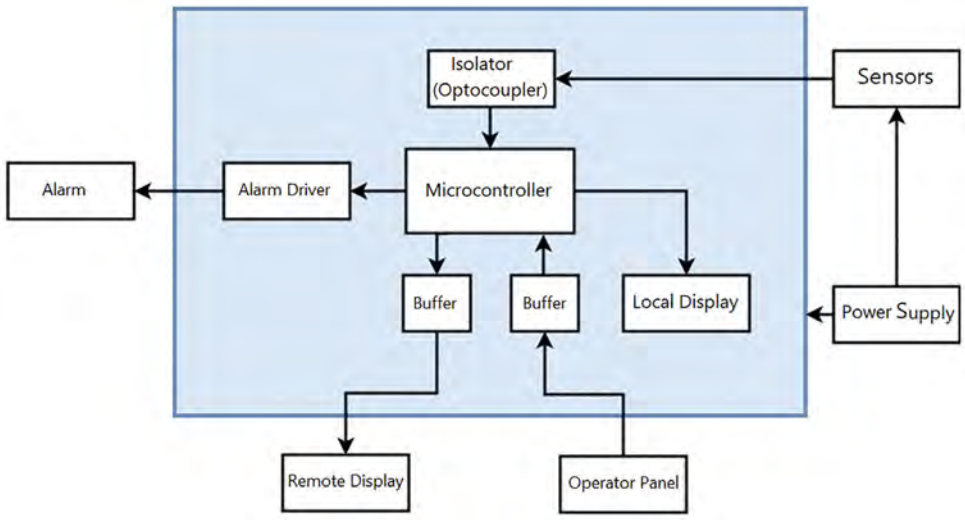

Figure 4: Block diagram of central electronic board of system for measuring and displaying yarn feeding speed in circular weft knitting machine

Figure 5: Remote display of yarn feeding speed monitoring system in circular weft knitting machine

2.3 Experiences

In order to measure the performance of the yarn speed monitoring system on an industrial circular weft knitting machine in actual working conditions, the system was installed on a Single Jersey knitting machine with a cylinder diameter of 34 inches, 26 gauges, 4 needle butts and 108 cams.

3 Results and discussion

3.1 Calculation of key performance and reliability indicators

In order to study the performance of the yarn feeding automation system, the reliability and maintenance indicators were compared in two 90-day production periods of the circular knitting machine.

The first period was performed without the presence of the automation system and the second period was performed with the presence of the yarn feeding monitoring system and under the same production conditions in terms of the type of texture, yarn count etc.

To monitor the reliability and maintainability of machines and equipment, several indicators are used in industrial engineering, and by measuring and comparing their trends, the effectiveness of the automation activities performed on the machines can be understood.

For this purpose, three well-known and widely used indicators in the maintenance and reliability of machines, including the mean time to repair (Equation 1), mean time between failures (Equation 2) and availability (Equation 3), were calculated and compared for two 90-day periods of tests on the knitting machine.

The most widely used indicator of maintainability is the mean time to repair, which expresses the average time required to perform a specific maintenance activity, adjustments or recovery, and is calculated with Equation 1 [16–18]:

$$\bar{t}_R = \frac{\Sigma t_R}{\Sigma N_R} \tag{1}$$

where $\bar{t}_R$ is time to repair, Σt_R is total repair time or adjustment time, and ΣN_R is total number of repair.

Mean time to repair (and restore) is the average time that takes to repair each machine when a failure is discovered. $\bar{t}_R$ is calculated by adding the total time spent repairing and dividing that by the number of repairs.

To calculate the $\bar{t}_R$ indicator in this research, the number of times the machine was stopped due to the need of adjustments of the yarn feeding mechanism, as well as the time spent for each stop (in minutes), were recorded in two periods of 90-day tests on a circular knitting machine.

The announcement of the need to adjust the yarn feeding mechanism could be due to several reasons, e.g. the unevenness of the fabric surface due to the lack of uniformity in the feeding speed of the yarns or the announcement of changes in the fabric weight (grams per square meter of fabric) etc.

In the reliability analysis, the average time leading to failure is very useful and is calculated with Equation 2:

$$\overline{t_{BF}} = \frac{(\Sigma t_{OH} - \Sigma t_{SH})}{\Sigma N_{TF}} \quad (2)$$

where $\bar{t}_{BF}$ is mean time between failures, Σt_{OH} is total number of operational hours, Σt_{SH} is total number of stop hours, and ΣN_{TF} is total number of failures.

The $\bar{t}_{BF}$ indicator is one of the most important elements and indicators of product development and design. $\bar{t}_{BF}$ indicates the average machine operating time until the next failure. In fact, this indicator shows the average operating time of the machine after a repair or adjustment and the need for repair or adjustment after the start-up.

In this research, $\bar{t}_{BF}$ to calculate the indicator, the total working time of the knitting machine (in minutes) was recorded in each 90-day period with and without the presence of the yarn feeding automation system. Then, the total time of machine stops due to the adjustment of the feeding mechanism was calculated and deducted from the total time of machine operation. The numbers obtained in each period were divided by the number of times the knitting machine was stopped solely due to the adjustment of the feeding mechanism.

Availability is an important indicator that shows the accessibility of the machine. Availability is expressed as a ratio or percentage and is calculated with Equation 3:

$$Availability = \frac{\bar{t}_{BF}}{(\bar{t}_{BF} + \bar{t}_{R})} \quad (3)$$

To calculate the indicators and the average machine stopping rate, the grading of the time unit is important. For this purpose, the unit of time in terms of minutes is used in the calculations. The results related to the calculation of indices are shown in Table 1.

Table 1: Calculating reliability and maintenance indicators of knitting machine in presence and absence of yarn feeding speed automation system after period of 90 days of operation of knitting machine

Using system of measuring and displaying speed of yarn feeding	$\bar{t}_R$ (min)	$\overline{t_{BF}}$ (min)	Availability (%)
Yes	5	21595	99.97
No	15	10785	99.92

Based on the results obtained from the comparison of the $\bar{t}_R$ indicator in two periods of tests by using the feeding speed monitoring system, the average machine stopping time to adjust the yarn feeding mechanism was reduced by 66.66%.

Examining the $\overline{t_{BF}}$ indicator also shows a 100.2% improvement in the average continuous operating times of the knitting machine without the need to stop due to the adjustment of the feeding mechanism using the automation system to measure the yarn speed.

Stoppages generally occur due to the inaccuracy in the initial setting of the feeders by the operator, which was greatly reduced by using the yarn feeding automation system.

A comparison of indicators between two operating periods of the circular weft knitting machine in the presence and absence of the measurement system and the display of the yarn feeding speed indicate appropriate response of the reliability and maintenance indicators of the knitting machine to the designed automation process.

3.2 Economic analysis and calculation of machine production parameters and operator

Considering the importance of the uniformity of yarn feeding speed in circular weft knitting machine, the use of a speed monitoring system improved the production process and efficiency parameters, which leads to the reduction of production costs. Table 2 shows the state of improved production parameters (the numbers in the table are rounded).

Table 2: Improved parameters of machine and operator production

Row	Parameter	Condition	Improvement (%)
1	The amount of remaining yarn in the form of non-knit cones due to the lack of uniformity in the speed of feeders	Reduction	63
2	The duration of the adjustment and equalisation of the speed of the positive yarn feeding system by the operator	Reduction	67
3	Total production efficiency	Increase	0.3

4 Conclusion

In this research, a new system was designed and built to measure and display the yarn feeding speed in circular weft knitting machines. This system accurately measures and displays the yarn feeding speed in the positive feeding mechanism of knitting machines.

The results of the comparison between two 90-day test periods in the same production conditions with and without the presence of the measuring system and the display of the yarn feeding speed on the industrial knitting machine proved the successful application of the machine key performance and reliability indicators to the designed automation process.

One of the construction advantages of this automation system is its proper accuracy and cost-effectiveness, which makes its use in the status measurement of knitting machines possible without incurring exorbitant costs.

Another advantage of this system is that it does not affect the natural flow of yarn feeding and does not change the basic structure of the knitting machines. In addition, this system can be installed on any type of a circular weft knitting machine and at different speeds without any special settings. This feature indicates the possibility of upgrading and equipping the existing knitting machines with a yarn feeding automation system without the need for fundamental changes in their structure.

References

1. DURU, S.C., CANDAN, C., MUGAN, A. Effect of yarn, machine and knitting process parameters on the dynamics of the circular knitting needle. *Textile Research Journal*, 2015, **85**(6), 568–589, doi: 10.1177/0040517514547216.
2. KOO, Y.S. Correlation of yarn tension with parameters in the knitting process. *Fibers and Polymers*, 2002, **3**(2), 80–84, doi: 10.1007/BF02875404.
3. SARKER, M.E., ISLAM, M.R., MAHMUD, M.S., ISLAM, M.Z., ALIMUZZAMAN, S., AHMED, A. F. Effects of yarn, fabric and machine parameters on the dimensional properties of weft knitted single jersey fabric. *Journal of Natural Fibers*, 2022, **19**(17), 15625–15636, doi: 10.1080/15440478.2022.2131682.
4. MUNDEN, D.L. 26–The geometry and dimensional properties of plain-knit fabrics. *Journal of the Textile Institute Transactions*, 1959, **50**(7), T448–T471, doi: 10.1080/19447025908659923.
5. FATKIĆ, E., GERŠAK, J., UJEVIĆ, D. Influence of knitting parameters on the mechanical properties of plain jersey weft knitted fabrics. *Fibres & Textiles in Eastern Europe*, 2011, **19**(5), 87–91.
6. EMIRHANOVA, N., KAVUSTURAN, Y. Effects of knit structure on the dimensional and physical properties of winter outerwear knitted fabrics. *Fibres & Textiles in Eastern Europe*, 2008, **16**(2), 69–74.

7. ZHAO, B., CONG, H., WU, G. Construction and system realization of the yarn tension model of fully fashioned flat knitting fabric. *Textile Research Journal*, 2021, **91**(11–12), 1380–1388, doi: 10.1177/0040517520982386.
8. CATARINO, A.P., ARAÚJO, M.D. de, HONG, H. Process control for total quality in circular knitting. *AUTEX Research Journal,* 1999, 1(1), 21–29.
9. CATARINO, A., ROCHA, A.M., MONTEIRO, J. Monitoring knitting process through yarn input tension: new developments. In *IEEE 2002 28th Annual Conference of the Industrial Electronics Society. IECON 02. Vol. 3.* IEEE, 2002, 2022–2027, doi: 10.1109/iecon.2002.1185283.
10. MOBAROK HOSSAIN, A.K.M., ALI, Abu Rayan Md. Effect of machine speed on yarn input tension and 'on-machine'course length for a circular weft knitting machine with positive storage feeding. *International Journal of Mechanical and Production Engineering Research and Development*, 2018, **8**(1), 339–352.
11. JEDDI, A.A.A., NOSRATY, H., ORDOUKHANY, D., RASHIDIAN, M. A comparative study on the performance of electronically-and mechanically controlled warp yarn let-off systems. *Indian Journal of Fiber and Textile Research*, 1999, **24**, 258–263.
12. DAYIK, M., KAYACAN, M.C., ÇALIŞ, H., CAKMAK, E. Control of warp tension during weaving procedure using evaluation programming. *Journal of The Textile Institute*, 2006, **97**(4), 313–324, doi: 10.1533/joti.2005.0132.
13. NOSRATY, H., JEDDI, A.A.A., KABGANIAN, M., NEJAD, F.B. Influence of controlled weft yarn tension of a single nozzle air-jet loom on the physical properties of the fabric. *Textile Research Journal*, 2006, **76**(8), 637–645, doi: 10.1177/0040517506065604.
14. JARDINE, A.K.S., LIN, D., BANJEVIC, D. A review on machinery diagnostics and prognostics implementing condition-based maintenance. *Mechanical Systems and Signal Processing,* 2006, **20**(7), 1483–1510, doi: 10.1016/j.ymssp.2005.09.012.
15. HERAVI, M.E.M., NAJAR, S.S., MOAVENIAN, M., YAZDANSHENAS, M.E. Effect of knitted loop length on the fluctuation amplitude of yarn fed into a circular weft-knitting machine using a new opto-electro device. *Fibres & Textiles in Eastern Europe*, 2014, **4**(106), 81–86.
16. GHEYSOPOUR, S., AHMADI, S.H., JAHROMI, A.E. Calculation of maintenance index and identification of critical case study: mahd khodro fesharaki. *Sharif Journal of Industrial Engineering & Management*, 2016, **31.1** (2.1), 107–115.
17. ANTOSZ, K., STADNICKA, D. Evaluation measures of machine operation effectiveness in large enterprises: study results. *Maintenance and Reliability*, 2015, **17**(1), 107–117.
18. BOŁOZ, L., RAK, Z., STASICA, J. Comparative analysis of the failure rates of shearer and plow systems – a case study. *Energies*, 2022, **15**(17), 1–17, doi.org/10.3390/en15176170.

Jamal Hossen, Subrata Kumar Saha
Ahsanullah University of Science and Technology, Department of Textile Engineering, 141–142, Love Road, Tejgaon, Industrial Area, Dhaka-1208, Bangladesh

Influence of Blending Method and Blending Ratio on Ring-spun Yarn Quality – a MANOVA Approach

Vpliv metode mešanja in mešalnega razmerja na kakovost prstanske preje (pristop MANOVA)

Original scientific article/*Izvirni znanstveni članek*
Received/*Prispelo* 04-2023 • Accepted/*Sprejeto* 7-2023

Corresponding author/*Korespondenčni avtor:*
Subrata Kumar Saha
E-mail: subratatex@gmail.com
Phone: +8801678112194
ORCID: 0000-0003-3275-9559

Abstract

Cotton-polyester is a common and popular fibre blend in the textile industry nowadays. Its main advantage is that it improves the functional properties of clothing and textile products. In this study, fibre-blended, sliver-blended and roving-blended yarns with a fineness of 23 tex were manufactured using a ring spinning system, with blend ratios of cotton and polyester fibres of 50:50, 60:40 and 70:30. The quality parameters of the produced yarn, such as mass variations, imperfections, hairiness and bundle yarn strength, were studied. The end breakage rate of the ring frame machine was also studied during the manufacturing of the yarns. The results were analysed using multivariate analysis of variance (MANOVA) to determine the significance of the impact of the blending method and blending ratio on yarn quality and the end breakage rate of the ring frame machine. The profile plots were analysed from statistical and technical points of view. Among the three blended yarns, fibre-blended yarn demonstrated the best results in terms of mass variations and imperfections due to better blending homogeneity, while roving-blended yarn demonstrated better results in terms of hairiness. Among the blended yarn, fibre-blended yarn demonstrated the highest bundle yarn strength value, while the corresponding end breakage rate of the ring frame machine recorded the lowest value. The yarn quality was improved in terms of mass variations, imperfections, hairiness and bundle yarn strength by increasing the polyester fibre percentage in the blend ratio.

Keywords: cotton-polyester, blending, ring-spun yarn, profile plot, Box's M-test, Leven's test

Izvleček

Mešanje bombaža in poliestrskih vlaken v tekstilni industriji je danes pogosto in priljubljeno. Glavna prednost tovrstnih mešanic je v izboljšanju funkcionalnih lastnosti oblačil in tekstilnih izdelkov. V tej raziskavi so bile primerjane prstanske preje z dolžinsko maso 23 tex, izdelane iz mešanic vlaken bombaž/poliester v razmerjih 50:50, 60:40 in 70:30, in sicer z mešanjem vlaken v predivu, z mešanjem pramenov in z mešanjem predprej. Proučevani so bili

naslednji parametri kakovosti: variacijski koeficient neenakomernosti mase (CVm), indeks nepopolnosti preje (IPI), kosmatost preje (H) in trdnost snopa preje (CSP). Med proizvodnjo prej je bila proučevana tudi hitrost števila pretrgov (EBR) na prstanskem predilniku. Da bi ugotovili vplive metode mešanja in mešalnega razmerja na kakovost preje na hitrost pretrgov prstanskega predilnika, so bili dobljeni rezultati parametrov kakovosti analizirani z multivariantno analizo variance (MANOVA). Profilni grafikoni so bili ovrednoteni s statističnega in tehnološkega vidika. Najboljše vrednosti CVm in IPI je imela preja, izdelana iz mešanice vlaken v predivu, kar je posledica boljše homogenosti mešanja, medtem ko je preja, izdelana z mešanjem pramenov, imela najnižjo kosmatost. Preja iz mešanice vlaken v predivu je imela najvišjo vrednost CSP in najnižjo vrednost EBR. S povečanjem odstotka poliestrskih vlaken v mešanici se je zaradi ugodnejših vrednosti CVm, IPI, H in CSP izboljšala kakovost preje.

Ključne besede: bombaž/poliester, mešanje, prstanska preja, profilni grafikoni, test Box-M, test Levin

1 Introduction

The textile and clothing industries represent the backbone of Bangladesh's economy, as 82% of the country's export income derives from the aforementioned sectors (trade information of BGMEA 2021–2022) [1]. Yarn manufacturing is the first and one of the vital stages of backward linkage on today's global textile market, with yarn produced from fibres and/or filaments [2]. The characteristic of yarn represent key criteria for manufacturing pleasing and essential clothing [3]. Globally speaking, short-staple spun yarns are manufactured using ring, rotor, air-jet and friction spinning systems, with ring spinning representing a universal system. The properties of fibre influence the quality of yarn, regardless of yarn structure [4]. Fibres of greater length are present in the core, while shorter fibres are present on the surface of spun yarn [5]. Clothing made from blended yarn consists of several fibres, and exhibits superior quality relative to clothing made from single-fibre yarn [6]. The critical factors that determine the properties of spun yarn are the ratio of fibre in a blend and type of fibre used in that blend [7, 8]. Blending consists of orientations of more than one type of fibre in the yarn body, such that the components of each element remain unchanged at every point of the yarn, throughout the yarn length [9]. The blending of cotton fibres with manmade fibres has specific benefits and more desirable features than that of pure cotton, such as the reduction of costs through the replacement of expensive cotton fibres with cheaper manmade fibres, comfort and ease of care, functionalities such as stretchability and wrinkle-resistance, and the aesthetic properties of clothing [6, 9–14]. However, the accumulation and association of fibres within the yarn surface represent challenges faced by manufacturers [15]. Among manmade fibre derivatives, the consumption of polyester fibres is the highest due to its higher tensile strength and blending liability. Ry et al. [16] studied the blending of cotton and dyed cotton fibre in the blow-room and draw-frame stages. They noted that incraesing the shade depth results in a deterioration in the quality of ring-spun yarn. Channa et al. [17] studied the properties of cotton/polyester blended yarn manufactured using both fibre and sliver blending. Their results showed that yarn made from fibre blending was better than sliver blending. Nawaz et al. [18] explored the impacts of roving position, spindle rpm and twist factor on the quality of cotton/polyester blended ring-spun yarn. They demonstrated that roving spacing and the amount of twist had a significant impact on yarn quality. Sawhney et al. [19] studied the quality of cotton/polyester blended yarn produced from roving blending in a ring frame. The results of that study showed that the tensile strength of roving-blended yarn was higher than that of yarn produced using conventional systems.

In literature, a large number of studies have been carried out regarding the impact of the blending of different fibres, spinning techniques and blending

stages on the blended yarn quality of different textile products (Table 1). In terms of insight, there are no studies comparing the performance of the three blending methods, using multivariate analysis of variance. The research gap thus remains. For the sake of precision, a statistical tool is used, i.e. multivariate analysis of variance (MANOVA), together a profile plot to evaluate the significance of the impact of the fibre-, sliver- and roving-blending methods on yarn characteristics. Consequently, this paper supplements existing literature, as a hands-on textile and apparel study, as follows:

- Firstly, the study was carried out on cotton/polyester blended manufactured yarn using the fibre-blending, sliver-blending and roving-blending methods, while maintaining different blending ratios.
- Secondly, it investigated the significance of yarn characteristics on blending method and blending ratio using MANOVA.

The main goal of this study was to analyse the impact of fibre, sliver and roving blending on the physical characteristics of cotton/polyester blended ring-spun yarn to achieve more reliable and realistic results.

Table 1: Overview of blending methodology studies in the textile spinning industry

No.	Authors	Aims	Scope of application
1	Ray et al. [16]	To investigate the effect of blending methodology on the quality of cotton melange yarn	Blow-room and draw-frame blending
2	Channa et al. [17]	To compare the properties of cotton/polyester blended yarn	Blow-room and draw-frame blending
3	Zhang et al. [20]	To determine the properties of blended ring-spun yarn made from jute and cotton	Blow-room and draw-frame blending
4	Tyagi et al. [21]	To study the properties of cotton/tencel, tencel/polyester blended ring-spun yarn	Blow-room blending
5	Kilic and Okur [22]	To investigate the properties of cotton/pro-modal, cotton/modal blended yarn in ring and vortex spinning	Draw-frame blending
6	Nawaz et al. [18]	To investigate the quality of cotton/polyester roving blended ring-spun yarn	Roving blending
7	Behera et al. [23]	To determine the impact of blending method and stages on cotton melange yarn	Blow-room and draw-frame blending
8	Sawhney et al. [19]	To produce cotton/polyester blended yarn using the ringspinning process	Roving blending

2 Materials

2.1 Raw materials

The quality of end products and the functional performance of textile machinery primarily depend on the physical and chemical properties of the raw materials that are processed in a factory. In the short-staple spinning industry, the main raw materials are natural fibre and/or manmade filament in staple form. Cotton and polyester fibres were used as the raw materials in this research. The most important properties of the fibres are given in Table 2.

Table 2: Properties of cotton and polyester fibre

Important properties	Cotton	Polyester
Upper half mean length (UHML)	2.80 cm (1.1024 inches)	3.4 cm (1.3386 inches)
Fineness	1.42 dtex (3.60 µg/inch)	2 dtex (5.07 µg/inch)
Strength	27.55 cN/tex	46.39 cN/tex
Country of origin	Chad	Indonesia

2.2 Blending and mixing

The main technological challenge in the textile spinning industry is to convert the high level of inconsistency in the features of raw fibres to an even yarn, so that critical work can be performed using the correct blending methods [24]. Today, it is quite difficult to produce higher-quality yarn with a single variety of raw material. Overcoming the challenge of mixing the variabilities of similar and/or different fibre components could be an obvious solution [25]. Hence, mixing is defined as random proportions of fibre components, where the quality of a product can not be predicted and is not reproducible, while in blending the proportions of fibre components are known and the properties of the resulting product can be predicted and are reproducible. Blending can be carried out at various stages in the spinning industry, as follows: fibre blending (also known as intimate blending) at the blow-room or carding stage, sliver blending (also known as creel blending) at the draw-frame or post-carding stage and roving blending, which can be carried out on a ring frame machine [26, 27].

2.3 Quality parameters of yarn

The properties of spun yarns are affected by fibre properties, such as blend ratio, process parameters and spinning systems [28]. Yarn irregularity is expressed by means of unevenness (Um) and coefficient of mass variation (*CVm*). The imperfection index (IPI) is the sum of +50% thick places, -50% thin places and +200% neps per 1,000 m length in yarn for ring-spun yarn. The hairiness of yarn (H) is the length of protruding fibre in 1 cm of yarn surface. Bundle yarn strength is expressed by count strength product (CSP) [29, 30]. The CSP of spun yarn was calculated using equation 1.

$$CSP = Lea\ strength \times N_e \qquad 1$$

where CSP represents count strength product, lea strength is expressed in pounds (1 lb = 0.4536 kg) and N_e represents yarn fineness (N_e × tex = 590.5).

The running performance of a ring frame machine is expressed by the end breakage rate (EBR). The EBR is one of the key factors for determining the quality of spun yarn and the productivity of a factory. A higher EBR indicates the faults in yarn that are created by the machine, material and people. It is mainly due to a higher spinning tension then actual yarn strength [25]. In the textile spinning industry, equation 2 is used to measure the EBR of a ring frame machine:

$$EBR = \frac{(N_{PDO} + BFT - BIT) \times 1000}{(N_{TS} - N_{IS}) \times t_{st}} \qquad 2$$

where EBR represents the number of breaks per 1,000 spindle-hours, N_{PDO} represents the number of piecing during observation, BFT represents breakage at finishing time, BIT represents breakage at initial time; N_{TS} represents the total number of spindles, N_{IS} represents the number of idle spindles, and t_{st} represents the total time of the study.

2.4 Multivariate analysis of variance (MANOVA)

To gain insight into the relationship between numerous definite independent variables and two or more continuous dependable variables, the statistical technique recommend is the multivariate analysis of variance [31]. It can be used when studying the impact of factors on several dependent variables at the same time in the same variance analysis. It is desirable to use multiple univariate analysis only when dependent variables are suitably correlated [32]. Four major multivariate analysis of variance are used in statistics to calculate p values: Wilk's lambda, Roy's largest root, Hotelling Lawley trace and Pillai's trace [33]. In this study, MANOVA was performed to determine the significance of the effect of three different blending methods, i.e. fibre blending, sliver blending and roving blending, on the yarn characteristics of unevenness, imperfections, strength, hairiness and EBR of the ring frame machine on which the yarn is manufactured.

2.5 Methodology

The physical properties of cotton fibres were tested using an Uster HVI instrument, while the properties of polyester fibres were provided by the supplier. The test results are shown in Table 2. First, cotton and polyester fibres were blended at the blow-room stage with blending ratios of 50:50, 60:40 and 70:30 separately, and chute matt was prepared as the output of the blow-room stage. After completion of the subsequent process following the blow-room stage, the yarns were produced using a ring frame machine. Second, cotton and polyester fibres were processed separately at the blow-room stage, and cotton and polyester carded slivers were produced using a carding machine. The carded slivers were then blended at the blending draw frame with blending ratios of 50:50, 60:40 and 70:30. After the processing of subsequent stages, 23 tex ring-spun yarn was produced. Figure 1 illustrates the blending stages during the manufacturing of yarn samples.

The end breakage rate (EBR) of the ring frame machine was remeasured during the manufacturing of yarn samples at each stage (equation 2).

In the roving blending method, two rovings of cotton and polyester with different fineness were fed in to the drafting system of the ring frame. Here, fibres were not blended in the drafting zone; the roving blended yarns were instead manufactured after twisting. This method is referred to as siro spinning. In this method, two rovings are fed in to a ring frame machine, with dividers to ensure that each roving is drafted separately. Two strands continuing from the drafting zone are formed into a single yarn by twisting [38]. Finally, 100% cotton and 100% polyester rovings were produced using a speed frame machine. The manufactured rovings were fed in to the drafting system of the ring frame and yarns were produced with blending ratios of 50:50, 60:40 and 70:30. The roving fineness in the ring frame for each blending ratio is shown in Table 3. The fineness of output materials for every blending method is presented in Table 4. The technical parameters of production machinery are presented in Table 5.

The produced ring cops were taken to a quality control laboratory and conditioned for 24 hours at standard atmospheric conditions. Yarn fineness and bundle yarn strength were measured using an electronic warp reel, an auto sorter machine and a lea strength tester in accordance with the D1907M-12 [34] and D1578-93 ASTM standards, [35] respectively. Yarn irregularity (*CVm*), hairiness and imperfections were measured using an Uster Evenness Tester-5 in accordance with the ASTM D1425M-14 standard [36]. The significance of the impact of

Table 3: Roving fineness for roving blended yarn

Blending ratio cotton:polyester	Roving fineness (tex)	
	Cotton	Polyester
50:50	748.00	748.00
60:40	748.00	498.40
70:30	748.00	327.75

Table 4: Fineness of output material for fibre, sliver and roving blending methods

Process	Output material	Fineness (tex)
Carding	carded sliver	6,500
Blending draw frame	drawn sliver	6,000
Breaker draw frame	drawn sliver	6,000
Finisher draw frame	drawn sliver	6,000
Speed frame	roving	748
Ring frame	yarn	23

blending methods and blending ratios on yarn quality and the EBR of machines were evaluated using multivariate analysis of variance (MANOVA). The tests were conducted using IBM SPSS Statistics software, version 25. The results of the tests were then analysed with the help of profile plots that originated from SPSS.

Table 5: Technical parameters of production machinery

Machine name	Company / Model	Important settings
Blow room	Rieter / Blow room line	Production: 800 kg/line
Carding	Rieter / C 60	Delivery speed: 180 m/min
Blending draw frame	Rieter / SB D 15	Delivery speed: 600 m/min Drafting system: 4 over 3 Zone setting (front-back): 38–42 mm Doubling: 6
Breaker draw frame	Rieter / SB D 15	Delivery speed: 600 m/min Drafting system: 4 over 3 Zone setting (front-back): 38–42 mm Doubling: 6
Finisher draw frame	Rieter / RSB D 35	Delivery speed: 500 m/min Drafting system: 4 over 3 Zone setting (front-back): 38–42 mm Doubling: 8
Simplex	Toyoda / FL 200	Flyer speed: 1200 rpm Drafting system: 4 over 4 Zone setting (front-middle-back): 39–45–51 mm
Ring frame	Toyota / RX-240	Spindle speed: 14500 rpm Drafting system: 3 over 3 Zone setting (front-back): 48–60 mm

a b c

Figure 1: Blending of: a) fibres at blow room, b) slivers at blending draw frame and c) rovings at ring frame

3 Results and discussion

3.1 Analysis with MANOVA

To explore the association between several definite independent variables and two or more dependent variables, the recommended statistical technique is MANOVA [31]. The main aim of MANOVA is to examine mean differences in linear combinations of multiple quantitative variables [37]. In the current research, the independent variables were the blending method and the blending ratio. The yarn quality parameters *CVm*, IPI, CSP, H and EBR were dependent variables. To determine the equality of covariance between the groups, a Box's M-test was performed. Levene's test of equality of variance was

used to examine whether the variance between independent variable groups was equal. Partial eta square ($\eta 2$) referred to as the estimate of effect size, which illustrates the amount of variance, was explained by the independent variable [38]. It can be calculated from the significant test statistics of F [39]. Multivariate F statistics were derived to determine variability within groups compared with the variability between different groups [40]. The higher F value indicated that the null hypothesis of no differences between group means was not true [41].

Table 6: Box's test of equality of covariance matrices of dependent variables

Box's M	284.877
F	2.023
df1	120
df2	17832.079
Sig.	0.000

The null hypothesis of the homogeneity of variance-covariance was rational based on the results of Box's M-test (Table 6) for the equality of variances where M = 284.877 and p = 0.000, which is less than 0.05. The null hypothesis of equal covariance metrics was thus rejected. It was also proven that if the p-value of the M-test returns results, Pillai's trace would be an emphatic test [42]. So, it would proceed for the MANOVA test with Pillai's trace, Wilks' Lambda, Hotelling Lawley trace and Roy's largest root. With regard to test strength, Pillai's trace has the greatest impact, followed by Wilk's Lambda, Hotelling Lawley trace and Roy's largest root in that order, as since each has its own interrelated F value [42, 43].

It is evident from Table 7 that the tests are significant for the different blending methods, blending ratios and the resulting products. The results of the MANOVA established that there was a statistically significant difference in yarn quality between different blending methods, blending ratios and their interrupt on the combined dependent variables of *CVm*, IPI, hairiness, CSP and the EBR of the machine, where Wilks value = 0.000, F (20. 406) = 26.938, $p < 0.001$, partial $\eta 2 = 0.504$ and observed power = 1.000. A multivariate eta squared of zero suggests that none of the total variances in the total data can be explained. Conversely, an eta squared of 1.00 indicates that all the variances in the total data can be explained [44]. Therefore, the discrepancy between multivariate and univariate results replicate the larger statistical effect related to the multivariate hypothesis test[45]. It would thus make sense to perform univariate tests with regard to manufactured yarn quality, such as *CVm*, IPI, hairiness, CSP and the EBR of the machine in terms of blending methods. It was clearly shown that yarn quality differs significantly with different blending methods, as the p values are less than 0.05 (0.0005) in all cases.

Table 7: Multivariate analysis of variance

Effect		**Value**	**F**	**df**	**Error df**	**Sig.**	**Partial eta squared**	**Observed power**
Blending ratio * blending method	Pillai's trace	1.666	17.850	20.000	500.000	0.000	0.417	1.000
	Wilks' Lambda	0.061	26.938	20.000	405.578	0.000	0.504	1.000
	Hotelling Lawley trace	5.728	34.511	20.000	482.000	0.000	0.589	1.000
	Roy's largest root	3.925	98.127	5.000	125.000	0.000	0.797	1.000

The results of Levene's test of equality of error variances (Table 8) indicate that the assumption of equality of variance through blending methods is also rational, as the properties of yarn are F (8.126) = 5.103, p = 0.00; F (8.126) = 5.501, p = 0.000; F (8.126) = 3.776, p = 0.001; F (8.126) = 7.302, p = 0.000 and F (8.126) = 1.031, p = 0.003, respectively, for *CVm*, IPI, CSP, H and EBR.

Table 8: Levene's test of equality of error variances

Values based on mean	Levene statistic	df1	df2	Sig.
CVm (%)	5.109	8	126	0.000
IPI	5.501	8	126	0.000
CSP	3.776	8	126	0.001
H	7.302	8	126	0.000
EBR	1.031	8	126	0.003

The sum of square values is expressed as the amount of the outcome of the independent variables on the response variables in a percentage [46]. The strength of the correlation between independent variables and response variables is described as 0 = 100%. The greater sum of square means, the better a model fits with data [46]. Table 9 shows that there was satisfactory reason to reject the null hypothesis for *CVm*, IPI, CSP, H and EBR. Using the Bonferroni method, the test was performed at an alpha value of 0.025 (0.05/2). The strength of the relationship between blending method and yarn quality is strong, as the *CVm* of the blending method is 95.5% of the variance of the dependent variable. The IPI, CSP, H and EBR and variance with the blending method were 97.30%, 98.00%, 94.90% and 89.90%, respectively. The observed power is 1.00, meaning that there is a 100% chance that the results could have a significant impact on the analysis.

Table 9: Tests of between-subjects effects

Source	Dependent variable	Type III sum of squares	df	Mean square	F	Sig.	Partial eta squared	Noncent. parameter	Observed power
Corrected model blending ratio * blending methods	*CVm*%	42.583	8	5.323	333.078	0.000	0.955	2664.627	1.000
	IPI	784056.415[b]	8	98007.052	563.619	0.000	0.973	4508.951	1.000
	CSP	1799961.526[c]	8	224995.191	778.185	0.000	0.980	6225.482	1.000
	H	13.714	8	1.714	292.212	0.000	0.949	2337.698	1.000
	EBR	2642.859	8	330.357	140.943	0.000	0.899	1127.540	1.000

3.2 Analysis with profile plots

A profile plot is a graphical suggestive method used to examine the relative performance of all variables in a multivariable data set [47, 48]. It can also be used to assess whether lines are indeed parallel, equal or flat within or across time. There is no interaction found between two or more factors when lines are parallel to each other [49]. The profile plots are fashioned at SPSS based on the estimated marginal mean values of the dependent variables across the two sets of independent variables of blending methods and blending ratios.

Figures 2 and 3 illustrate the differences in the profiles of blending methods and blending ratios of yarn mass variation (*CVm*) and imperfection index (IPI). It is evident that the profiles are indeed not parallel. There is thus an interaction between the dependent and independent variables. The *CVm* and IPI are higher for sliver- and roving-blended yarn than fibre-blended yarn. The reason lies in the variation in length of fibre, cotton and polyester. The length of cotton fibre is shorter than polyester fibre (Table 2). Two types of fibre were processed in a unique drafting system whose setting was higher than cotton fibre. Consequently, the movement of shorter fibres was unrestrained during the drafting of roving in the ring frame machine. As a result, *CVm* in yarn increased. Blending homogeneity was better for the fibre blending process. For this reason, mass variation is lower than the other two blending process. Consequently, the IPI is also lower than the other two blending processes. Increasing

the percentage of polyester fibres also increases the variations for all blending methods.

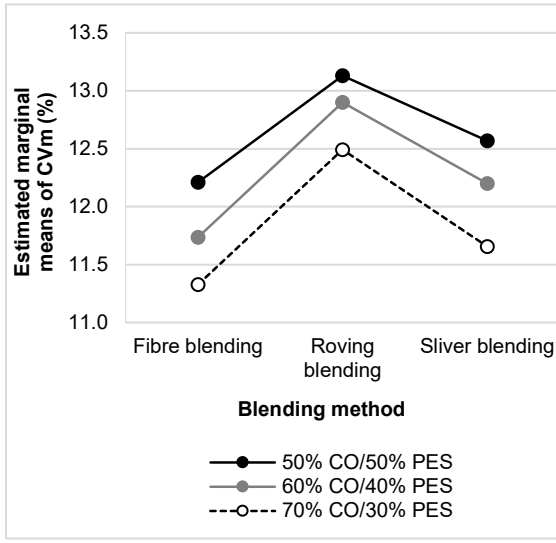

Figure 2: Estimated marginal means of CVm with corresponding blending method and blending ratio

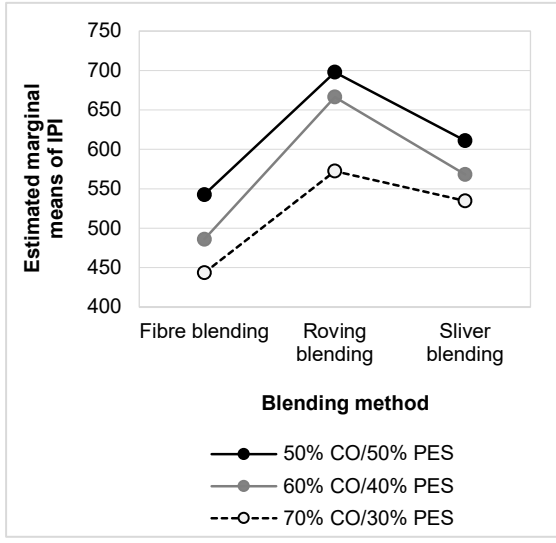

Figure 3: Estimated marginal means of IPI with corresponding blending method and blending ratio

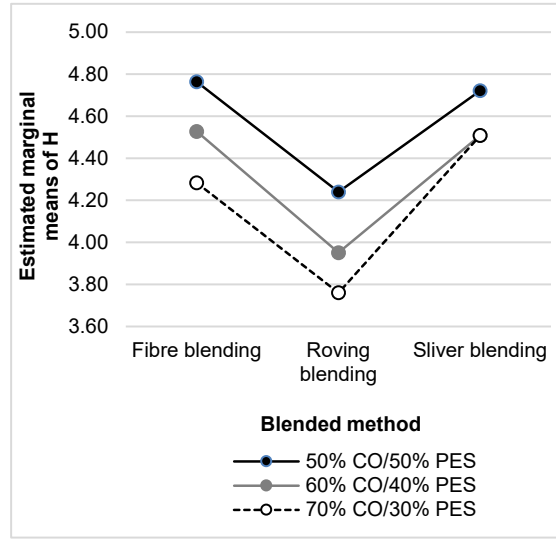

Figure 4: Estimated marginal means of H with corresponding blending method and blending ratio

Figures 4 and 5 illustrate the differences in the profiles of blending method and blending ratio of yarn hairiness value (H) and strength of yarn (CSP). It is evident that there are strong correlations between the groups, as the lines are not parallel to each other. When polyester was blended with cotton, the average length of fibre in the blended yarn increased. As a result, better twist distribution was seen in the blended yarn, while hairiness decreased. On the other hand, there was no significant difference in hairiness values for sliver- and fibre-blended yarn. However, hairiness decreased for roving-blended yard. This was because the yarn was produced using the siro spinning method. Increasing the percentage of polyester in blend ratios resulted in a decrease in the corresponding H value for the three blending methods. In the case of CSP (Figure 5), the blending homogeneity was higher in fibre blending than in the other two process, meaning the CSP value was higher in fibre blending than in the other two process. By incorporating polyester fibre in the blend, the strength of yarn also increased for all blending methods.

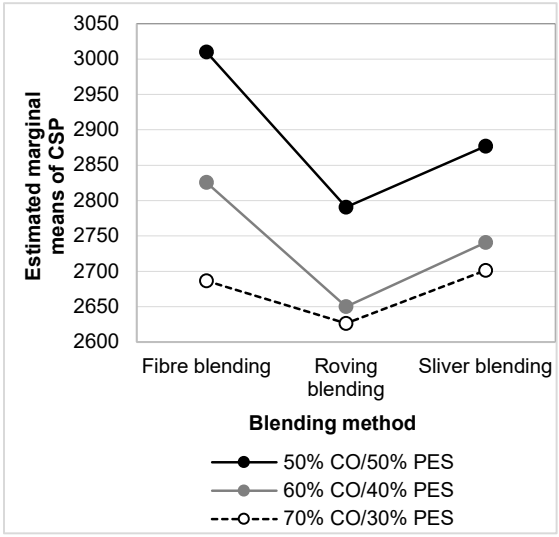

Figure 5: Estimated marginal means of CSP with corresponding blending method and blending ratio

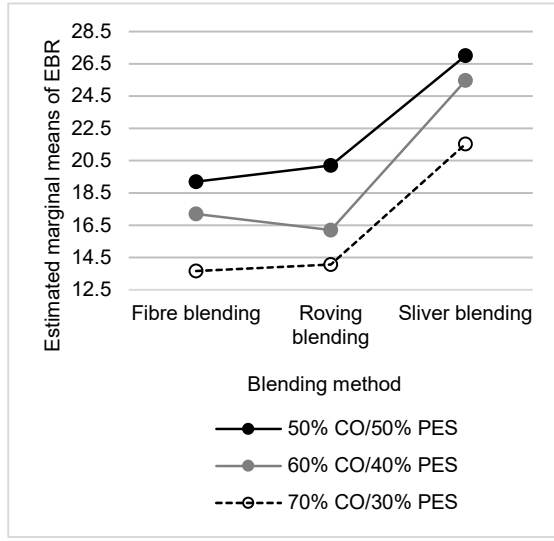

Figure 6: Estimated marginal means of EBR with corresponding blending method and blending ratio

Figure 6 presents the differences in the profiles of blending method and blending ratio of the end breakage rate (EBR) of the ring frame machine. The profile lines are not parallel to each other, which means the difference between the mean values of the EBR of the ring frame are not the same for the fibre-, sliver- and roving-blending processes, together with different blending ratios [42]. The breakage of yarn is higher with a higher winding tension and higher spinning tension, together with yarn strength. The yarn produced using the fibre-blending process and a blend ratio of 50/50 exhibited a higher strength. Thus, the EBR of the ring frame was lowest in the fibre-blending process and at a cotton/polyester blending ratio of 50/50. This can also be attributed to the contribution of polyester fibre to yarn strength.

4 Conclusion

The study was concerned with the impact of blending methods and blending ratios on the physical properties of blended ring-spun yarn. For that purpose, 23 tex cotton/polyester blended yarns were manufactured at blending ratios of 50/50, 60/40 and 70/30. The blending stage of fibre blending is the blow-room stage, the draw-frame stage in sliver blending and at the ring frame in roving blending. After analysing yarn characteristics using MANOVA and a profile plot, it was determined that the impact of blending method and blending ratio are statistically significant for the physical characteristics of ring-spun yarn. The characteristics of yarn were also studied based on technical facts relating to the settings of machinery and properties of raw materials. Among the three blending methods, fibre-blended yarn demonstrated the best results for *CVm*, IPI and EBR, while roving-blended yarn demonstrated the best results for H and bundle yarn strength (CSP). CSP increased as polyester fibre was blended with cotton. The CSP value is the highest for fibre-blended yarn due to better blending homogeneity. When polyester was blended with cotton, the average length of fibre in the blended yarn increased. As a result, better twist distribution was seen in the blended yarn, while the hairiness value decreased. For the blending process, there is no significant difference in hairiness values for fibre- and sliver-blended yarn. However, hairiness decreased in the roving-blending process. This was because the yarn was produced using the siro spinning method. However, the blending

method and ratio can be adapted based on the functional properties and potential uses of the yarn from the viewpoint of the consumer. The results achieved in this study can also be used for blended yarn manufactured using cotton and regenerated cellulosic fibres or/and bast fibres.

Acknowledgement

The research work was conducted at Matin Spinning Mills Ltd., situated in Shardaganj, Kashimpur, Gazipur. The authors acknowledge the employees of Matin Spinning Mills Limited for their support in the successful completion of our research work.

References

1. HOSSEN, J., AHMAD, N., ALI, S. M. An application of Pareto analysis and cause-and-effect diagram (CED) to examine stoppage losses: a textile case from Bangladesh. *The Journal of the Textile Institute*, 2017, **108**(11), 2013–2020, doi: 10.1080/00405000.2017.1308786.
2. AHMAD, N., HOSSEN, J., ALI, S. M. Improvement of overall equipment efficiency of ring frame through total productive maintenance: a textile case. *The International Journal of Advanced Manufacturing Technology*, 2018, **94**(1–4), 239–256, doi: 10.1007/s00170-017-0783-2.
3. TEKLEHAIMANOT, M., FISSEHA, K., AYELE, M. Combined effect of carding machine process parameters on yarn properties; process optimization. *Tekstilec*, 2022, **65**(1), 58–66, doi: 10.14502/tekstilec.65.2021020.
4. KOPITAR, D., PAVLOVIC, Z., SKENDERI, Z., VRLJICAK, Z. Comparison of double jersey knitted fabrics made of regenerated cellulose conventional and unconventional yarns. *Tekstilec*, 2022, **65**(1), 25–35, doi: 10.14502/tekstilec.65.2021026.
5. DUCKETT, K. E., GOSWAMI, B. C., RAMEY JR, H. H. Mechanical properties of cotton/polyester yarns. Part I: contributions of interfiber friction to breaking energy. *Textile Research Journal*, 1979, **49**(5), 262–267, doi: 10.1177/004051757904900504.
6. ISLAM, M. R., MIA, R., UDDIN, A. J. (2022). Investigation of the performance of okra fiber in woven fabric. *Heliyon*, 2022, **8**(4), 1–9, doi: 10.1016/j.heliyon.2022.e09307.
7. SEKERDEN, F. Investigation on the unevenness, tenacity and elongation properties of bamboo/cotton blended yarns. *Fibres & Textiles in Eastern Europe,* 2011, **19**(3), 26–29.
8. SHAD, S. S., MUMTAZ, A., JAVED, I. Effect of blending ratios and techniques on the quality parameters of 30's polyester/cotton yarn. *Pakistan Journal of Agricultural Sciences*, 2001, **38**(3–4), 35–37.
9. SAMANTA, A. K. Effect of blend ratio on yarn evenness and imperfections characteristics of wool/polyester ring-spun yarn. *Indian Journal of Fibre & Textile Research (IJFTR)*, 2014, **39**(1), 89–92.
10. BOULTON, J., CHARNLEY, F. Machinery problems in blending cotton and man-made fibres. *Journal of the Textile Institute Proceedings*, 1955, **46**(8), P534–P548, doi: 10.1080/19447015508665065.
11. LAWRENCE, C. A. *Fundamentals of spun yarn technology*. Boca Raton : CRC Press, 2003.
12. *Advances in yarn spinning technology*. Edited by C.A. Lawrence. Oxford : Woodhead Publishing, 2010.
13. MALIK, S. A., FAROOQ, A., GEREKE, T., CHERIF, C. Prediction of blended yarn evenness and tensile properties by using artificial neural network and multiple linear regression. *Autex Research Journal*, 2016, **16**(2), 43–50, doi: 10.1515/aut-2015-0018.
14. AKTER, N., REPON, M. R., MIKUČIONIENĖ, D., JALIL, M. A., ISLAM, T., KARIM, M. R. Fabrication and characterization of stretchable denim fabric using core spun yarn. *Heliyon*, 2021, **7**(12), 1–9, doi: 10.1016/j.heliyon.2021.e08532.
15. AFROZ, F., ISLAM, M. M. Study on mechanical property of woven fabrics made from 50/50

cotton-tencel blended siro yarn. *Heliyon*, 2021, 7(10), 1–11, doi: 10.1016/j.heliyon.2021.e08243.

16. RAY, S., GHOSH, A., BANERJEE, D. Effect of blending methodologies on cotton melange yarn quality. *Fibres & Textiles in Eastern Europe*, 2018, **5**(131), 41–46, doi: 10.5604/01.3001.0012.2529.
17. CHANNA, A. A., SOLANGI, W. H., NOONARI, Z. A., MEMON, A. H. Comparison of Quality & Propertiesof pc (52:48) blended ring spun yarn, produced by 'intimate' & 'creel' blending. *International Journal of Emerging Technology & Research*, 2014, **1**(3), 33–52.
18. NAWAZ, M., SHAHBAZ, B., IFTIKHAR, M., ILYAS, M. Cotton and polyester double rove feeding effect on blend yarn imperfections. *International Journal of Agriculture & Biology*, 2003, **5**(3), 364–366.
19. SAWHNEY, A. P. S., RUPPENICKER, G. F., KIMMEL, L. B., SALAUN, H. L., ROBERT, K. Q. New technique to produce a cotton/polyester blend yarn with improved strength. *Textile Research Journal*, 1988, **58**(10), 601–604, doi: 10.1177/004051758805801007.
20. ZHANG, A. F., XIA, Z. P. Properties of jute blended yarns spun on ring spinning system. *Advanced Materials Research*, 2013, **779**, 290–293, doi: 10.4028/www.scientific.net/AMR.779-780.290.
21. TYAGI, G. K., GOYAL, A., CHATTOPADHYAY, R. (2013). Influence of twist and blend ratio on characteristics of ring-spun tencel blended yarns. *Indian Journal of Fibre & Textile Research (IJFTR)*, 2013, **38**(2), 138–143.
22. KILIC, M., OKUR, A. The properties of cotton-Tencel and cotton-Promodal blended yarns spun in different spinning systems. *Textile Research Journal*, 2011, **81**(2), 156–172, 2011, doi: 10.1177/0040517510377828.
23. BEHERA, B. K., HARI, P. K., BANSAL, S., SINGH, R. Effect of different blending methods and blending stages on properties of Milange yarn. *Indian Journal of Fibre & Textile Research (IJFTR)*, 1997, **22**(2), 84–88.
24. *Process control and yarn quality in spinning*. Edited by G. Thilagavathi and T. Karthik. New Delhi : CRC Press, 2015, doi: 10.1201/b18797.
25. *Process management in spinning*. Edited by R. S. Kumar. New York: CRC Press, 2015.
26. LORD P. R. *Handbook of yarn production*. Cambridge : Woodhead Publishing, 2003, doi: 10.1533/9781855738652.
27. KLEIN W. *The Rieter manual of spinning - vol. 1*. Rieter Holding, 2014.
28. REGAR, M. L., AMJAD, A. I., JOSHI, S. Effect of solvent treatment on siro and ring spun TFO polyester yarn. *Tekstilec*, 2021, **64**(1), 1–8, doi: 10.14502/Tekstilec2021.64.47-54.
29. AMJAD, A. I., KUMAR, R. Evaluation of mechanical and physical characteristics of eco blended melange yarns. *Tekstilec*, 2020, **63**(2), 94–103, doi: 10.14502/Tekstilec2020.63.94-103.
30. KRETZSCHMAR S. D., FURTER R. *Application Report*, USTER® TESTER 5-S800 Version 1.1, 2009 SE 629.
31. PEREIRA, J. M., BASTO, M., FERREIRA-DA-SILVA, A., RIBEIRO, H. Financial risk analysis of portuguese textile and tourism companies. *Mediterranean Journal of Social Sciences*, 2015, **6**(3), 1–7, doi: 10.5901/mjss.2015.v6n3p471.
32. CLEFF, T. *Applied statistics and multivariate data analysis for business and economics*. Cham : Springer, 2019, doi: 10.1007/978-3-030-17767-6.
33. PEI, J., PARK, H., ASHDOWN, S. P. Female breast shape categorization based on analysis of CAESAR 3D body scan data. *Textile Research Journal*, 2019, **89**(4), 590–611, doi: 10.1177/0040517517753633.
34. *Test method for liner density of yarn (yarn number) by the skein method*. ASTM International, West Conshohocken, PA, 2018, doi: 10.1520/D1907_D1907M-12R18.
35. *Test method for breaking strength of yarn in skein form*. ASTM International, West Conshohocken, PA, 2016, doi: 10.1520/D1578-93R16.

36. *Test method for evenness of textile strands using capacitance testing equipment*. ASTM International, West Conshohocken, PA, 2020, doi: 10.1520/D1425_D1425M-14.
37. GRICE, J. W., IWASAKI, M. A truly multivariate approach to MANOVA. *Applied Multivariate Research*, 2008, **12**(3), 199–226.
38. RICHARDSON, J. T. Eta squared and partial eta squared as measures of effect size in educational research. *Educational Research Review*, 2011, **6**(2), 135–147, doi: 10.1016/j.edurev.2010.12.001.
39. HULLETT, C. R., LEVINE, T. R. The overestimation of effect sizes from F values in meta-analysis: the cause and a solution. *Communication Monographs*, 2003, **70**(1), 52–67, doi: 10.1080/715114664.
40. GEORGE, D., MALLERY P. *IBM Statistics 25 step by step: a simple guide and reference.* New York : Routledge, 2018, doi: 10.4324/9781351033909.
41. ANDERSON, M. J. A new method for non-parametric multivariate analysis of variance. *Austral Ecology*, 2001, **26**(1), 32–46, doi: 10.1111/j.1442-9993.2001.01070.pp.x
42. SARMA, K. V. S., VARDHAN, R. V. *Multivariate statistics made simple: a practical approach*. Boca Raton : CRC Press, 2019.
43. PALANIVEL, R. V., GANESH, K. S., NYANGOSI, R. A study on socio-economic conditions and work life balance of women workers in textile spinning mills. *International Journal of Business Management Insight & Transformations*, 2019, **3**(1), 1–8.
44. HAHS-VAUGHN, D. L. *Applied multivariate statistical concepts*. New York: Routledge, 2016, doi: 10.4324/9781315816685.
45. GHOSH, Anil K. Applied MANOVA and discriminant analysis. *Journal of the American Statistical Associatio*n, 2007, **102**(479), 1075–1076, doi: 10.1198/jasa.2007.s203.
46. SARIOĞLU, E., KAYNAK, H. K. PET bottle recycling for sustainable textiles. In *Polyester-production, characterization and innovative applications*. Edited by Nurhan Onar Camlibel. London : IntechOpen, 2017, 5–20, doi: 10.5772/intechopen.72589.
47. BULUT, Okan, DESJARDINS, Christopher David. *Profile analysis of multivariate data: a brief introduction to the ProfileR package*. 2020 Feb 10; Available from: http://dx.doi.org/10.31234/osf.io/sgy8m.
48. DAVISON, M. L., KIM, S. K., CLOSE, C. Factor analytic modeling of within person variation in score profiles. *Multivariate Behavioral Research*, 2009, **44**(5), 668–687, doi: 10.1080/00273170903187665.
49. KIM, S. K., FRISBY, C. L., DAVISON, M. L. Estimating cognitive profiles using profile analysis via multidimensional scaling (PAMS). *Multivariate Behavioral Research*, 2004, **39**(4), 595–624, doi: 10.1207/s15327906mbr3904_2.

Slavenka Petrak, Ivona Rastovac, Maja Mahnić Naglić
University of Zagreb, Faculty of Textile Technology, Department of Clothing Technology,
Prilaz baruna Filipovića 28a, 10000 Zagreb, Croatia

Dynamic Anthropometry – Research on Body Dimensional Changes

Dinamična antropometrija – raziskave sprememb telesnih dimenzij

***Original scientific article**/Izvirni znanstveni članek*
Received/*Prispelo* 4-2023 • Accepted/*Sprejeto* 9-2023

Corresponding author/*Korespondenčna avtorica:*
Maja Mahnić Naglić, mag. ing. techn. text.
E-mail: maja.mahnic@ttf.unizg.hr
ORCID: 0000-0001-9216-5483

Abstract

Dynamic anthropometry is a research field that refers to the physical characteristics and considers the measuring of a human body in dynamic positions. In dynamic positions, specific body measurements and surface dimensions change significantly compared to the measurements in a resting state. In that sense, this paper presents a research on dimensional changes conducted on a group of male test subjects in three dynamic positions with a defined set of body measurements relevant for the analysis of body measurement changes compared to the upright standing position. Using a Vitus Smart 3D body scanner and the Anthroscan program, the test subjects were scanned and measured in the upright standing position according to ISO 20685 and in three dynamic positions. Depending on the defined measurements for the analysis in each dynamic position, scanning markers were attached to test subjects' bodies to ensure the precise determination of anthropometric measuring points. Based on the obtained measurement results, dimensional changes and correlations of the three dynamic positions relative to the measurements in the upright standing position were analysed. The analysis showed significant differences in dynamic positions measurements compared to the upright standing position and indicated the assumption that the dimensional changes of body in motion within a specific body constitution group depend on the initial body part dimensions. The determined results can be used in the design and construction process of functional clothing, since the target values of the garment ease allowances can be determined based on the measurement changes.

Keywords: dynamic anthropometry, 3D body scanning, body dimensions, dynamic body positions

Izvleček

Dinamična antropometrija je raziskovalno področje, ki zajema proučevanje fizičnih značilnosti človeškega telesa in njegovo merjenje v dinamičnih položajih, kjer so specifične telesne mere in površinske mere bistveno drugačne kot v mirovanju. V tej raziskavi je bil na skupini moških testirancev raziskan definirani nabor dimenzijskih sprememb telesnih mer v treh dinamičnih položajih in primerjan s pokončnim stoječim položajem. S telesnim skenerjem Vi-

tus Smart 3D in programom Anthroscan so bili skladno s standardom ISO 20685 testiranci skenirani in izmerjeni v pokončnem stoječem položaju in treh dinamičnih položajih. V vsakem dinamičnem položaju so bili na telesa testirancev pritrjeni skenirni markerji, ki so zagotavljali natančno določitev antropometričnih merilnih točk. Na podlagi rezultatov meritev so bile analizirane dimenzijske spremembe in korelacije treh dinamičnih položajev glede na meritve v pokončnem stoječem položaju. Analiza je pokazala pomembne razlike v meritvah dinamičnih položajev v primerjavi s pokončnim stoječim položajem in nakazala domnevo, da so dimenzijske spremembe telesa v gibanju v posamezni skupini telesne konstitucije odvisne od začetnih dimenzij delov telesa. Rezultate lahko uporabimo pri načrtovanju in konstrukciji funkcionalnih oblačil, saj lahko na podlagi sprememb meritev določimo ciljne vrednosti dodatkov za lahkotnost oblačila.

Ključne besede: dinamična antropometrija, 3-D skeniranje telesa, dimenzije telesa, dinamični položaji telesa

1 Introduction

The main goal of anthropometry is to quantify the human body characteristics as accurately as possible. In the process, it is necessary to take into account the anthropometric characteristics of the population involved, the way in which these characteristics affect product design and the criteria that determine the appropriate relationship between users and products. Body measurements can be determined with a variety of methods, where positions of body measurements depend on the applied standard [1–5]. Non-contact methods for body measurements determination involve the use of modern devices, e.g. 3D and 4D body scanners, and the measurement process is performed on a computer 3D model [6–9]. The application of modern computer technologies has greatly contributed to the development of research in the field of anthropometry. In addition to the application in the development of sizing standards and clothing construction methods, where the measurements of human subjects in a static upright position are used [10, 11], 3D scanners have also enabled an accurate analysis of the human body both in static and dynamic positions [12–14]. 4D body scanners capture and reproduce digital human models in motion where an accurate analysis of body shape can be obtained from a sequence of scans. This is the newest technology, which requires more research in order to establish a reliable methodology for anthropometric surveys [9].

Dynamic anthropometry has its application in the areas such as ergonomics, automotive industry, workplace design and clothing technology. Dynamic anthropometry refers to the physical characteristics of a person in motion or measuring the human body in different positions. It is based on body biomechanics, the broad concept of which includes the knowledge of physics, chemistry and psychology, while the primary interest is in the application of mechanics to biological systems [15]. It is assumed that during body movement, specific body length and surface dimensions will change significantly with respect to the resting state. There are several aspects of measurement in dynamic anthropometry, the most common of which are the measurements of body dimensions and range of movements required for work, observed from the aspect of safety and practicality [15, 16].

In the field of clothing technology, dynamic anthropometric measurements are performed to determine the dimensions and shape of the human body in different positions, the results being applied in the development of products and garments for better functionality and fit [13, 17, 18]. The main issue in obtaining dynamic measurements is the lack of standardised methodology and protocols, where particular dimensions on 3D models in different positions are still mostly taken manually using interactive measurement tools [19, 20]. Since the conventional construction of clothing is based on body measurements in upright standing position, it is necessary to consider dynamic anthropometry when developing high

quality functional garment models. Body dimensions in different body positions significantly differ from static ones and the main goal is to determine those dimensional changes and possibly define their relationships to initial static measurements and body shapes to ensure suitable ease and comfort of products in the designing and construction process [21–25].

2 Test subjects and methods

The experimental part of the study was set up as preliminary research in the field of dynamic anthropometry with the aim of determining differences in body measures depending on the measurement method, dynamic body position and the analysis of possible relationship of those deviations with initial body dimensions.

2.1 Sample of test subjects and preparation of test subjects for 3D body scanning

The study was conducted on a small sample of 35 male test subjects, age group 25–35 years, with a body without any deformities, size range from 88 to 112,5 cm in chest circumference. Scanning markers were placed on the test subject bodies in order to enable the most accurate determination of anthropometric points and measures between them in the measurement process. The positions of the markers were defined according to characteristic anthropometric points, and based on the body positions and relevant measures for which the measurement was performed (Figure 1). Three dynamic positions were defined, i.e. forward bend (P1), squat (P2) and upper limbs pre-extension (P3), as Figure 2 shows.

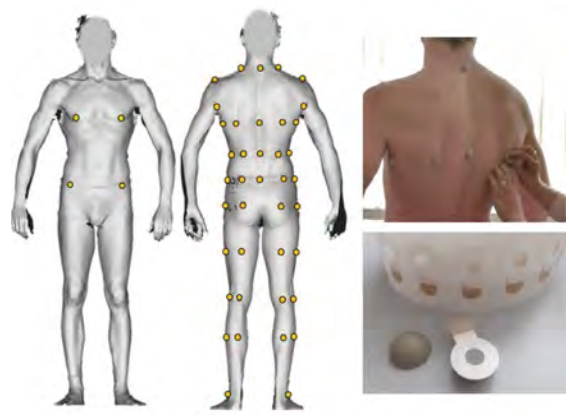

Figure 1: Preparation of test subjects – body markers positioning

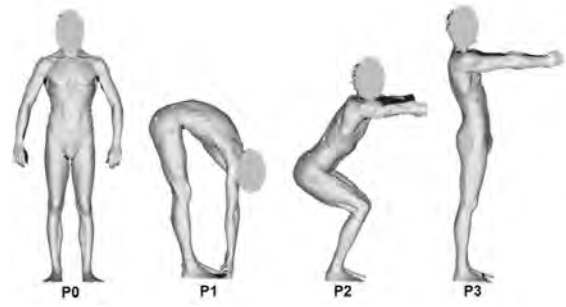

Figure 2: Scanned body model in upright standing position according to ISO 20685 [3] and three dynamic positions

2.2 Variables

A set of body measures for a dimensional changes analysis were defined for each of the three positions (Table 1), i.e. four variables for the dynamic positions P1 and P3, and three variables for the position P3, making a total of 11 variables for the analysis.

Table 1: Set of most significant body measurements for analysis in three dynamic positions

Variable	Measure description	Position
BW1	Back width measured at armpit level	P1, P3
BW3	Back width measured at chest height	P1, P3
SW1	Shoulders width measured between acromion points	P1, P3
BL3	Lower back length measured between waist and hips lines	P1
HW	Hips width measured on hips circumference line between outseams	P2
ULC	Upper leg circumference	P2
LLC	Lower leg circumference	P2
CC	Chest circumference	P3

2.3 Determination of body measurements using conventional measurement method

The sample of male test subjects was measured with a conventional method using an anthropometer and a measuring tape. Body measurements were precisely determined according to the positions of the anthropometric points marked with markers. They were measured in all three dynamic positions (P1–P3) and in the upright standing position (P0), as it can be seen in Figure 3.

Figure 3: Conventional measurement of test subject

2.4 3D body scanning of test sample

Using a laser body scanner VitusSmart, the sample of male test subjects was scanned in three dynamic body positions (P1–P3) and in the upright standing position (P0) defined by the standard for 3D body scanning ISO 20685 (Figure 2). The measuring of the scanned body models was performed using the Anthroscan program. The automatic measurement method in the upright standing position according to ISO 20685 [1] was applied on the scanned models whereby 154 body measures were determined for each test subject for a subsequent comparison with defined variables in dynamic positions.

2.5 Determination of body measurements on scanned body models in dynamic positions

Using the tools for the interactive measurement within the Anthroscan program, the measurements of the scanned body models in three different dynamic positions were determined. The anthropometric points and positions of body measurements on scanned models in dynamic positions were precisely determined according to the positions of markers attached to the bodies of the test subjects (Figure 1). In the measurement process, the most widely used functions were the measurements between points over a curve and the function of intersecting a body model with a plane defined by three points (Figure 4). By intersecting a body model with a plane through three points, it is possible to visualise and analyse any particular cross-section in the dynamic position, given that in dynamic positions, characteristic body circumferences are usually not parallel to any of the basic anatomical planes.

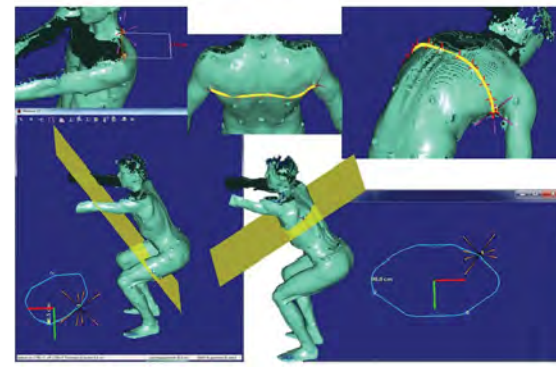

Figure 4: Interactive measuring of scanned body model in dynamic positions

Based on the measurements performed on body models in upright standing and dynamic body positions, differences in body measurements and average values of changes for each of the three dynamic positions were calculated for the defined set of variables. In addition, a correlation analysis between the values of the determined measures in the upright standing position and the measurement differences determined in the dynamic positions was performed for variables with significant dynamic changes.

3 Results and discussion

Based on the measurement results determined with a conventional method and 3D scanning, differences and deviations in individual body measures

were calculated depending on the applied method. No major deviations in the measurement results between the conventional and 3D scanning methods were observed in any of the scanned positions. All deviations ranged up to 1 cm. Higher changes can be observed on the measures of widths and circumferences, while with linear measures, the deviations were smaller. In the performed measurements, significantly smaller differences in values were found depending on the applied method compared to previously conducted research where similar comparisons were made [1]. In this study, the accuracy of measurements between the two methods was achieved by attaching scanning markers to the test subject bodies, which enabled precise positioning of anthropometric measurement points in both methods, resulting in concordance of the results.

At the bend forward position (P1), the greatest stress and changes in body dimensions occurred in the area of the upper and lower back, while shoulders width was decreasing. From the measurements results of scanned models in the dynamic position P1, it can be seen that the measurements of the back width (BW1 and BW3) significantly increased compared to the measurements in the upright standing position. The average change value of the back width measured at the height of the armpit (BW1) in the P1 position was 12.02 cm, which is 30.5% of the same measure average value in the static position. The lower back length measured between the waist and hips lines (BL3) also increased significantly by an average of 10.58 cm, which is 47.8% of the same measure average value in the upright standing position. The shoulder width measure (SW1) decreased on average by 19.7% (Table 2).

Table 2: Measurement differences in dynamic position P1 and correlation with initial measurements and other relevant characteristic measurements in standard position (P0)

P1 variables	Change percent. (%)	Average change (cm)	Standard deviation	Correlation with initial measurement (P0) – r	Correlation with chest circumference (P0) – r	Correlation with body height (P0) – r
SW1	–19.74	–7.66	2.00	–0.35	–0.12	–
BW1	30.46	12.02	5.27	–0.64	–0.07	–
BW3	31.04	12.28	3.31	–0.58	–0.02	–
BL3	47.82	10.58	3.05	–0.51	–	–0.14

In the dynamic position P2, the most significant changes were obtained in the hips area (HW) and the circumferences of the upper (ULC) and lower leg (LLC). The average change of the hips width measured on hips circumference line between outseams (HW) was 5.83 cm, which is 11.5% of the average value of the same measure in the static position. The average change of the upper leg circumference (ULC) was 8.15 cm, which is 16.6% of the same measure average value in the static position. The average change in the lower leg circumference (LLC) was 2.54 cm, which is 6.8% of the measure average value in the static position (Table 3).

Table 3: Measurement differences in dynamic position P2 and correlation with initial measurements and other relevant characteristic measurements in standard position (P0)

P2 variables	Change percentage (%)	Average change (cm)	Standard deviation	Correlation with initial measurement (P0) – r	Correlation with hips circumference (P0) – r
HW	11.49	5.83	2.84	0.12	0.11
ULC	16.61	8.15	2.75	–0.29	–
LLC	6.77	2.54	1.34	0.14	–

From the measurements results of scanned models in the dynamic position P3, it can be seen that the measurements of back width at armpit level and back width at chest height level increased (BW1, BW3), while the measurement of shoulder width measured between acromia (SW1) decreased significantly. The average change of back width at armpit level (BW1) was 18.30 cm, which is 45.6% of the same measure average value in the static position. The average change of shoulder width measured between the acromia was 6.13 cm, which is a decrease of 15.8% compared to the same measure average value in the static position (Table 4).

Table 4: Measurement differences in dynamic position P3 and correlation with initial measurements and other relevant characteristic measurements in standard position (P0)

P3 variables	Change percentage (%)	Average change (cm)	Standard deviation	Correlation with initial measurement (P0) – r	Correlation with chest circumference (P0) – r
SW1	–15.75	–6.13	2.00	–0.47	–0.19
BW1	45.61	18.30	4.28	–0.17	0.20
BW3	27.99	11.13	3.76	–0.28	0.02
CC	–2.88	–2.98	1.46	–0.09	

In the dynamic position P1, a small to moderate correlation between the measurement changes and initial measurements was found in all measures with a significant difference. The changes in shoulders width showed a small negative correlation, while the measurement changes on back width and back length showed moderate negative correlation with the initial measurements. The results lead to the assumption that the changes on back width measurements in position P1 depend on body size and can be predicted based on the initial dimensions (Table 2). The analysis of the dimensional changes with basic body measurements, body height and chest circumference did not show any correlation. Significant differences in the measurements in the dynamic position P2 did not show any correlation (< 0.3), which leads to the assumption that changes in body dimensions in this position do not depend on body size and cannot be predicted based on the initial dimensions (Table 3). In the dynamic position P3, a moderate negative correlation was found on shoulders width measures (SW1, r = –0.47), while the other observed measurements did not show any correlation (< 0.3), as it is depicted in Table 4. Previously conducted similar researches were mostly investigating the dynamic body changes in length dimensions [24, 25]. Research performed on a group sample of the same body type but different body height [24] showed similar results considering the correlations with initial dimensions. The research hypothesis was that the length body dimensions will increase in change in specific dynamic positions according to the increase in body height; however, this was not the case and there was no correlation found.

Additionally, we divided the test sample according to body constitutions [26], since the primary results indicated certain similarities in dynamic body changes within the test subjects with similar proportions of body dimensions, and we obtained more interesting and meaningful results. Within each group, an increased correlation of individual body measurement changes compared to the initial measurement was visible, which confirms the hypothesis that changes of body in dynamic positions do not depend only on body dimensions in general, but on the type of body constitution and its muscularity. Based on the observed preliminary study, it can be concluded that the research on a larger number of test subjects, based on body constitution, can lead to the definition of general percentage of changes in individual measurements for each type. This has an extremely important and great role in the development of functional clothing and the standardisation of the ease allowance values implemented in the construction of

such clothing and adjustments according to individual measurements. The defined values of the percentage change of an individual measure in the targeted dynamic position can also be used in the segment of selecting textile materials with targeted properties that meet the criteria of unrestricted movement and optimal pressure against the body in the zones of greatest garment stress when performing various tasks of physical work.

Table 5: Correlation of measurement differences in three dynamic positions (P1–P3) with initial measurements (P0) for three body constitutions groups

Body position	Measurement variable	Body constitutions					
		Leptosome		Athletic		Picnic	
		Δ (%)	r	Δ (%)	r	Δ (%)	r
P1	SW1	–14.87	–0.57	–21.05	–0.09	–21.99	–0.46
	BW1	34.80	–0.80	29.50	–0.75	28.03	–0.56
	BW3	31.85	–0.49	30.55	–0.63	31.22	–0.74
	BL3	44.80	–0.34	45.38	–0.67	55.71	–0.22
P2	HW	12.17	0.42	10.21	0.01	13.36	–0.18
	ULC	19.87	–0.43	16.09	–0.44	14.38	0.17
	LLC	8.23	–0.15	5.88	0.45	7.08	0.28
P3	SW1	–12.01	–0.45	–17.11	–0.44	–16.78	–0.26
	BW1	55.56	0.12	43.26	–0.27	40.36	–0.16
	BW3	36.73	0.08	24.91	–0.45	25.43	–0.55
	CC	–2.27	0.26	–3.28	0.18	–3.08	0.62

4 Conclusion

Body measurements determined in dynamic positions are the starting point for the analysis of changes on characteristic body parts that affect the functionality and comfort of clothing. Body dimension changes in dynamic positions cannot be considered only from the aspect of basic anthropometric measurements. The use of 3D body scanners enables the non-contact measurement of scanned models and by using an interactive measurement method, it is possible to determine measurement points anywhere on the body and perform measurements between them. In this way, the measurements of scanned body models in dynamic positions are performed, whereby the characteristic anthropometric points are defined with the application of scanning markers on subjects' bodies in the scanning process. Scanning markers ensure precise positioning of measuring points in the interactive measurement process and enable the repeatability and comparison of the results, since the measurement is always performed in the same way and between the same defined points, which is especially important when measuring in different positions where body surface deformation occurs, thereby shifting the position of the measures. A comparative analysis of the determined measurement results between the conventional measurement method and 3D scanning of the subjects did not show significant deviations in the obtained measurements. The analysis of body measurement changes in dynamic positions in relation to the upright standing position revealed significant differences in individual measures. The determined results can be used in the design of functional and special-purpose clothing, since the target values of the garment ease allowances can be determined based on the measurement changes. The results of the preliminary research indicated the assumption that the dimensional changes of body in motion within a specific body constitution group depend on the initial body part dimensions. In that sense, further research will focus on expanding the test sample to a larger range of body sizes and constitutions, and

implementation of the obtained results in the design and construction customisation process of functional clothing.

References

1. ISO 7250-1:2017. Basic human body measurements for technological design. Part 1: Body measurement definition and landmarks. Geneva : International Organization for Standardization, 2017, 51 p.
2. SIST EN 13402-3:2017. Size designation of clothes. Size labelling based on body measurements and intervals. Geneva : International Organization for Standardization, 2017, 36 p.
3. ISO 20685-1:2018. 3-D scanning methodologies for internationally compatible anthropometric databases. Part 1: Evaluation protocol for body dimensions extracted from 3-D body scans. Geneva : International Organization for Standardization, 2018, 19 p.
4. UJEVIĆ, D., SZIROVICZA, L., HALÁSZ, M., TAMÁS, P., PETRAK, S., DOLEŽAL, Ksenija, DOMJANIĆ, Žaklina, ŠAJATOVIĆ, B. B., KISFALUDY, M., VAS, L. M., KOLESZÁR, András, SZABÓ, Orsolya. Comparison of conventional and computerized human body measurement methods. In *Proceedings of the 5th International Textile, Clothing and Design Conference – Magic World of Textiles*. Edited by Z. Dragčević et al. Zagreb : University of Zagreb Faculty of Textile Technology, 2010, 523–528.
5. DABOLINA, Inga, LAPOVSKA, Eva. Sizing and fit for protective clothing. *In Anthropometry, apparel sizing and design (2nd edition)*. Edited by D. Gupta and N. Zakaria. Cambridge : Woodhead Publishing, 2020, 289–316, doi: 10.1016/B978-0-08-102604-5.00011-1.
6. D'APUZZO, Nicola. Overview of 3D surface digitization technologies in Europe. In *Three-Dimensional Image Capture and Applications VII (vol. 6056)*. Edited by Brian D. Corner, Peng Li and Matthew Tocheri. San Jose : SPIE – The International Society for Optical Engineering, 2006, doi: 10.1117/12.650123.
7. DAANEN, Hein, PSIKUTA, Agnes. 3D body scanning. In *Automation in Garment Manufacturing*. Edited by Rajkishore Nayak and Rajiv Padhye. Elsevier, 2018, 237–252, doi: 10.1016/B978-0-08-101211-6.00010-0.
8. KLEPSTER, Ank, MORLOCK, Simone. Investigating fit in motion with 4D photogrammetry scanner system. In *3DBODY.TECH 2021. Proceedings of 12th International Conference and Exhibition on 3D Body Scanning and Processing Technologies,* 2021, doi: 10.15221/21.13.
9. URIEL, J., RUESCAS, A., IRANZO, S., BALLESTER, A., PARRILLA, E., REMÓN, A., ALEMANY, S. A methodology to obtain anthropometric measurements from 4D scans. In *Proceedings of the 7th International Digital Human Modeling Symposium,* **7**(1), 12, 2022, doi: 10.17077/dhm.31758.
10. PETROVA, Adriana, ASHDOWN, Susan P. Three-dimensional body scan data analysis: body size and shape dependence of ease values for pants fit. *Clothing and Textile Research Journal*, 2008, **26**(3), 227–252, doi: 10.1177/0887302X07309479.
11. LU, Jun-Ming, WANG Mao-Jiun J. Automated anthropometric data collection using 3D whole body scanners. *Expert Systems with Applications*, 2008, **35**(1–2), 407–414, doi: 10.1016/j.eswa.2007.07.008.
12. CHI, Liu, KENNON, William R. Body scanning of dynamic posture. *International Journal of Clothing Science and Technology*, 2006, **18**(3), 166–178, doi: 10.1108/09556220610657934.
13. DABOLINA, Inga, LAPOVSKA, Eva, VILUMSONE Ausma. Dynamic anthropometry for investigation of body movement comfort in protective jacket. In *Functional Textiles and Clothing.* Edited by Abhijit Majumdar, Deepti Gupta and Sanjay Gupta. Singapore : Springer, 2019, 241–259, doi: 10.1007/978-981-13-7721-1_20.

14. WU, Xinzhou, KUZMICHEV, Victor. A design of wetsuit based on 3D body scanning and virtual technologies. *International Journal of Clothing Science and Technology,* 2021, **33**(4), 477–494, doi: 10.1108/IJCST-02-2020-0021.
15. WINTER, David A. *Biomechanics and Motor Control of Human Movement*. New Jersey : John Wiley & Sons, 2004.
16. BROLIN, Erik. *Anthropometric Diversity and Consideration of Human Capabilities (PhD Thesis)*. Gothenburg : Chalmers University of Technology, Department of Product and Production Development, Division of Production Systems, 2016.
17. AVADANEI, Manuela. Dynamic anthropometry – a solution for improving the shape of individual protective garments. *International Journal of Engineering Research & Technology,* 2020, **9**(7), 162–165, doi: 10.17577/IJERTV9IS070131.
18. LEE, Heeran, HONG, Kyunghi, LEE, Yejin. Ergonomic Mapping of Skin Deformation in Dynamic Postures to Provide Fundamental Data for Functional Design Lines of Outdoor Pants. *Fiber and Polymers*, 2013, **14**(12), 2197–2201, doi: 10.1007/s12221-013-2197-6.
19. PETRAK, Slavenka, MAHNIĆ NAGLIĆ, Maja. Dynamic Anthropometry – Defining a Protocols for Automatic Body Measurement. *Tekstilec*, 2017, **60**(4), 254–262, doi: 10.14502/Tekstilec2017.60.254-262.
20. LOERCHER, C., MORLOCK, S., SCHENK, A. Design of a motion-oriented size system for optimizing professional clothing and personal protective equipment. *Journal of Fashion Technology & Textile Engineering,* 2018, **S4**, 1–4, doi: 10.4172/2329-9568.S4-014.
21. MAHNIC NAGLIC, Maja, PETRAK, Slavenka. Analysis of surface segments deviations between different female body types based on 3D flattening method. In *AHFE 2020. Advances in Simulation and Digital Human Modeling*. Vol. 1206. Edited by Daniel N. Cassenti, Sofia Scataglini, Sudhakar L. Rajulu and Julia L. Wright. Cham : Springer, 2020, 241–247, doi: 10.1007/978-3-030-51064-0_31.
22. MAHNIČ NAGLIC, M., PETRAK, S., GERŠAK, J., ROLICH, T. Analysis of dynamics and fit of diving suits. *IOP Conference Series: Materials Science and Engineering,* 2017, **254**(15), 1–7, doi: 10.1088/1757-899X/254/15/152007.
23. AVADANEI, M. L., OLARU, S., DULGHERIU, I., IONESI, S. D., LOGHIN, E. C., IONESCU, I. A new approach to dynamic anthropometry for the ergonomic design of a fashionable personalised garment. *Sustainability,* 2022, **14**(13), 1–24, doi: 10.3390/su14137602.
24. BOGOVIĆ, S., STJEPANOVIČ, Z., CUPAR, A., JEVŠNIK, S., ROGINA-CAR, B., RUDOLF, A. The use of new technologies for the development of protective clothing: comparative analysis of body dimensions of static and dynamic postures and its application. *AUTEX Research Journal,* 2018, **19**(4), 301–311, doi: 10.1515/aut-2018-0059.
25. TAMA, Derya, ÖNDOĞAN, Ziynet. Calculating the percentage of body measurement changes in dynamic postures in order to provide fit in skiwear. *Journal of Textiles and Engineer (Tekstil Ve Mühendis),* 2020, **27**(120), 271–282, doi: 10.7216/1300759920202712007.
26. Body constitution. In *Medical Encyclopedia (Medicinska enciklopedija)*. Zagreb: Leksikografski zavod Miroslav Krleža, 1986.

SHORT INSTRUCTIONS FOR AUTHORS OF SCIENTIFIC ARTICLES

Scientific articles categories:

- **Original scientific article** is the first publication of original research results in such a form that the research can be repeated and conclusions verified. Scientific information must be demonstrated in such a way that the results are obtained with the same accuracy or within the limits of experimental errors as stated by the author, and that the accuracy of analyses the results are based on can be verified. An original scientific article is designed according to the IMRAD scheme (Introduction, Methods, Results and Discussion) for experimental research or in a descriptive way for descriptive scientific fields, where observations are given in a simple chronological order.
- **Review article** presents an overview of most recent works in a specific field with the purpose of summarizing, analysing, evaluating or synthesizing information that has already been published. This type of article brings new syntheses, new ideas and theories, and even new scientific examples. No scheme is prescribed for review article.
- **Short scientific article** is original scientific article where some elements of the IMRAD scheme have been omitted. It is a short report about finished original scientific work or work which is still in progress. Letters to the editor of scientific journals and short scientific notes are included in this category as well.

Language: The manuscript of submitted articles should be written in UK English and it is the authors responsibility to ensure the quality of the language.

Manuscript length: The manuscript should not exceed 30,000 characters without spacing.

Article submission: The texts should be submitted only in their electronic form in the format *.doc (or *docx) and in the format *.pdf (made in the computer program Adobe Acrobat) to the address: tekstilec@a.ntf.uni-lj.si. The name of the document should contain the date (year-month-day) and the surname of the corresponding author, e.g. 20140125Novak.docx. The articles proposed for a review need to have their figures and tables included in the text. The article can also be submitted through a cloud-based file transfer service, e.g. "WeTransfer" (www.wetransfer.com).

Publication requirements: All submitted articles are professionally, terminologically and editorially reviewed in accordance with the general professional and journalistic standards of the journal Tekstilec. Articles are reviewed by one or more reviewers and are accepted for publication on the basis of a positive review. If reviewers are not unanimous, the editorial board decides on further proceedings. The authors can propose to the editorial board the names of reviewers, whereas the editorial board then accepts or rejects the proposal. The reviewers' comments are sent to authors for them to complete and correct their manuscripts. The author is held fully responsible for the content of their work. Before the author sends their work for publication, they need to settle the issue on the content publication in line with the rules of the business or institution, respectively, they work at. When submitting the article, the authors have to fill in and sign the Copyright Statement (www.tekstilec.si), and send a copy to the editors by e-mail. They should keep the original for their own personal reference. The author commits themselves in the Copyright Statement that the manuscript they are submitting for publication in Tekstilec was not sent to any other journal for publication. When the work is going to be published depends on whether the manuscript meets the publication requirements and on the time reference the author is going to return the required changes or corrections to the editors.

Copyright corrections: The editors are going to send computer printouts for proofreading and correcting. It is the author's responsibility to proofread the article and send corrections as soon as possible. However, no greater changes or amendments to the text are allowed at this point.

Colour print: Colour print is performed only when this is necessary from the viewpoint of information comprehension, and upon agreement with the author and the editorial board.

More information on: www.tekstilec.si